TASK REPORT

Title: Durability of Concrete Using Low Slag Cement Contents

FDOT Contract Number: BEC98

Draft Final Report

Submitted to

The Florida Department of Transportation Research Center
605 Suwannee Street, MS 30 Tallahassee, FL 32399

c/o Thomas Frank
Concrete Field Operations Manager
FDOT State Materials Office

Submitted by:

Dr. Kyle A. Riding (kyle.riding@essie.ufl.edu) (Principal Investigator)
Dr. Christopher C. Ferraro (Co-Principal Investigator)
Sristi Das Gupta
Engineering School of Sustainable Infrastructure and Environment
University of Florida
Gainesville, Florida 32611
Dr. Abla Zayed (Co-Principal Investigator)
Department of Civil and Environmental Engineering
University of South Florida

November 2023
Department of Civil Engineering
Engineering School of Sustainable Infrastructure and Environment
College of Engineering

i

DISCLAIMER

SI (MODERN METRIC) CONVERSION FACTORS (FROM FHWA)

Symbol	When You Know	Multiply By	To Find	Symbol
Length				
in	inches	25.4	millimeters	mm
ft	feet	0.305	meters	m
yd	yards	0.914	meters	m
mi	miles	1.61	kilometers	km
Area				
in^2	square inches	645.2	square millimeters	mm^2
ft^2	square feet	0.093	square meters	m^2
yd^2	square yard	0.836	square meters	m^2
mi^2	square miles	2.59	square kilometers	km^2
Volume				
fl oz	fluid ounces	29.57	milliliters	mL
gal	gallons	3.785	liters	L
ft^3	cubic feet	0.028	cubic meters	m^3
yd^3	cubic yards	0.765	cubic meters	m^3
NOTE: volumes greater than 1000 L shall be shown in m^3				
Mass				
oz	ounces	28.35	grams	g
lb	pounds	0.454	kilograms	kg
Temperature (exact degrees)				
°F	Fahrenheit	5 (F-32)/9 or (F-32)/1.8	Celsius	°C
Illumination				
fc	foot-candles	10.76	lux	lx
fl	foot-Lamberts	3.426	candela/m^2	cd/m^2
Force and Pressure or Stress				
lbf	pound-force	4.45	newtons	N
lbf/in^2	pound-force per square inch	6.89	kilopascals	kPa

TECHNICAL REPORT DOCUMENTATION PAGE

1. Report No.	2. Government Accession No.	3. Recipient's Catalog No.
4. Title and Subtitle Durability of Concrete Using Low Slag Cement Contents		**5. Report Date** October, 2023
		6. Performing Organization Code
7. Author(s) Kyle A. Riding, Christopher C. Ferraro, Sristi Das Gupta, Abla Zayed		**8. Performing Organization Report No.**
9. Performing Organization Name and Address Department of Civil and Coastal Engineering Engineering School of Sustainable Infrastructure & Environment University of Florida 365 Weil Hall P.O. Box 116580 Gainesville, FL 32611-6580		**10. Work Unit No. (TRAIS)**
		11. Contract or Grant No. BEC98
12. Sponsoring Agency Name and Address Florida Department of Transportation 605 Suwannee Street, MS 30 Tallahassee, FL 32399		**13. Type of Report and Period Covered** Final Report
		14. Sponsoring Agency Code

15. Supplementary Notes – N/A

16. Abstract

Supplemental cementitious materials (SCMs), such as fly ash, slag, silica fume, and metakaolin have become commonplace in Florida concrete, particularly for high durability or high-strength concrete. The Florida Department of Transportation (FDOT) currently allows fly ash to be used as a cement replacement at 18-50% levels and slag cement to be substituted at 50-70% when incorporated into binary blends for general use, mass concrete, or precast concrete products in extremely aggressive environments. Some precast concrete producers would like to use slag cement instead of fly ash. High volumes of slag cement in the concrete can reduce early-age strength gain. The research objectives of this study were to determine the maximum amount of slag cement that could obtain high enough compressive strength to detension prestressed concrete products in 18 hrs after concrete placement in FDOT class V and above mixtures, and the minimum amount of slag cement required to achieve comparable durability against chloride ingress to a control mixture containing 20% ASTM C618 Class F fly ash, and durable in a very severe sulfate attack environment. Compressive strength results showed that it is possible to achieve early-age strengths needed for precast concrete production, however some slags may require additional heat or accelerators to achieve such strengths. Accelerated curing of concrete gave bulk and surface resistivity results in between that measured for 56 and 91 days of curing at lab temperature. All mixtures tested for sulfate attack resistance that contained slag cement with a Type IL would qualify as high sulfate resistant cementitious systems. Based on the resistivity and sulfate attack test results, it is recommended that the minimum slag replacement level required for chloride durability in Class V, VI, and VII concrete be changed to allow slag cement replacement levels of 35% when used with Type IL cement.

17. Key Word Slag cement, Durability, Sulfate Attack, Resistivity		**18. Distribution Statement** No restrictions.		
19. Security Classif. (of this report) Unclassified		**20. Security Classif. (of this page)** Unclassified.	**21. No. of Pages** 91	**22. Price**

EXECUTIVE SUMMARY

1.1. Background

Supplemental cementitious materials (SCMs), such as fly ash, slag, silica fume, and metakaolin have become commonplace in Florida concrete, particularly for high durability or high-strength concrete. FDOT currently allows fly ash to be used as a cement replacement at 18-50% levels and slag cement to be substituted at 50-70% when incorporated into binary blends for general use, mass concrete, or precast concrete products in extremely aggressive environments. Fly ash has traditionally been used by precast concrete producers to meet FDOT durability requirements. Because of limited availability of fly ash in recent years, some precast concrete producers would like to use slag cement instead of fly ash. High volumes of slag cement in the concrete can reduce early-age strength gain. Some precast concrete producers have stated that it is difficult for them to meet strength requirements to detension prestressing steel in time to begin the fabrication process for new product the next day. They would like to have the option of using lower slag cement replacement levels to help them maintain similar productivity as with their mixtures containing fly ash. Different slag cements can have different rates of strength gain and durability based on their chemical composition and fineness [1].

1.2. Research Objectives

The research objectives of this study were to determine the maximum amount of slag cement that could obtain high enough compressive strength to detension prestressed concrete products in 18 hrs after concrete placement in FDOT class V and above mixtures, and the minimum amount of slag cement required to achieve comparable durability against chloride ingress to a control mixture containing 20% ASTM C618 [2] Class F fly ash, and durability in a very severe sulfate attack environment. This project also examined the potential for a rapid test to determine the sulfate durability of concrete based on ASTM C1202 [3] but using sodium sulfate solution instead of sodium chloride.

1.3. Research Approach

To address the objectives of this study, published literature were reviewed to document the existing knowledge on the durability of slag cement. Concrete constituent materials were then obtained to carry out an experimental plan to measure the strength and durability development of concrete containing slag cements of different chemical compositions. An ASTM C595 [4]Type IL cement, a Class F fly ash, three ASTM C989 [5] slag cements from different sources, and an ASTM C1240 [6] silica fume were procured and their physical and chemical compositions were characterized using X-ray fluorescence (XRF), semi-quantitative X-ray diffraction (QXRD), laser particle size distribution, and specific gravity. The slags were found to have 8.8% (slag 9), 13.4% (slag 13), and 17.6% (slag 18) Al_2O_3 contents.

Binary-blended concrete mixtures incorporating 20% fly ash, 30%, 40%, and 50% slags with the three different slags, and ternary-blended concrete mixtures of slag 13 with 30% and 50% cement replacement having 4% and 6% silica fume were used. Compressive strengths were measured after elevated temperature curing (120°F) at 18 and 24 hr after mixing, and lab

temperature curing (73°F) at 18 hr, 24 hr, 7 days, and 28 days after mixing. Surface and bulk resistivity were tested using two different curing approaches, lab temperature curing (73°F) at 28, 56, and 91 days and accelerated curing according to the method prescribed in ASTM C1202 at 28 days. The accelerated curing was done to determine if the accelerated curing approach could be used to reduce the time required to perform long-term durability tests. For assessing sulfate durability, mortar bars with a w/cm of 0.485 were prepared with the same cementitious material system as the concrete mixtures. To measure the sulfate expansion rate of mortar bars till 6 months, two different exposures, standard ASTM C1012 and accelerated, were followed where the accelerated exposure method was implemented by drying the bars at 100°F for 14 days after which they were vacuum impregnated with a 5% sulfate solution to accelerate the sulfate expansion rate.

1.4. Main Findings

The findings from compressive strength, resistivity, and external sulfate durability testing of binary and ternary blended concrete mixtures can be summarized as follows:

1. At elevated temperature curing, all mixtures tested containing slag with an alumina content $\geq$ 13% (slag 13 and slag 18) were capable of reaching the 5200 psi target strength at 18 hr and were above that of the 20% fly ash mixes. However, the low alumina slag had slightly lower strength. These results show that it is possible to achieve early-age strengths needed for precast concrete production, however some slags may require additional heat or accelerators to achieve such strengths.
2. Accelerated curing of concrete gave bulk and surface resistivity results in between that measured for 56 and 91 days of curing at lab temperature.
3. The worst performing slag for resistivity, slag 18, required 30.9% slag to achieve equivalent surface resistivity as 20% fly ash at 91 days, and 36.2% slag to achieve equivalent bulk resistivity as 20% fly ash at 91 days.
4. All mortar mixtures made with slag cement had a 6 month expansion in ASTM C1012 less than 0.05% when used with a Type IL cement and would be classified as having a high sulfate resistance. According to the ACI 201 Guide to Durable Concrete, these materials would qualify to be used in very severe sulfate environments (S3) when used with a w/cm at or below 0.40. Because FDOT class V, VI, and VII concrete limits the w/cm to 0.37, all the slags studied could be used in these classes with replacement levels of 30% or greater.

1.5. Recommendations

The following recommendations can be made based on the project findings:

1. Accelerated curing of concrete samples should be considered by FDOT for future acceptance testing.
2. Based on the resistivity and sulfate attack test results, it is recommended that the minimum slag replacement level required for chloride durability in Class V, VI, and VII concrete be changed to allow slag cement replacement levels of 35% when used with Type IL cement.

TABLE OF CONTENTS

LIST OF FIGURES

LIST OF TABLES

1. INTRODUCTION

1.1. Background

The Florida Department of Transportation requires the use of supplementary cementitious materials (SCMs) in concrete in extremely aggressive environments to improve durability. SCMs commonly used in FDOT concrete include ASTM C618 [2] Class F fly ash, ASTM C989 [5] slag cement, ASTM C1240 [6] silica fume, and ASTM C618 [2] Class N metakaolin. Due to their filler effect and pozzolanic effect, these materials have the potential to enhance durability, principally against chloride penetration, corrosion resistance, and sulfate attack [7]. The Florida Department of Transportation (FDOT) currently allows fly ash to be used at a 18-50% cement replacement level and slag cement to be used at 50-70% portland cement replacement levels when used in binary blends for general use, mass concrete, or precast concrete products. Precast concrete producers have traditionally used fly ash to help meeting the durability criteria for concrete in extremely aggressive environments. Fly ash has become less available and consistent due to coal-burning power plants closing [8]. Precast concrete producers would like to be able to use slag cement in lieu of fly ash when fly ash supplies are low, however large slag replacement levels can reduce the early age strength development [9]–[11]. Precasters they have had a difficult time in the past meeting the compressive strength required to detension prestressing reinforcement in a timely manner.

While lower slag cement replacement levels could help precast concrete producers meet early-age strengths desired, there is a concern that they could provide a lower level of durability than desired by the FDOT. The premature deterioration of concrete caused by sulfate attack significantly decreases its service life and increase its cost of maintenance. Some types of SCMs can contribute to a significant improvement in sulfate performance, however not all of them [12]. Slag cements with varying alumina content display different behaviors when exposed to sulfate-aggressive environments [13]. ASTM C989 [5] states that the sulfate resistance of a slag cement mix is dictated by the slag cement replacement amount, the alumina content, and addition of calcium sulfate and/or limestone fines. High alumina slags can promote the formation of monosulfoaluminate, increasing susceptibility to sulfate attacak [1], [14], [15]. When calcium sulfate or limestone fines are added to the slag cement, ettringite is favored to form over monosulfoaluminate [16].

Laboratory-based external sulfate attack tests take at least 6 months. A method has been proposed to accelerate further external sulfate attack tests. In this test, samples are vacuum impregnated with a sodium sulfate solution to accelerate the sulfate ingress into the mortar, thus reducing the time needed for damage to occur.

1.2. Research Objectives

This project had the following research objectives;

1

- Determine the minimum slag cement replacement level required to provide similar durability against chloride ingress and sulfate attack as a mixture containing 20% Class F fly ash used as a benchmark for service life.
- Determine the maximum slag replacement level that can provide the strength required to detension prestressed concrete members at 18 hr.

1.3. Research Scope

To address the objectives of this study, published literature were reviewed to document the existing knowledge on the durability of slag cement. Concrete constituent materials were then obtained to carry out an experimental plan to measure the strength and durability development of concrete containing slag cements of different chemical compositions. An ASTM C595 [4] Type IL cement, a Class F fly ash, three ASTM C989 [5] slag cements from different sources, and an ASTM C1240 [6] silica fume were procured and their physical and chemical compositions were characterized using X-ray fluorescence (XRF), semi-quantitative X-ray diffraction (QXRD), laser particle size distribution, and specific gravity. The slags were found to have 8.8% (slag 9), 13.4% (slag 13), and 17.6% (slag 18) Al_2O_3 contents.

Binary-blended concrete mixtures incorporating 20% fly ash, 30%, 40%, and 50% slags with the three different slags, and ternary-blended concrete mixtures of slag 13 13 with 30% and 50% cement replacement having 4% and 6% silica fume were used. Compressive strengths were measured after elevated temperature curing (120°F) at 18 and 24 hr after mixing, and lab temperature curing ($100°$F) at 18 hr, 24 hr, 7 days, and 28 days after mixing. Surface and bulk resistivity were tested using two different curing approaches, lab temperature curing ($73°$F) at 28, 56, and 91 days and accelerated curing according to the method prescribed in ASTM C1202 at 28 days. The accelerated curing was done to determine if the accelerated curing approach could be used to reduce the time required to perform long-term durability tests. For assessing sulfate durability, mortar bars with a w/cm of 0.485 were prepared with the same cementitious material system as the concrete mixtures. To measure the sulfate expansion rate of mortar bars till 6 months, two different exposures, standard ASTM C1012 and accelerated, were followed where the accelerated exposure method was implemented by drying the bars at 100°F for 14 days after which they were vacuum impregnated with a 5% sulfate solution to accelerate the sulfate expansion rate.

2

2. LITERATURE REVIEW

2.1. Background

Utilization of concrete as a building material is prominent throughout the world due to its adaptability, robustness, durability, and low cost [17]. Concrete is a mixture of different types and amounts of hydraulic cement, aggregates, and water, and sometimes chemical admixtures, fibers, or other cementitious materials [8], [17]. Concrete that has been properly designed, proportioned, finished, and cured can last for decades with little maintenance. Certain situations might cause concrete to deteriorate if the materials are not designed accordingly. Exposure to moisture, temperature or other aggressive environment can augment the severity of concrete degradation and reduce the concrete service life [18]. Fluids and ions from the environment can flow through the concrete because it is a multiphase medium made up of a porous cement paste matrix with aggregates. Concrete degradation mechanisms from fluid and ion transport through the concrete can be chemical or physical in nature [19]. Moreover, the development of cracks will enhance the rate of fluid and ion (chloride and sulfate) infiltration in concrete and thus worsen the concrete performance. Chloride attack is the trigger for reinforcing steel corrosion whereas sulphate attack engenders extensive micro-cracking in concrete. This concrete cracking impairs the structure's load capacity, serviceability, and durability. With the increasing demand for concrete performance, researchers are currently incorporating SCMs (fly ash, slag) in concrete to fortify concrete durability [20].

Concrete permeability and diffusivity can be considerably reduced by incorporating SCMs into the mixture. These materials may not significantly lower total porosity, but they subdivide pores, making them less continuous in the concrete matrix [21]. Fly ash has long been utilized by precast concrete makers to achieve the durability requirements for concrete in aggressive environments. In addition, fly ash can reduce the amount of water required in concrete mixtures because of their spherical particle shape, allowing for lower w/c ratio while ensuring the same workability [19]. Due to the closure of coal-fired power stations, fly ash availability has become inconsistent and, in some locations, difficult to obtain, and expensive. To alleviate this issue, precast concrete manufacturers want to use slag cement instead of fly ash [18]. When slag is used to replace a portion of portland cement, it has various advantages including decreased usage of energy, reduced greenhouse gas emissions, and minimal use of virgin raw material [22].

Depending on the application and performance goals, the optimal cement substitution level can vary. Users must assess and analyze all characteristic aspects of slag cement binders, such as workability, strength, and durability to ensure it is appropriate for its intended application when proposing them. Figure 1 shows typical slag substitution levels used for different concrete applications. Other performance requirements, aside from compressive strength, will affect the quantity of slag cement being used in some high-strength concrete. For instance, to curb the increase in concrete temperature caused by the heat of hydration, high-strength concrete may require a slag cement amount of more than 50 percent (usually 60 to 80 percent). With increasing slag cement content, early-age strength may be reduced, leading to the lower slag replacement levels typically seen with precast concrete [23]. Concrete mixtures made with slag at the 50-70%

3

replacement levels currently permitted by FDOT have a low early strength gain rate and have difficulty achieving strength required to detension prestressing steel and begin creating new products in a timely way for cost-effective precast productions. Concrete mixtures that use less than 50% slag cement used in precast operations in other states may be able to be used by Florida precast concrete producers if they have sufficient durability required for FDOT structures.
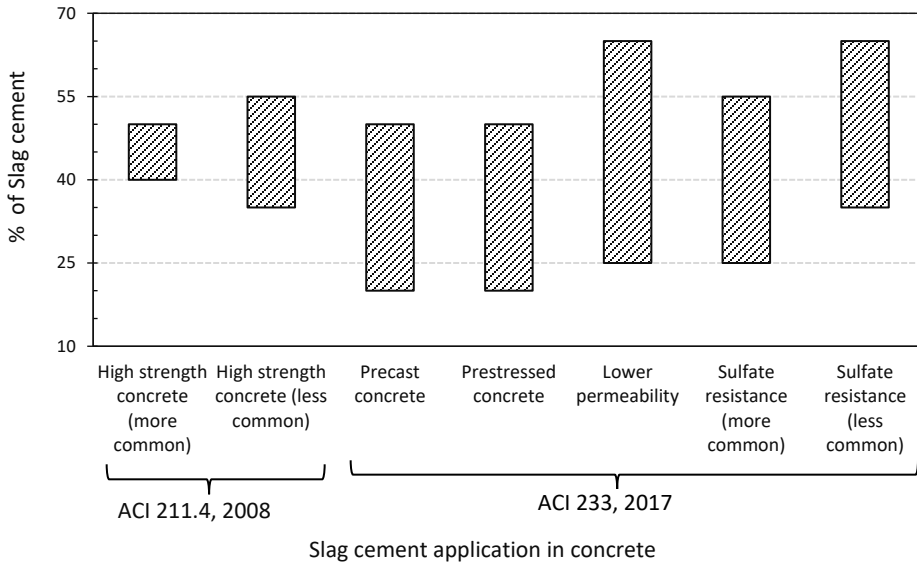
Figure 1: Replacement rate of slag cement for individual application [8], [21]

2.2. Slag Cement Hydration

Slag cement reacts in both hydraulic and pozzolanic reactions, changing the hydration products formed from those in systems with only portland cement as the cementitious material. Factors such as slag chemical composition, concentration of alkalis in the system, fineness of cement and slag, and temperature during hydration process influence slag hydration [24]–[26]. A high amount of calcium and silica is present in slag cement and factors into the hydration products formed.

When slag is exposed to water, there is a small and slow hydraulic reaction that can occur. Slag dissolution increases as the pH increases. Activators such as lime or alkalis can be incorporated to speed up the slag dissolution and hydration reactions. The predominant slag chemical reaction is with an alkali hydroxide as represented in Equation 1 [27].

$$\text{Slag + Water +} \begin{cases} \text{CH} \\ \text{NH} \\ \text{KH} \end{cases} \rightarrow \text{C- (N, K)-S-H} \qquad \text{Equation 1}$$

4
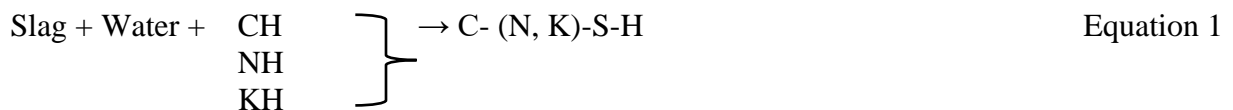
During portland cement hydration, calcium silicate hydrate (C-S-H) and calcium hydroxide are formed. Calcium silicate hydrate (C-S-H) is the primary adhesive that holds concrete together and provides a majority of the strength. On the other hand, portlandite that is formed from cement hydration does not add much to the concrete strength. Additional C-S-H forms however when the silica from the slag combines with water and portlandite. Alkalis can also substitute in the C-S-H as shown in Equation 1. This added C-S-H strengthens the concrete composite by densifying the pore system [28]. On the other hand, MgO may have a deleterious effect in the hydration reaction when it is over 10%. Based on British standards, the mass ratio of CaO plus MgO-to-SiO_2 must be greater than 1.0 (Table 1) to maintain high alkalinity in the hydration phase without which hydraulic activity of slag is unproductive [29]. Figure 2 shows a ternary diagram of possible reaction phases after the hydration of portland cement and slag.

Table 1: Chemical ratios for the evaluation of hydraulic activity of slag cement [30]

No.	Chemical ratio	Requirement
1	CaO/SiO_2	1.3-1.4
2	$(CaO + MgO)/ SiO_2$	>1.4
3	$(CaO + MgO)/ (SiO_2 + Al_2O_3)$	1.0-1.3
4	$(CaO + MgO + Al_2O_3)/ SiO_2$	3
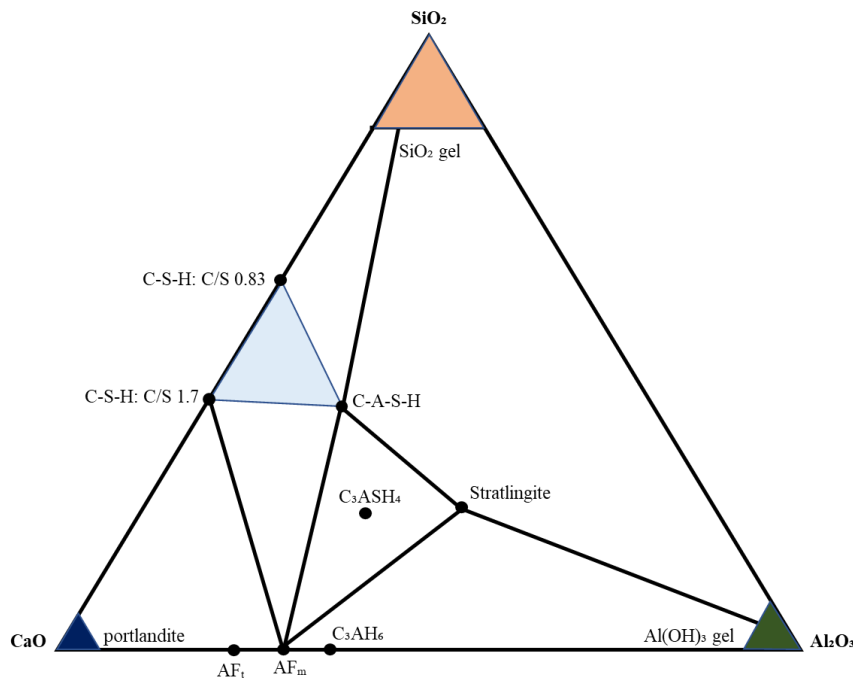
Figure 2: Hydration phases of slag cement with portland cement in CaO-SiO$_2$-Al$_2$O$_3$ system, after [29]

2.3. Fresh Properties

Concrete made with slag cement can have excellent fresh properties. When compared to concrete without slag cement, the workability and placeability of concrete with slag cement are enhanced. The impact of slag cement substitution level on workability is shown in Figure 3 [8]. Slump has been shown to increase as the slag substitution of cement increases in concrete with a constant w/cm. Several experimental studies confirmed this tendency by showing that as the proportion of slag cement in the concrete rose, the w/cm had to be lowered to retain workability qualities comparable to that of concrete without slag cement [23]. Depending on the substitution level and other conditions, the water consumption for a particular slump in concrete with slag cement may be 3 to 5% lower than in concrete without slag cement [31]. Finer cementitious particle dispersion and higher specific surface area of slag particles contribute to increased workability by generating smooth slip planes in the paste with increasing water film thickness and therefore imbibe little water [32], [33]. Another reason for the improved workability properties may be the increased volume of paste. This decreases the aggregate interconnection which in turn decreases the concrete viscosity [33]. Moreover, slag particles have a lower specific gravity (2.85-2.94) than cement particles [21]. When cement is replaced on a mass basis by slag, it results in an increased volume of cementitious particles and consequently higher paste content, aiding workability [29]. Research findings have showed that the rate of slump loss of concrete containing slag cement is decreased compared to OPC mixtures [34]
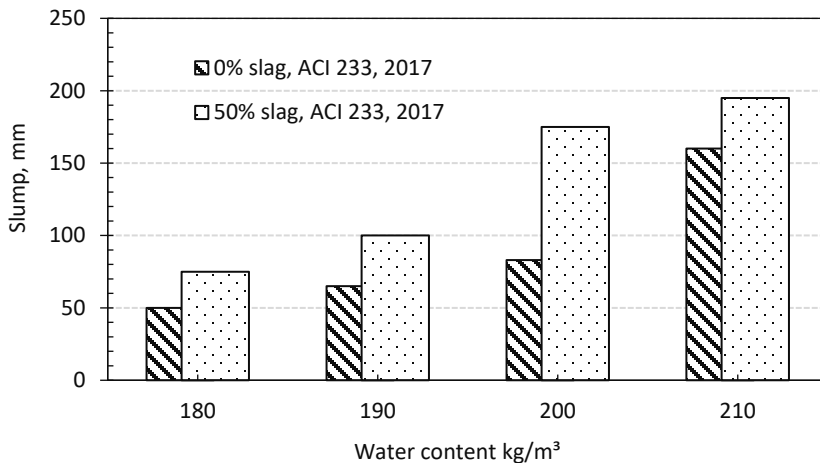
.
Figure 3: Influence of water content on concrete slump with and without slag cement [8]

The incorporation of slag cement can reduce concrete bleeding. The ratio of solid surface area to water unit volume, air voids, and concrete member depth all affect the bleeding capacity and rate of concrete bleeding. When using slag cement in concrete, bleeding properties can be determined based on the slag cement fineness relative to portland cement and the interactive influence of the two cementitious materials. When slag cement is used as a replacement of portland cement on an equal-mass basis, bleeding may be decreased if the slag cement is finer than portland cement. On

6

the other hand, the bleeding rate may increase from the control if the slag cement is coarser than the portland cement [29]. The bleeding rate is more stable at higher than 60% substitution levels, regardless of the slag cement fineness. Furthermore, adding the finer particles can improve grain size distribution and particle filling, resulting in increased cohesiveness of concrete paste and reduced concrete bleeding [35]. Another potential cause of changes in bleeding is the slowdown of hydration reaction and subsequent decrease in the production of hydration products [36].

2.4. Mechanical Properties

2.4.1.   Setting Time

ASTM C403/C403M "Standard Test Method for Time of Setting of Concrete Mixtures by Penetration Resistance [37] is commonly used to evaluate the time that concrete takes to set and complete the transition between fluid concrete and a hardened solid. [38]. Increasing the substitution level of slag cement in concrete lengthened the time it takes for the cement to set [39], however the relative amount depends on the slag and cement compositions, replacement level, and temperature. When more than 25% slag cement is substituted for portland cement in concrete compositions, an increase in setting time might be expected [40]. This is to be expected because the slag has a very low reaction until setting, contributing very little to hydration products and particle bridging. The mostly filler effect of the slag particles at this age means that the higher the replacement level, the more bridging required by the cement hydration reaction and the longer it takes to set.

Several research studies have shown that over a range of 400 to 1400 m^2/kg, slag cement fineness had no effect on concrete setting time prepared with 40% slag cement [38]. Unlike conventional slag cement, which is slow to react and mainly promotes the later formation of the microstructure, ultra-fine slag decreases both initial and final strength of concrete. In comparison to the same slag cement binder with a lower fineness, ultra-fine slag cement binder causes quick setting of the concrete and faster strength gain rate after setting. The high surface area of these slag particles provides nucleation sites for cement hydration products and react quickly with CH [41].Slag cement hydration is very dependent on the temperature. At 25% slag replacement, a slight reduction in setting time was seen at room temperature, whereas at $41^{°}$F ($5^{°}$C), the impact of the slag on setting time depended on the cement used [42]. As demonstrated in Figure 4 and Figure 5, concrete blends with slag cement take longer to set at lower temperature. At high temperatures concrete sets significantly quicker than the similar concrete blended and cured at relatively low temperatures. In cold weather, lowering the ratio of the slag cement-portland cement may be suggested to avoid excessive setting times and potential settlement cracking. In most circumstances, the prolonged setting time is preferable at elevated temperatures, and thus increasing the slag cement-portland cement ratio may be beneficial for concrete mixing, placing, and consolidating. Because of this, many precast operations will use a cold weather mixture with a low slag content in the winter, and a high slag content mixture in the summer. Despite the fact that substantial slowdown in setting can occur at relatively low temperatures, accelerators such as $CaCl_2$ or other non-chloride containing admixtures can mitigate this impact. Based on the chemical composition of the admixture, the setting time can be shortened by 40 to 50% [34].

7
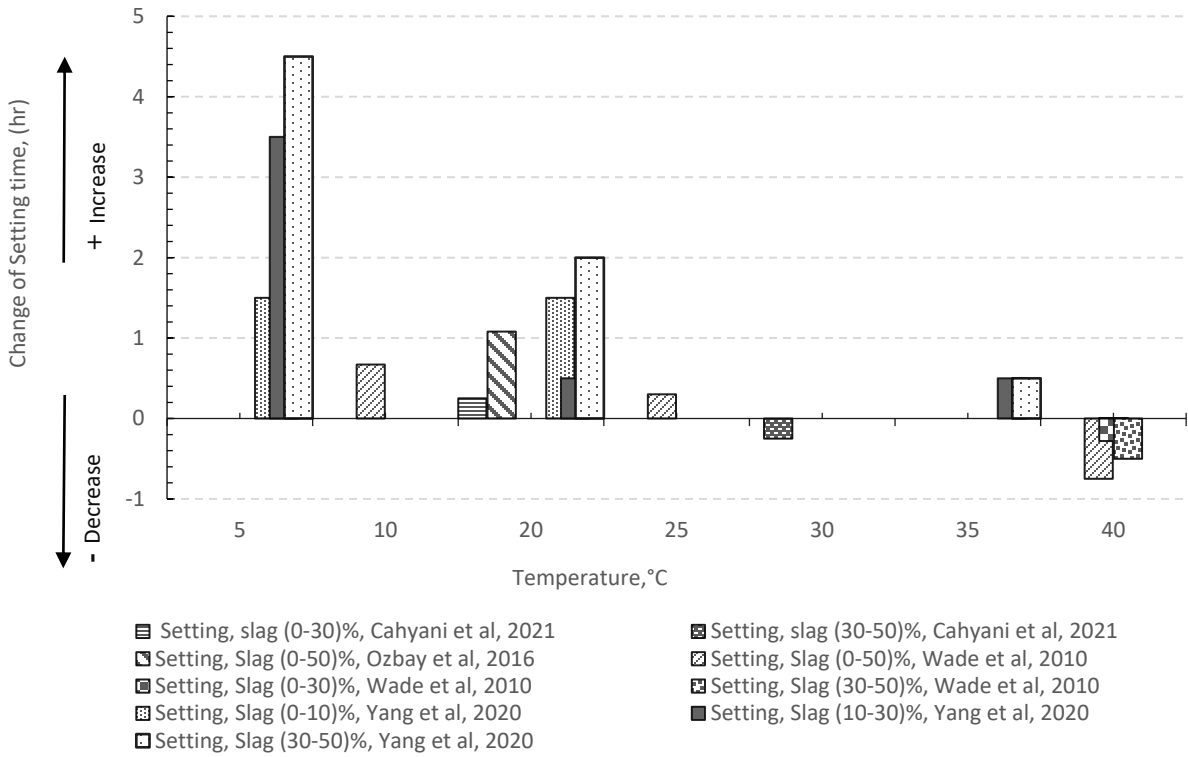
Figure 4: Change of initial setting time with different temperatures [29], [34], [43], [44]
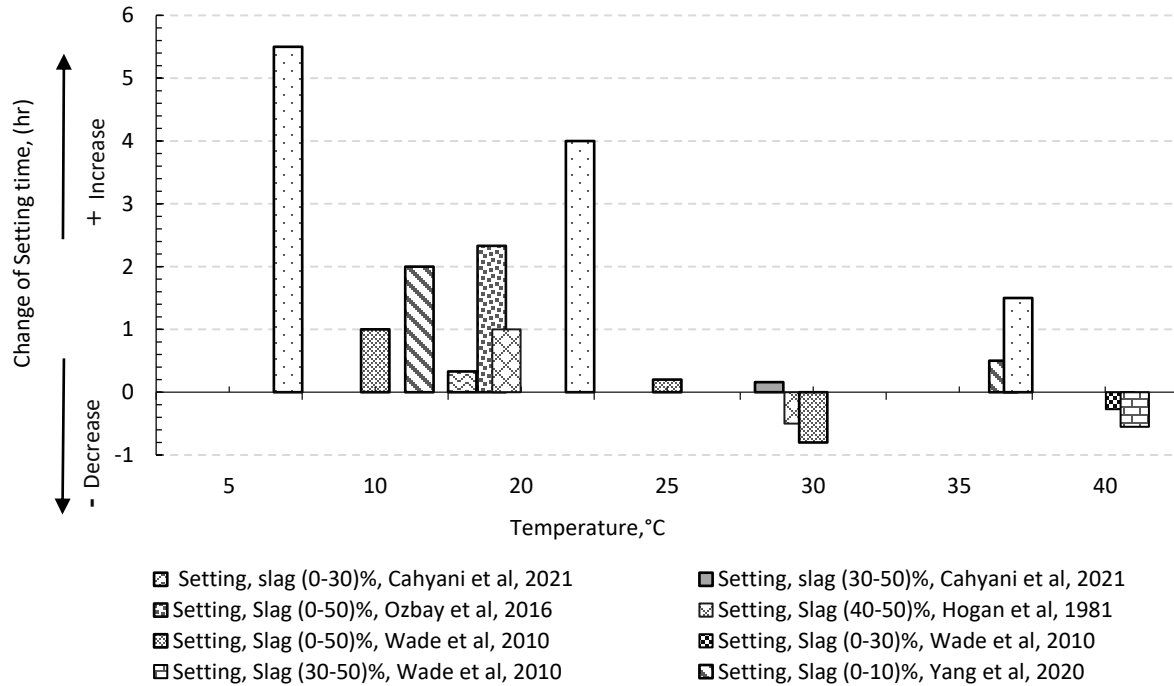
Figure 5: Change of final setting time with different temperatures [29], [34], [43], [44]

2.4.2. Effect of Slag Cement Fineness on Compressive Strength

The fineness of cement with slag addition has a significant impact on the heat of hydration and concrete compressive strength. The Blaine air permeability test (ASTM C204/AASHTO T 153) is generally used to evaluate specific surface area (fineness) which indirectly measures cement particle surface area per unit mass. Slags typically have a surface area of between 450 to 550 m^2/kg in the United States [30]. The surface area of slag contributes to its reactivity because dissolution occurs only where the slag comes in contact with pore solution the surface. The finer the cement, the faster the reaction, the higher the heat of hydration (HOH), and the faster the concrete strength development. However, increased hydration rate can cause reduced bleeding, decreased workability, rapid shrinkage development and better early strength [45].

Slag fineness can greatly impact the material reaction rate and strength gain. Isothermal calorimetry has been extensively used to study the reaction rate and consequent strength gain rate of cementitious systems containing slag. Incorporating slag cement reduced the peak heat of hydration rate and increased the time to reach peak heat of hydration compared to ordinary portland cement, as shown in Figure 6 [29]. Furthermore, the peak heat evolution occurs later with decreasing fineness of slag. Concrete made with high fineness slag exhibits remarkable strength growth at an early age and can reach very high strengths at 28 days compared to concrete made with slag, as shown in Figure 7. These findings provide evidence that finer slag can help with early strength development [46].

9
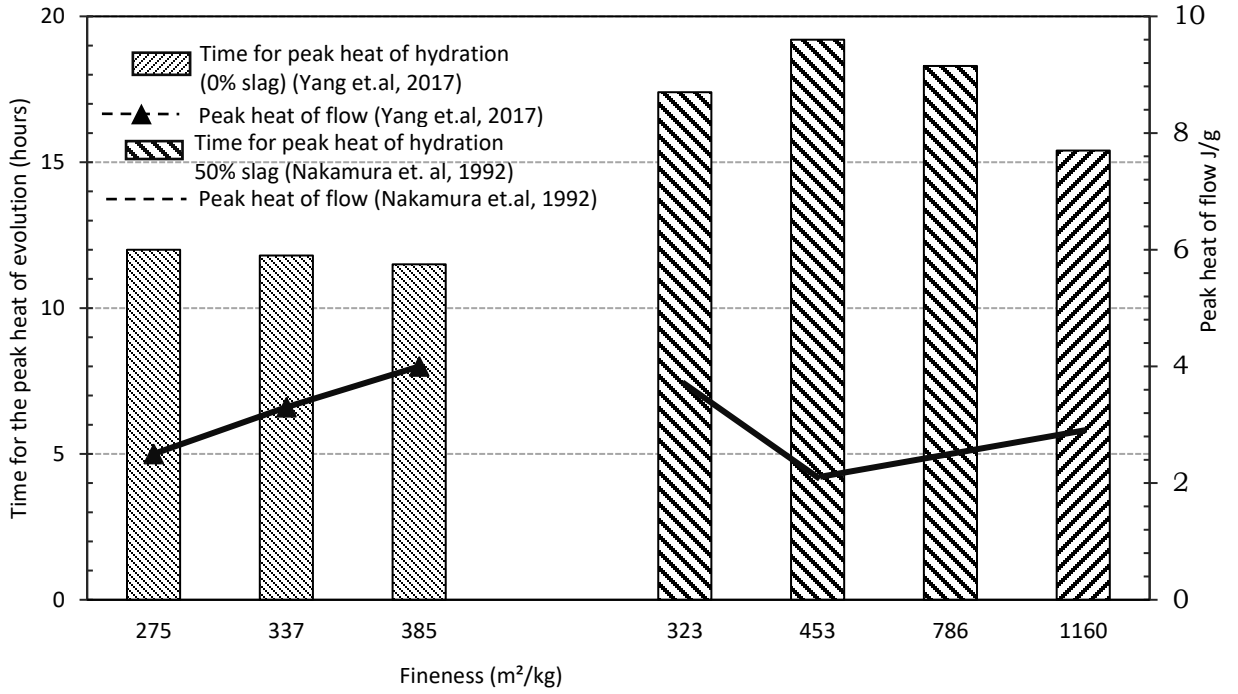
Figure 6: Effect of OPC and slag cement fineness on duration of peak heat of hydration and peak heat of flow [46], [47]
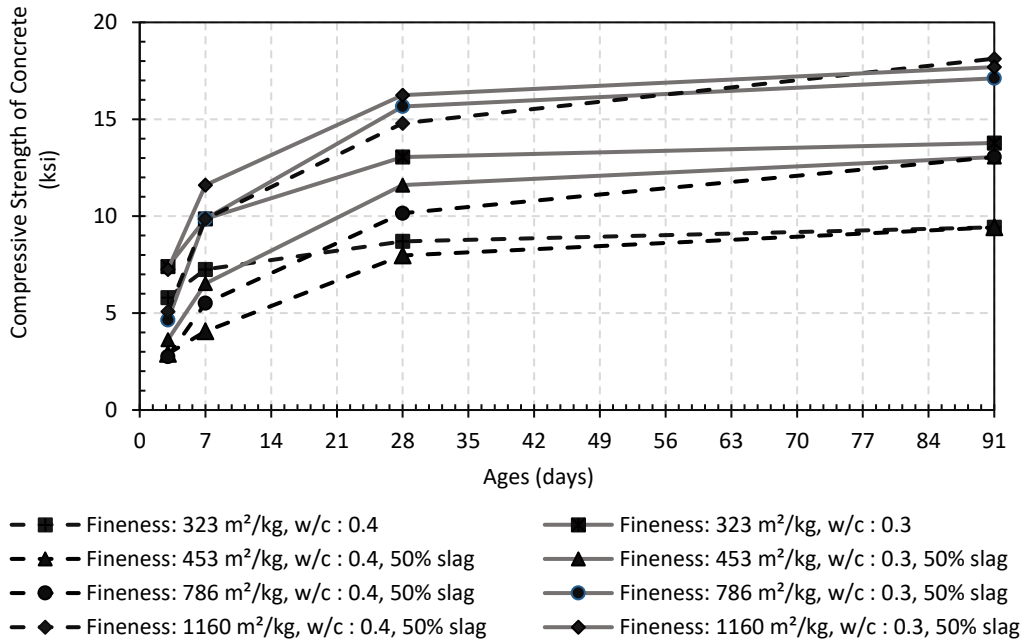
Figure 7: Effect of slag cement fineness on compressive strength of concrete [46]

2.4.3. Temperature Sensitivity

Concrete strength development is a function of the concrete temperature history. Concrete maturity is often used to quantify the effects of the curing history on strength. Concrete maturity assumes that two concrete with different temperature histories, but the same maturity, will have the same strength. Two maturity methods have been developed for this purpose. The Nurse-Saul method is the simpler method of the two and calculates the maturity as the integral of the time-temperature history of the concrete. The equivalent age method is commonly used for the assessment of strength gain because it takes into account the concrete curing temperature range, the precision of the prediction result, and the cement's chemical reaction rate as illustrated in Equation 2. This method is generally regarded as more accurate than the Nurse-Saul method, but more difficult to calculate [44].

$$k_T = A. \, exp^{\frac{E_a}{R.T}}$$ Equation 2

Where, k_T is reaction rate constant, A is proportionality constant, E_a is apparent activation energy (kJ/mol), R is 8.314 J/mol·K (gas constant), and T is absolute temperature (Kelvin). The equivalent age (t_e) can be calculated using Equation 3:

$$t_e = \int_0^t exp^{\frac{E_a}{R}(\frac{1}{T_r} - \frac{1}{T})} \, dt$$ Equation 3[29]

Where T is the average curing temperature of the concrete and T_r is the fixed temperature, i.e., 20^0C (293 K).

The apparent activation energy is used to measure the reaction temperature sensitivity. The activation energy follows the chemical reaction rate principles outlined by the Arrhenius law for a single chemical reaction. For cement, multiple chemical reactions occur simultaneously. A single coefficient called the apparent activation energy is used that gives the average sensitivity for the several hydration reactions occurring in the system. High activation energies are associated with higher substitution levels of slag cement [43]. Slag cement is far more temperature sensitive than portland cement when it comes to hydration. The strength of slag cement in concrete is greatly boosted at elevated early age temperatures [48].

ASTM C1074 is used to calculate the activation energy of cementitious material from mortar cubes. According to ASTM C1074-11, the activation energy is calculated from the slope of the relationship between the natural log of the compressive strength development rate at different tempreatures plotted against the reciprocal of the test absolute temperature [44]. Isothermal calorimetry performed at different temperatures is also used to calculate the apparent activation energy for mixtures containing slag [43], [49]. The apparent activation energy of slag cement is proportional to the cement substitution level by slag as illustrated in Figure 8. Slag cement has a greater activation energy (50-60 kJ/mol) than portland cement (30-40 kJ/mol) [50].

11
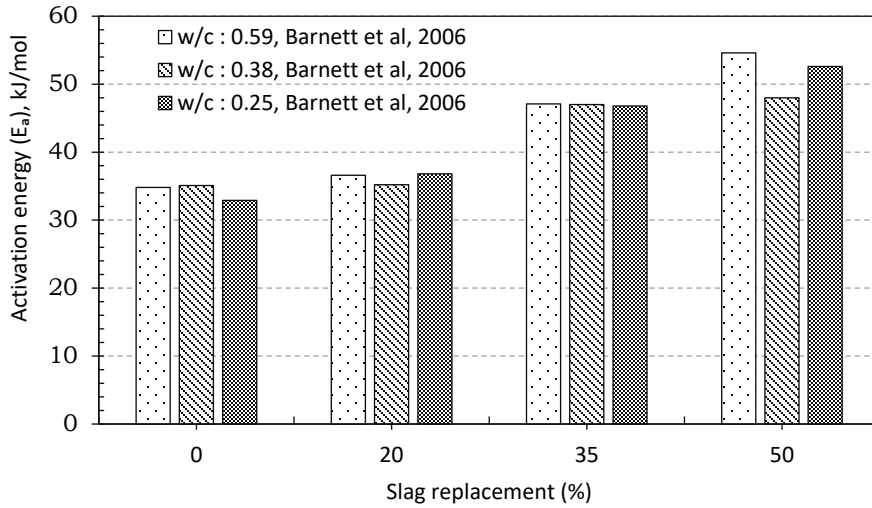
Figure 8: Activation energy with different slag replacement levels [48]

The increased activation energies manifest the higher temperature reactivity of slag cement concrete or mortar in strength development as demonstrated in Figure 9. As a result, curing concrete with slag cement at a high temperature is particularly beneficial in enhancing the strength at an early stage (Figure 9). Hence, slag cement is better suited to thermal treatment as a means of accelerating slag hydration [50]. Slag cement response to heat treatments may allow precast concrete producers to increase strength levels at early ages sufficient to detension prestressing steel before 24 hrs as required for daily member production.
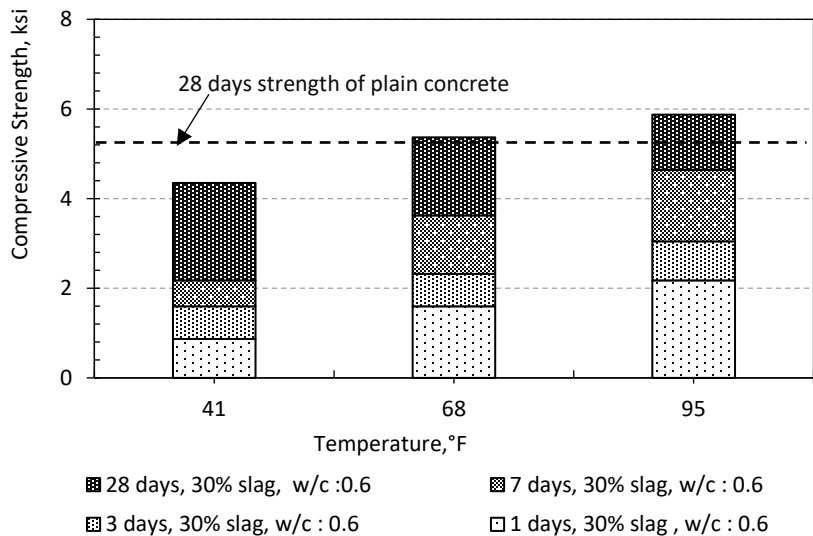
Figure 9: Temperature effect on slag cement mortar [44]

12

Two different methods have been developed to calculate apparent activation energy considering the type and percentage of substitution of supplementary cementitious materials (SCM) in the cementitious system. One is the Bogue calculation method as presented in Equation 4. This method says that a rise in C_3A and C_4AF or gypsum content in cement as calculated using the Bogue equations increases the activation energy. Whereas the other method of calculation uses the cement composition estimated from quantitavie X-ray diffraction, as shown in Equation 5. That method implies that an increment of the aluminate or total soluble sulphate content raises the apparent activation energy [51].

$$E_a = 41{,}230 + 1416{,}000\,[\,(C_3A + C_4AF)\cdot p_{cement} \cdot SO_3 \cdot p_{cement}] \qquad \text{Equation 4}$$
$$-347{,}000 \cdot Na_2O_{eq} - 19.8 \cdot Blaine +29{,}600 \cdot p_{fly\ ash} \cdot p_{CaO\text{-}fly\ ash}$$
$$+ 16{,}200 \cdot p_{GGBFS} - 51{,}600 \cdot p_{SF} - 3090{,}000 \cdot WRRET$$
$$- 345{,}000 \cdot ACCL$$

$$E_a = 39{,}200 + 1069{,}000\,[\,(C_3A)\cdot p_{cement} \cdot (CaSO_4 \cdot xH_2O + K_2SO_4) \qquad \text{Equation 5}$$
$$p_{cement}] - 12.2 \cdot Blaine +12{,}400 \cdot p_{fly\ ash} \cdot p_{CaO\text{-}fly\ ash} + 12{,}000 \cdot p_{GGBFS}$$
$$- 53{,}300 \cdot p_{SF} - 3020{,}000 \cdot WRRE - 343{,}000 \cdot ACCL$$

Where p_{cement} is the total cementitious content in the mixture (%); $p_{fly\ ash}$ is the fly ash mass to total cementitious content ratio; p_{GGBFS} is the slag mass to total cementitious content ratio; p_{SF} is the silica fume mass to total cementitious content ratio; $p_{CaO\text{-}fly\ ash}$ is the fly ash CaO mass to the total fly ash content ratio; Blaine is the Blaine fineness of cement; Na_2O_{eq} is the percentage of Na_2O_{eq} in the cement ($0.658 \times \%\ K_2O + \%\ Na_2O$); C_3A is the amount of C_3A in the cement (%); C_4AF is the amount of C_4AF in the cement (%); SO_3 is the amount of SO_3 in the cement (%); $WRRET$ is the ASTM Types A and D water reducer or retarder, percent solids per gram of cementitious material; $ACCL$ is the ASTM Type C calcium-nitrate-based accelerator, percent solids per gram of cementitious material $CaSO_4 \cdot xH_2O$ is the sum of the percentage by mass of gypsum, hemihydrate, and anhydrite; K_2SO_4 is the percentage by mass of arcanite; and C_3A is the aluminate in the cement (%).

2.4.4. Compressive Strength Gain with Temperature and Replacement Level

Slag cement has been successfully used for precast applications. The ability of slag cement to achieve early-age target strengths will depend on a number of factors. The Slag Cement Association states that "Without heat curing, early strength may be less than plain portland cement concrete members. Ultimate compressive strengths will be higher using slag cement. Engineering requirements and plant processes will influence mixture proportions [52]." For this reason, any discussion about concrete strength gain with slag cement must be coupled to a discussion about the temperatures used.

The slag cement replacement level, w/cm, curing temperature, evaluating period, and other factors can all influence the strength gain of slag cement containing concretes. At laboratory temperature, slag cement mortars or concretes achieve compressive strength slower than portland cement mortars or concrete during the initial stage of curing [48] as depicted in Figure 10.

13

However, after 28 days curing compressive strength of slag cement concrete surpasses the portland cement concrete (Figure 10). For precast applications that need early strength, the trend is clear. At laboratory temperature an increase in slag replacement level decreases 24 hrs strength, as shown in Table 2. The 1-day strength without heat curing or accelerators will almost always be lower slag cement than the control portland cement mixture. Whether a replacement level is acceptable for precast applications will depend on productivity requirements for strand detensioning, strand detensioning strength required, heat curing available, and accelerators used.
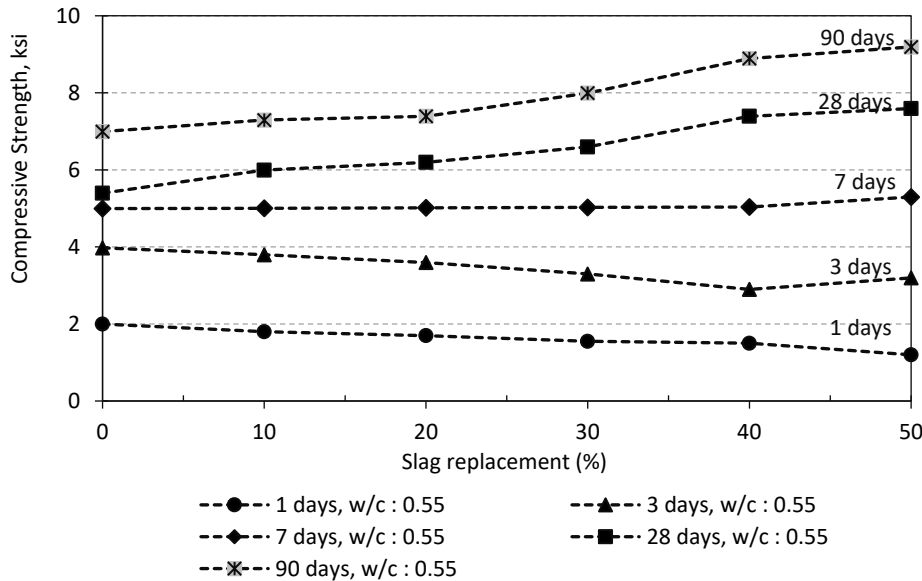
Figure 10: Compressive strength of mortar with different proportion of slag substitution [8]

Table 2: Mortar and concrete compressive strength measurements take from the literature with different slag cement replacement levels and curing temperatures

Slag Cement Replacement Level (≤50%)	Mixture Type	w/cm	Temp. (⁰F)	Compressive Strength (ksi) with Age (days)						Ref.
				1	3	7	28	56	90	
0%	Mortar	0.55	73	1.99	3.97	4.99	5.39		6.99	[8]
10%				1.80	3.80	5.00	5.99		7.29	
20%				1.70	3.60	5.02	6.19		7.39	
30%				1.55	3.30	5.03	6.60		7.99	
40%				1.50	2.90	5.04	7.39	-	8.89	
50%				1.20	3.20	5.30	7.59		9.19	
0%	Concrete			0.80	2.30	2.80	3.32		-	
40%				0.90	2.20	3.30	5.40		-	
50%				0.50	1.50	2.90	3.90		-	

14

%	Material	w/c	Temp							Ref
30%	Concrete	0.65	68	-	-	2.49	4.03	-	-	[53], [54]
		0.82		0.36	0.88	1.88	2.95	3.48		
50%	Concrete	0.40		-	-	3.77	6.10	-		
		0.61		0.70	1.60	2.93	5.08	5.98		
		0.61	133	1.45	3.48	6.53	7.98	-		
0%	Concrete	0.30	68	8.44	9.24	10.05	12.37		13.37	[50]
40%				5.29	6.65	8.48	11.80		12.96	
0%	Concrete		104	9.22	10.15	10.67	12.05		12.82	
40%				6.56	8.23	9.98	12.34		13.40	
0%	Concrete		140	9.23	10.47	11.05	11.48		12.41	
40%				8.02	9.15	10.79	12.35		13.51	
0%	Concrete	0.4	68	6.08	7.60	8.73	10.45		11.83	
40%				3.67	4.87	6.26	9.76		11.83	
0%	Concrete		104	6.54	8.00	9.06	9.79	-	10.90	
40%				4.42	6.05	7.70	10.37		10.79	
0%	Concrete		140	6.80	7.80	8.06	8.64		9.67	
40%				5.57	6.95	8.47	9.74		10.67	
0%	Concrete	0.5	68	2.42	5.21	6.90	8.71		9.56	
40%				1.68	3.25	4.96	8.50		9.31	
0%	Concrete		104	4.26	5.61	7.28	8.38		9.00	
40%				2.29	4.23	5.92	9.35		9.79	
0%	Concrete		140	4.54	5.39	6.70	7.71		8.18	
40%				2.74	4.52	6.16	8.28		8.95	
0%	Mortar		68	-	4.16	5.80	7.74	-	9.18	[24]
10%					3.48	4.71	7.42		9.14	
20%					2.68	3.94	7.25		9.11	
30%					2.15	2.90	7.09		9.00	
40%					1.45	2.09	6.82		8.90	
50%					1.33	1.74	6.53		8.70	
0%	Mortar	0.5	86		4.35	6.02	8.40		9.73	
10%					3.96	5.68	8.28		9.66	
20%					3.35	5.32	8.16		9.58	
30%					2.87	4.92	8.09		9.54	
40%					2.36	4.35	7.93		9.41	
50%					2.18	4.33	7.63		9.06	
0%	Mortar		122		5.08	6.22	8.70		10.15	
10%					4.63	6.12	8.66		10.12	
20%					4.18	6.06	8.56		10.02	
30%					3.63	5.97	8.48		9.96	
40%					2.90	6.02	8.27		9.86	
50%					2.78	5.80	7.98		9.74	
0%	Mortar	0.59	50	-	-	-	0.73	1.41	2.90	[48]
			86	-	-	0.87	2.54	2.90	3.77	

15

%	Material	w/c	Temp							Ref
			122	0.29	0.72	1.08	3.19	3.48	4.06	
35%			50	-	-	-	0.36	0.97	1.33	
			86	-	-	0.17	1.31	2.47	3.63	
			122	0.12	0.29	0.65	2.47	3.63	4.35	
0%			41	1.89	2.39	3.19	4.64	5.08	-	
			68	2.32	3.77	4.71	5.22	5.37	-	
			95	2.90	3.92	4.93	5.44	5.51	-	
10%			35	1.60	2.03	3.05	4.50	4.79	-	
	Mortar		68	2.18	2.90	3.92	5.08	5.66	-	
			95	2.90	3.48	4.93	5.37	5.80	-	
30%			41	1.89	2.39	3.19	5.08	4.64	-	
			68	2.32	3.77	4.71	5.37	5.8	-	
			95	2.90	3.92	4.93	5.51	-	-	
50			41	1.60	2.03	3.05	4.79	4.93	5.22	
		0.60	68	2.18	2.90	3.92	5.66	5.8	-	
			95	2.90	3.48	4.93	5.80	5.95	-	[44]
0			41		1.74	2.68	3.63			
			68		2.18	3.05	3.77			
			95		2.90	3.55	3.92			
10%			41		1.16	2.18	3.19			
			68		1.74	2.47	3.57			
	Concrete		95	-	2.47	2.97	3.70	-	-	
30%			41		0.70	1.45	2.90			
			68		1.38	2.18	3.63			
			95		2.18	2.90	3.77			
50%			41		0.36	0.87	2.39			
			68		0.87	1.67	3.26			
			95		1.67	2.54	3.63			

The impact of heat curing on concrete strength gain is often calculated using the maturity method. Concrete maturity methods assume that the concrete strength at the same maturity is equal, independent of the temperature history. This assumption works pretty well at early ages, however differences in long-term strength can occur depending on the concrete curing temperature [29]. There can be a decrease in the concrete ultimate strength owing to changes in hydration products formed at high temperatures. High early temperatures lead to increased early-age strengths over that of concrete cured at lower temperatures because of the faster chemical reaction rate [50]. Eventually, the concrete strength at the lower temperatures will overtake or cross-over that of the concrete cured at the higher temperature, as shown in Figure 11.
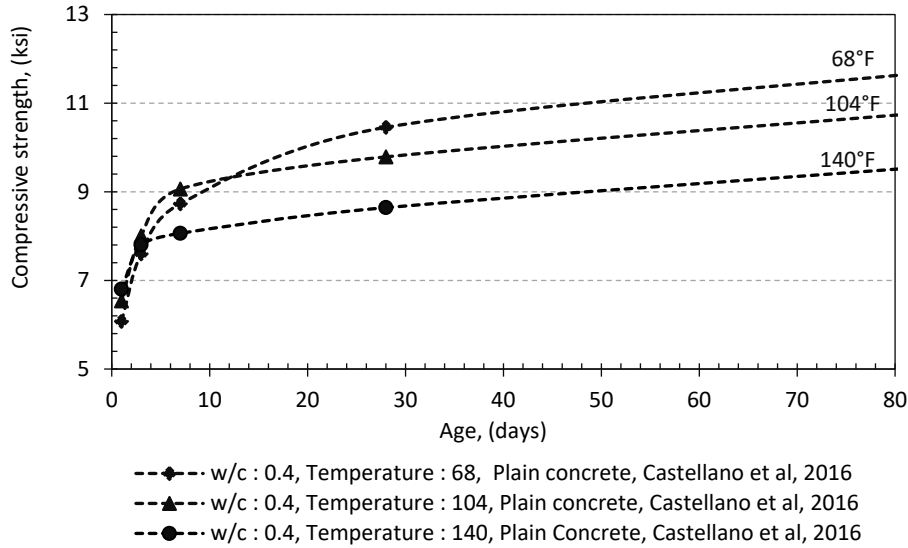
Figure 11: Cross over effect on plain concrete [50]

One theory has been that the hydration products do not have enough time to evenly disperse throughout the capillaries of the hardening paste at elevated temperatures and around the cement particles a less permeable hydrated layers form, preventing subsequent hydration. Large capillaries result from the less homogeneous dispersion of hydrates, lowering the ultimate strength. The faster rate of hydration caused by a rise in temperature, which improves the volume of hydrates and reduces the capillary pores of the matrix, is ascribed to the gain in early strength [55]. Other more recent studies have shown that the C-S-H that forms at high temperatures has less water in the structure and a higher density. Because hydration products provide strength by filling space with solid material, the higher the density, the lower the space filled by solids and the higher the pore volume. Concrete strength is an inverse function of the pore volume, giving lower strengths with high density C-S-H [56][50].

For portland cements, the crossover effect can arise as early as seven to ten days of age (Figure 11). The hydration reaction of slag cement concrete slows down when the slag replacement level is increased. As a result, the age at which the compressive strength crossover occurs is delayed (Figure 12) in comparison to portland cement concrete [57]. Moreover, when the curing temperature rises, the crossover effect occurs quickly as demonstrated in Figure 12 [44]. The crossover effect is less likely to happen when greater percentages of slag (>70%) are utilized as a supplement for portland cement in concretes or mortars [55].

17
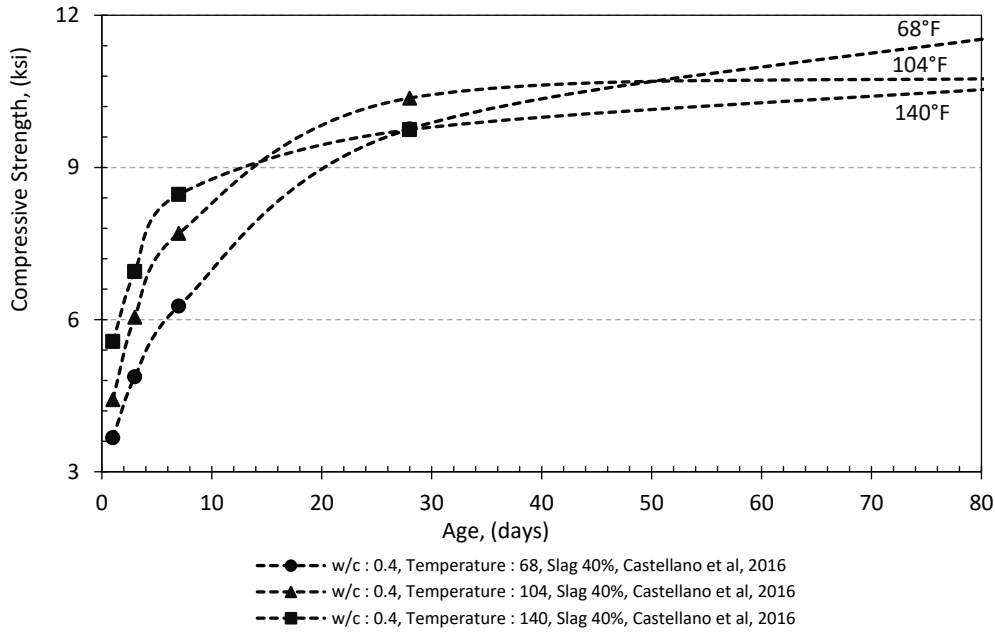
Figure 12: Cross over effect on slag cement concrete [50]

2.5. Durability

2.5.1.   Chloride Attack

Many concrete structure deterioration mechanisms occur because of fluid and ion transport inside the microstructure. Corrosion of steel reinforcement induced by chloride ingression is a major cause of structural degradation [58]. The main two parameters that control the transport mechanism of Cl- into the slag cement mixes are chloride diffusivity governed by the pore system and the ability to bind chlorides to keep them from penetrating further into the concrete [59]. Cement hydration and subsequent transport properties are mainly controlled by the w/cm and the usage of SCMs such as slag cement [60]. Slag cement has a long history of application in coastal structures to reduce permeability and improve durability. Concrete permeability decreases as the slag cement replacement level rises [29].

2.5.1.1.   Porosity

Concrete's diffusivity is influenced principally by its capillary porosity volume, pore size distribution, pore connectivity, and pore diffusivity [61]. Slag cement can in some cases lower total porosity, while in others even though the total porosity is not reduced significantly, slag cement hydration products can subdivide pores, reducing pore size and connectivity [18]. Making the pore network more tortuous inhibits water passage and increases the time needed for aggressive ions to penetrate in to cause cracking or to the reinforcing steel and cause corrosion. [39]. Figure 13 shows concrete water permeability and porosity measured for concrete made with different quantities of slag, illustrating the benefits of slag use in concrete on transport properties.

18
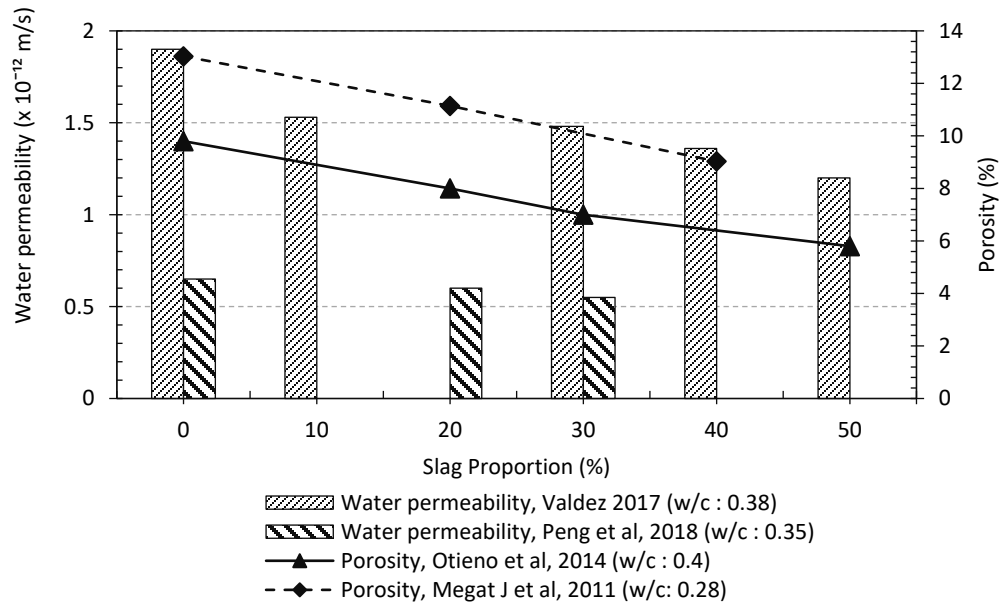
Figure 13: Effect on water permeability and porosity of concrete containing slag [23], [60], [62], [63]

Concrete pore size distribution has a large influence on the concrete transport properties. Micropores or pore volume and pore size distribution influence the penetrability of concrete. Concrete pores are split into two types namely, gel pores (<50 nm), and capillary pores (>50 nm) [23]. Mesopores and micropores (pores <50 nm) are found within the C-S-H gel. There are four categories of pore diameter in concrete: pores with <15 nm size that do not participate in ion transport, pores between 15-50 nm size that are not as detrimental to ion transport as larger pores, and pores >50 nm that principally determine the ion transport properties [64]. The secondary production of C-S-H gel by slag cement hydration reaction can improve the concrete microstructure, making it denser. These gels encapsulate and plug pores, resulting in decrease of capillary macropores (>50 nm) that can transmit water and chlorides. As the slag cement replacement level rises, the more capillary pores get filled with C-S-H with gel pores that do not participate significantly in water and ion transport [64][65]. Figure 14 shows the pore size distribution of cementitious systems containing slag, illustrating how slag decreases capillary porosity and increases the gel porosity as a percent of the total porosity [23].

19
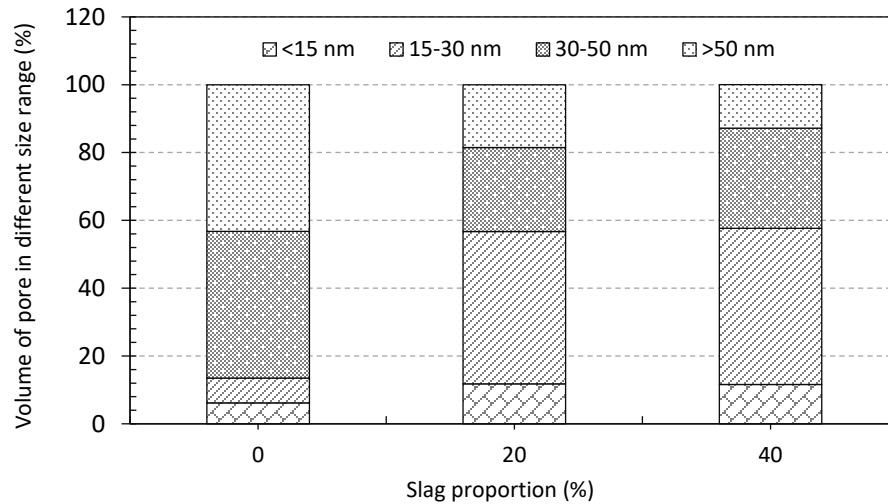
Figure 14: Concrete pore size distribution containing slag [23]

2.5.1.2. Chloride Diffusivity

Slag cement is very successful at reducing the chloride transport properties [66]. Figure 15 shows the chloride penetrability of concrete containing slag cement as measured by ASTM C1202 "Standard Test Method for Electrical Indication of Concrete's Ability to Resist Chloride Ion Penetration" [3]. As the slag replacement level increased, the chloride ion penetrability decreased. This formation of supplementary Ca-based hydration products (C-S-H and C-A-S-H) from the slag cement reaction is mostly responsible for the improved behavior [66]. Moreover, improved particle packing from the finer slag cement particles can better fill space and reduce the concrete permeability [67]. While the chloride penetrability measured in ASTM C1202 has been found to decrease when replacement levels up to 50% were used, they do not necessarily decrease further when replacement levels are increased above 70%. This may be because calcium exhaustion can be reached at really high replacement levels from cement dilution and pozzolanic reactivity. This can lead to increased porous microstructure and more interlinked apertures that would enhance ion diffusion [68].
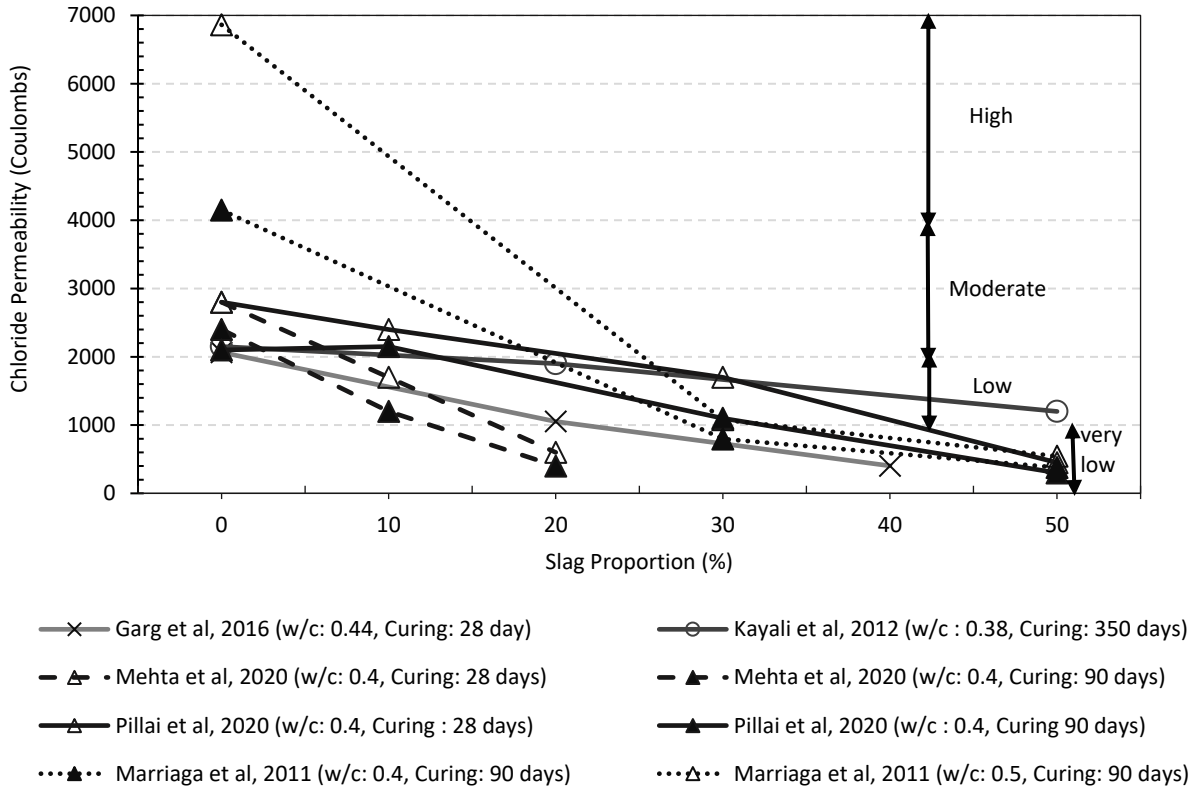
Figure 15: Concrete chloride permeability with slag addition [67]–[71]

Slag cement decreases the quantity of portlandite in the cement-aggregate interfacial transition zone (ITZ), reducing its average size and resulting in a denser interfacial transition zone (ITZ). According to the previous research findings, when the slag supplement level reaches 40% with a surface area surpass 425 m^2/kg, the poorly developed ITZ almost disappears. This could considerably reduce the penetrability of concrete and the risk of reinforcing steel corrosion [72].

In addition to slag cement replacement level, the concrete curing period helps determine how well it resists the passage of corrosive ions (Cl⁻ ions). Figure 16 shows that the concrete is more impervious to chloride mobility and dispersion when it is cured over a long period of time. This is because extended curing allows the portland cement and slag cement to achieve a higher degree of hydration and reduced porosity [73]. Even with lower curing, the effect of increased slag replacement level is evident [74], [75].

21
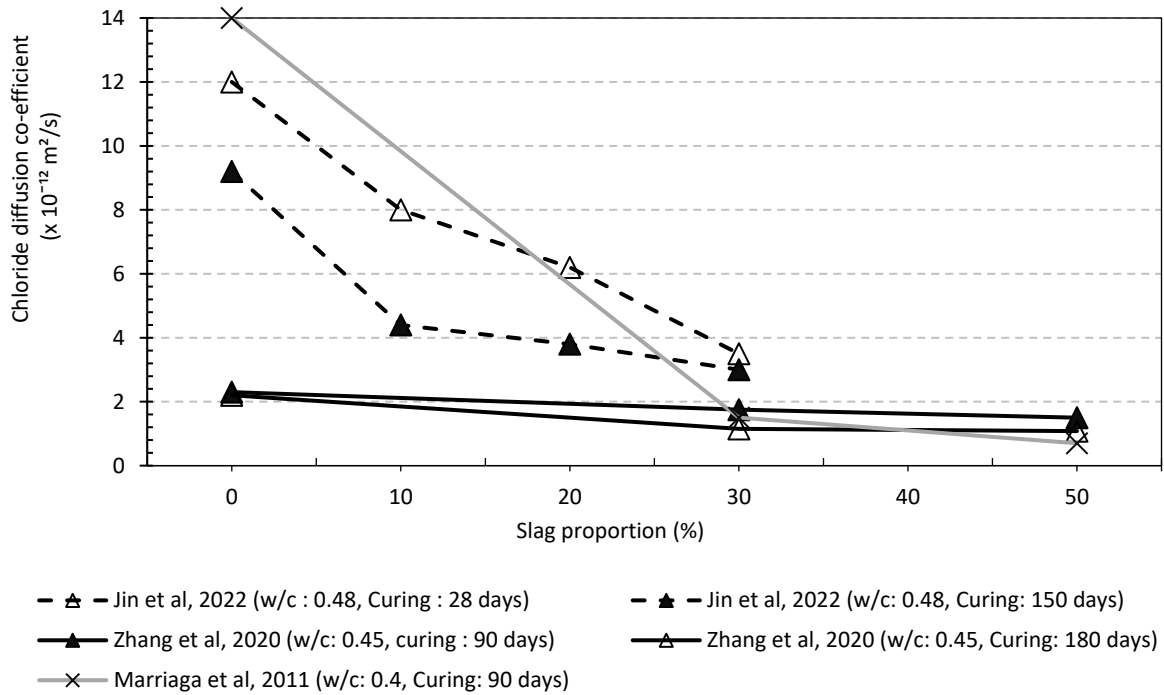
Figure 16: Chloride diffusion rate of concrete with different slag proportions [64], [71], [76]

2.5.1.3. Chloride Binding

One of the potential ways to reduce the chloride penetration rate is to raise the cementitious material's chloride bonding capability (CBC) [77]. Slag has a high chloride binding capability where free chloride ions that permeate the concrete pore spaces could be bound by the slag cement element, reducing their ability to migrate further into the concrete. The effects of slag chemical composition and replacement level are illustrated in Figure 17 and Figure 18. Al_2O_3 is a catalyst for chloride bonding, with a greater Al_2O_3 percentage promoting increased chloride binding capacity [78]. Some of the increased chloride penetration resistance can be attributed to the ability of hydrated elements to obstruct the probable passageways for corrosive ion mobility [79]. Alumina in the slag cement can react with chloride ions to form AFm phases, effectively immobilizing them and preventing them from penetrating deeper into the concrete [71]. C-S-H can also impede diffusion and trap additional chloride ions [80]. Only unbound chlorides in sufficiently high quantities can cause reinforcement deterioration, making chloride binding in addition to low porosity helpful in increasing the concrete service life [81]–[83].

22
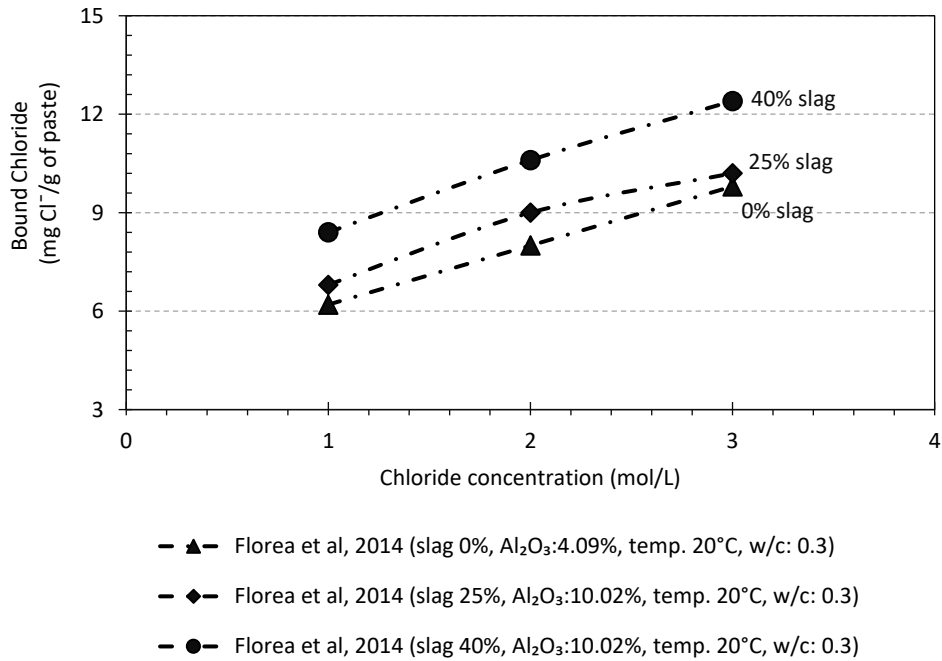
Figure 17: Bound chloride of concrete mixed with different proportion of slag [84]
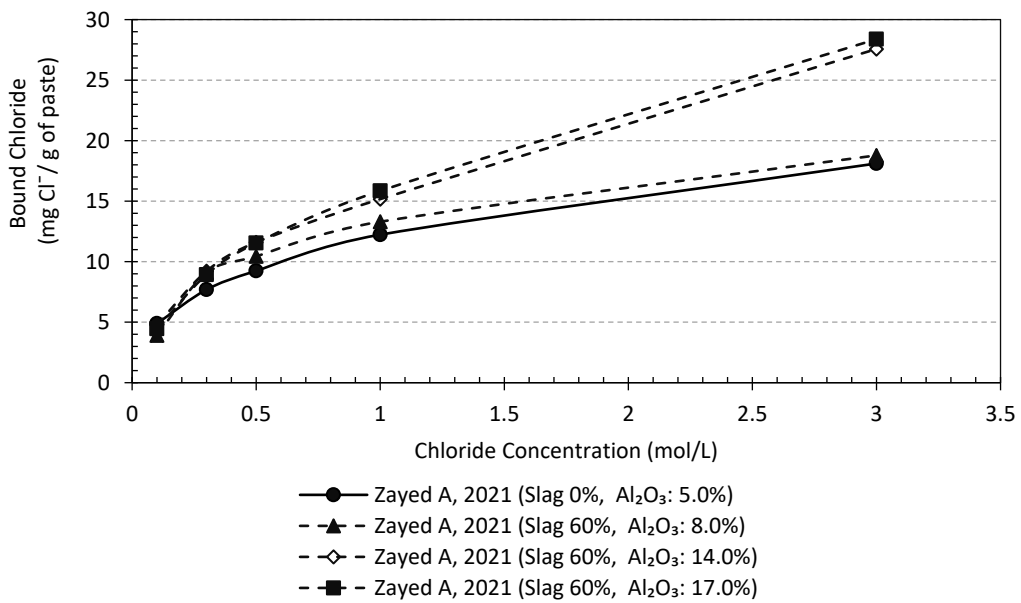
Figure 18: Bound chloride of concrete mixed with different amounts of Al_2O_3 [85]

23

During cement and slag hydration, alumina-bearing compounds form that can react with chlorides chemically to bind them (Figure 18) [86]. The incorporation of low slag content (20%) with greater alumina (>13%) content enhances the aluminate concentration of the hydrates, allowing more Cl^- ions to be bound. Moreover, Ca/Si proportion affects the physical adsorption of Cl^- ion bonding in C-S-H with a smaller ratio giving less binding. Slag cement brings down the Ca/Si percentage of the calcium silicate hydrate (C-S-H), although it contains more alumina (Al_2O_3). This increases the production of calcium alumina silicate hydrate (C-A-S-H) to increase chloride binding [87]. Slag cement and portlandite undergo a pozzolanic interaction, which results in the solubility of a greater number of aluminate molecules. Aluminate ions interact with sulfates, carbonates or other functional molecules to form aluminate ferrite monosulfate (AFm) phases such as calcium sulfoaluminate (SO_4-AFm) or calcium carboaluminate (CO_3-AFm). In specific circumstances such as with the outlay of Ca-ions, AFm phases can uptake chloride ions by swapping sulfates or carbon dioxide for chlorides to form Friedel's salts, [88], [89]. The interchange of ions between chloride ions and AF_m phases in the presence of calcium ions that lead to the formation of Freidel's salt are described in Equation 6 and Equation 7 [90], [91]. In addition, Kuzel's salt can also be formed through the replacement of sulphate in monosulfate by a Cl^- ion. Based on kinetic explanations, Kuzel's salt (KS) formation is a middle stage from monosulfate to Friedel's salt (FS) [92]. In the initial stage with low concentration of Cl^-, the sulfates in monosulfate (SO_4-AFm) can be substituted by chloride ions to form KS as presented in Equation 8. The liberated sulfates have high propensity to react with SO_4-AFm to produce ettringite (Equation 8). Moreover, when a significant amount of Cl^- are in pore solution, KS subsequently changes to FS as shown in Equation 9 [92], [93].

$$C_4A\mathbb{C}H_{11} + 2Cl^- + C \rightarrow C_4ACl_2H_{10} + C\mathbb{C} + H \hspace{2cm} \text{Equation 6}$$
$$C_4A\$H_{12} + 2Cl^- + C \rightarrow C_4ACl_2H_{10} + G \hspace{2cm} \text{Equation 7}$$
$$1.25C_4A\$H_{12} + Cl^- + 0.5CH + 5H \rightarrow C_4A\$_{0.5}ClH_{12} + 0.25C_6A\$_3H_{32} + H \hspace{1cm} \text{Equation 8}$$
$$0.25C_4A\$H_{12} + C_4A\$_{0.5}ClH_{12} + Cl^- + 0.5CH + 3H \hspace{2cm} \text{Equation 9}$$
$$\rightarrow C_4ACl_2H_{10} + 0.25C_6A\$_3H_{32} + H$$
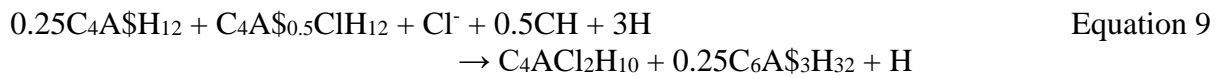
C-S-H gel can tie up chloride ions through physical adsorption. The higher the C-S-H gel from pozzolanic activity, the greater the physisorption of chlorides. The Ca/Si ratio in the C-S-H affects the physical adsorption of Cl^- ions. As the Ca/Si ratio decreases, chloride physisorption decreases [94], [95]. Slag cement decreases the Ca/Si percentage of the calcium silicate hydrate (C-S-H), although it contains more alumina (Al_2O_3). Formation of C-A-S-H helps offset this and provides for increased chloride bonding [96]. The electrical double layer (EDL) concept helps explain the physisorption of chlorides and the role of alumina in the C-A-S-H in the process. The potential of calcium silicate hydrate (C-S-H) might be positive (+), balanced, or negative (-), depending on the CaO/SiO_2 or C/S ratio [94], [95]. Abundant Ca inside the intermediate layer can switch the charge neutrality of calcium silicate hydrate (C-S-H) from minus to positive because of a rise in C/S ratio. The overall charge turns "+" above a threshold CaO/SiO_2 ratio, and as a result, chloride is entrapped to balance out the total positive electrical charge created by surplus calcium, when calcium silicate hydrate (C-S-H) comes into contact with Cl^- ions. On the contrary, calcium adsorption is accelerated by AlO_2^- on the negatively loaded calcium alumina silicate hydrate (C-A-S-H) interfacial configurations and the resulting C-A-S-H becomes positively loaded. As illustrated in Figure 19, this positively packed interface of C-A-S-H is

24

counterbalanced by the Cl⁻ in the interfacial region of the calcium alumina silicate hydrate when it is interacted with Cl⁻ ions. As a result, calcium alumina silicate hydrate (C-A-S-H) has a larger chloride physical adsorption capability than calcium silicate hydrate (C-S-H) [96].
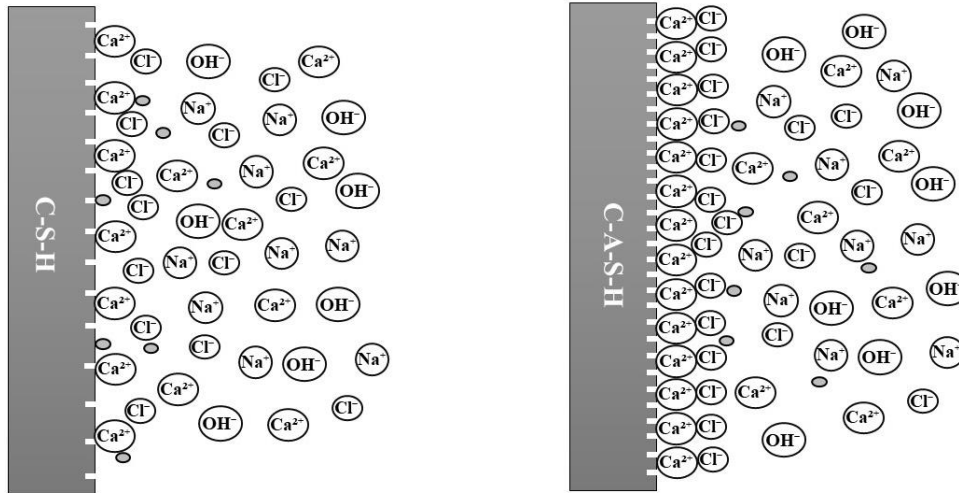
Figure 19: Chloride ion adsorption model on the C-S-H and C-A-S-H surface, after [96]

Other factors such as external sulphate ions have been shown to inhibit chloride binding or free previously bonded chlorides [97]. Apart from the external sulphate ions, slag proportions, slag chemical characteristics, temperature, and quantities of striking unbound chlorides all have a significant impact on the cement hydration phase and chloride solubility [98]. The amount of bound chlorides are increased at elevated temperatures as demonstrated in Figure 20 [99]. This can be attributed to the greater level of hydration during curing at elevated temperatures of slag cement concrete [100]. At both low and high temperatures, high alumina slag cement bound more chlorides than less alumina-rich slag cement [98]. In general, mixed solutions such as sodium chloride and sodium sulfate have lower chloride binding tendency than pure sodium chloride [101] [102]. Figure 20 depicts the influence of external sulfate. When the unbound chloride content is below 1.0 mol/l, the inclusion of sulphates gives a minuscule reduction in chloride binding. Sulphate predominantly reacts with tricalcium aluminate ($3CaO. Al_2O_3$) and tetracalcium aluminoferrite ($4CaO.Al_2O_3.Fe_2O_3$) or their hydration products to generate ettringite. This increase in preference for ettringite formation reduces slightly the amount of chlorides from becoming bound in Friedel's salt (FS) or Kuzel's salt (KS).
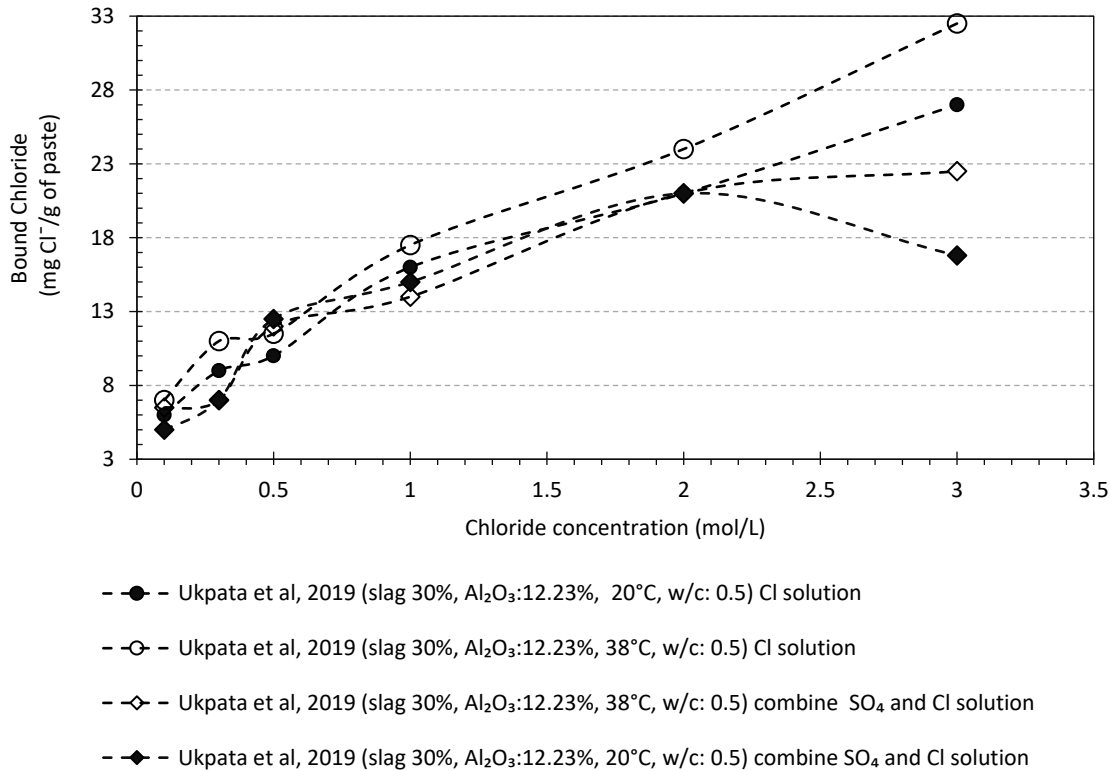
Figure 20: Chloride binding of slag cement concrete with combine chloride and sulfate solutions [98]

2.5.2. Sulfate Attack

Concrete's resistance to the diffusion of deleterious ions through its pores helps ensure its durability. Concrete durability degrades due to sulfate attack. Sulfate attack is a complicated process that comprises physical salt attack carried on by salt crystallization and chemical sulfate attack caused by sulfates in the groundwater, seawater, or soil [35] . The production of substances like ettringite, gypsum, and thaumasite in concrete caused by groundwater and seawater carrying sulfate chemicals that are transferred through the concrete pores has been recognized to promote concrete degradation [103]. The concrete may expand, crack, lose strength, and disintegrate as a result of sulfate attack.

2.5.2.1. External Sulfate Attack

Sulfate salts can damage concrete composites and are typically often found in soil, in freshwater, seawater, agrarian and manufacturing pollutants, and with residential effluents [104]. Sulfate attack occurs when sulfate ions enter the concrete microstructure with water and react chemically with cement hydration products, especially those from the aluminate reactions [105]. Because of these chemical reactions, the cement C_3A concentration is often associated with the cement's sulfate resistance. In more recent years, the C_4AF phase has been identified as a contributor to

26

sulfate attack. Besides reducing the aluminate phases in the cement, lowering the w/cm can improve sulfate durability by minimizing the entrance and mobility of soluble SO_4^{2-} ions. The severity of the sulfate attack is influenced by a variety of factors, including soil moisture, water flow, air temperature and relative humidity, sulfate intensity, and the sulfate salt cations present [18].

Sulfate ions that penetrate into the concrete lead to the formation of ettringite (AFt) and gypsum [106]. During portland cement hydration at early ages, ettringite will form from the reaction of C_3A, as shown in Equation 10. After the sulfate in the cement is exhausted, any additional C_3A will react with ettringite to form monosulfoaluminate, as shown in Equation 11. If there are carbonates in the system from limestone fines, the C_3A can react with the carbonates to form monocarboaluminate instead of sulfate-bearing AFm phases, as shown in Equation 12. This leaves more sulfate available to form ettringite instead of forming monosulfoaluminate, stabilizing early-age ettringite formation. After the concrete has hardened, when sulfate enters the concrete, it can react with the monosulfoalumiante to revert back to ettringite, as shown in Equation 13 [16].

$$C_3A + 2C + 2\$^- + 26H \rightarrow C_6A\$_3H_{32} \text{ (ettringite)}$$

Equation 10

$$2C_3A + C_6A\$_3H_{32} + 4H \rightarrow C_4A\$H_{12} \text{ (monosulfoaluminate)}$$

Equation 11

$$C_3A + 0.5C\mathbb{C} + 0.5CH + 12H \rightarrow C_4A\mathbb{C}_{0.5}H_{12} \text{ (monocarboaluminate)}$$

Equation 12

$$C_4A\$H_{12} + 2C + 2\$ + 20H \rightarrow C_6A\$H_{32} \text{ (ettringite)}$$

Equation 13
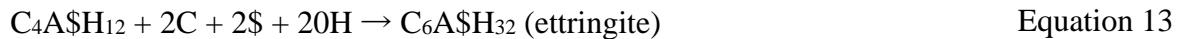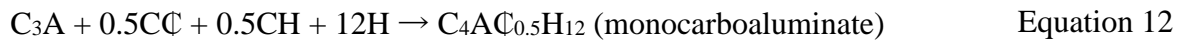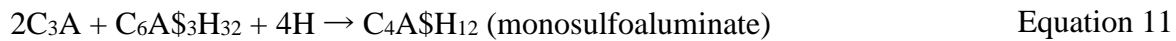
Concrete is deteriorated in two ways by outer sulfate exposure. In mature concrete, structural swelling and fracturing are caused by ettringite formation. Ettringite and gypsum cause pressure on the interior pore walls, causing crack formation owing to pore dilation. Stresses (tensile) are produced by crystal growth when the size of the crystalline matrix in the solidified concrete mixture increases, and once the paste's specific tensile capacity is surpassed, microcracks appear [107]. Weakening and breakdown of cohesiveness are additional damage mechanisms linked to sulfate intrusion from external source [108].

The sulfate salt cation influences the deterioration caused by sulfate attack. Calcium sulfate has a fairly low solubility, limiting the amount of sulfate that will enter the concrete. Calcium sulfate typically causes less damage than the other sulfate salts. Magnesium sulfate will react chemically with the C-S-H, causing strength loss. Sodium sulfate follows the chemical reactions described previously but will also cause physical salt attack [109]. In case of magnesium sulfate, both magnesium and sulfate ions are engaged in the sulfate attack mechanism [110]. The formation of brucite ($Mg(OH)_2$) results from the magnesium ion's reaction with calcium hydroxide or C-S-H. This drops the concrete pores fluid's pH and gives a supply of calcium that can combine with sulfate to form gypsum. The interactions continue until the paste is depleted of calcium hydroxide and calcium silicate hydrates. Ultimately, the degradation action linked to magnesium sulfate ($MgSO_4$) ingress is breakdown of cohesiveness, making it a particularly destructive form of attack [110].

27

Sodium sulfate (Na_2SO_4) is the most prevalent sulfate agent that causes degradation owing to physical salt intrusion. Besides damage from the chemical reactions between the sulfate ions and the cement hydration products, damage can occur from phase change of the sodium sulfate in the concrete pores [111]. Capillary rise and evaporation at the surface may induce salts near the concrete surface to become supersaturated and crystallize. This tends to occur where concrete elements are built near salty groundwater or the sea, causing sulfates to chemically and physically damage concrete. Thenardite, the anhydrous form of sodium sulfate, forms in the pores of the concrete under hot and dry conditions. When the temperature decreases sufficiently and/or relative humidity increases, the thenardite can change phase to mirabilite, the hydrated version of sodium sulfate. Mirabilite formation is accompanied by a volume increase, causing pressure on the pores, cracking, and scaling. This phase change can occur at typical diurnal temperature and humidity changes.

When concrete infrastructures are submerged in sea water, the parts over the brine are typically the most damaged, while the parts completely submerged are significantly less damaged [112]. However, the degree and form of the chemical activity are changed by the existence of chloride ions, resulting in reduced damage. It can be attributed to the fact that chloride ions have the propensity to combine with aluminates in cement to generate calcium chloroaluminates (Friedel's salt). Development of calcium chloroaluminates reduces the amount of monosulfoaluminate in the system, consequently diminishing degradation by sulfate intrusion [108]. Brucite (MH) formation in the pores may block sulfates from entering cementitious pore spaces [110]. In addition, thaumasite production is possible in concrete if there is a supply of highly solvable limestone ($CaCO_3$) and sulfate as shown in [103].

$$CaCO_3 + CaSO_4 + C\text{-}S\text{-}H + H_2O \rightarrow CaCO_3.CaSO_4. CaSiO_3.15H_2O \qquad \text{Equation 14}$$

In disintegrating concrete, ettringite and thaumasite are usually observed simultaneously [18]. Use of sulfate-resisting concrete does not necessarily stop the growth of thaumasite as it can form without aluminates present. Once thaumasite has formed, the concrete matrix turns into a white cohesionless mass, eliminating any load-bearing properties of the concrete [111]. Similar to ettringite, thaumasite can form in crevices and fissures with no overt indications of sulfate attack. Temperatures under 59°F (15°C) are ideal for the formation of thaumasite. In addition, the rate of formation is slower when it occurs at temperatures as high as 77°F (25°C) [103].

2.5.2.2.   Internal Sulfate Attack

Delayed ettringite formation (DEF) is another type of sulfate attack that can occur when the concrete has been subjected to high temperatures, typically during curing. Formation of ettringite after the concrete has hardened does not need sulfate from an outside origin. When concrete is exposed to high heat during production, the typical early development of ettringite that happens in concrete at room temperature does not occur because ettringite is soluble at high temperatures [113]. Weakly crystallized monosulfate is the predominant sulfate component not in solution. The soluble sulfates that at cooler temperatures would form ettringite get trapped by C-S-H. As the concrete cools and is exposed to moisture in operation, the majority of the sulfate and a

28

minor quantity of the alumina is liberated by the C-S-H [112]. The sulfate is released from the C-S-H into the pore solution. Because of the widening of ettringite crystallites in the microscopic pores of about 100 nm, this late ettringite production may in some cases cause the concrete mixture to dilate, causing the development of voids surrounding agglomerates and fracturing of the cement matrix [108][18]. Heat-cured precast structures are not the only things at danger from DEF deterioration. Owing to the heat emitted in the hydration reactivity of the concrete mixture, inner concrete temperatures may rise enough in mass concrete to encourage DEF [113].

DEF-related enlargement is unlikely to be the case except if cement mortar or concrete samples are heated to temperatures over 158°F (70°C). Some experts suggest that the highest vulnerability to DEF is in cements with high fineness that are made with high amounts of C_3A, and Na_2O, consequently containing a substantial amount of SO_3 [113]. The probability of concrete expansion is often smaller for concrete with low strength enhancement at initial stage. The concrete temperature should be maintained so that it never exceeds 70°C in order to reduce the possibility of deterioration caused by detrimental DEF [18].

2.5.2.3.   Slag Effect on Sulfate Attack Durability

Sulfate durability can be improved by increasing the chemical stability of the hydration products in the presence of sulfate ions and reducing the concrete penetrability to prevent sulfate ions from entering the concrete. Based on this information, sulfate-resistant cements and mix compositions for concrete mixtures to be employed in sulfate-laden conditions have been developed [114]. Slag cement can significantly reduce sulfate attack damage when used in sufficient quantities and low w/cm [115].

Slag cement exhibits a good pozzolanic response, binding portlandite to interact with sulfate and lowering gypsum levels. Slag can effectively lessen the dilation brought on by sulfate exposure. Replacing cement with slag cement enhances concrete efficiency in sulfate environments by in some cases lowering the cement's aluminates composition, consuming calcium hydroxide in the slag cement hydration, and minimizing penetrability [116]. With the inclusion of relatively low-Al_2O_3 slag, sulfate tolerance for slag cement is significantly boosted. Moreover, the development of monosulfoaluminate phase from the hydration of high Al_2O_3 slag cement suggests that these combinations may be less durable owing to the transformation to secondary ettringite upon sulfate invasion unless additional measures are taken [1].

Addition of calcium sulfate and optionally limestone fines to the slag cement can improve significantly the performance of high alumina slags in sulfate attack as demonstrated in Figure 21, although high replacements levels may be needed [16], [105]. High alumina slags can change the sulfate balance in the system, resulting in more monosulfoaluminate produced instead of ettringite. Addition of calcium sulfate to the slag can balance the sulfate levels in the system to produce more ettringite instead of monosulfoaluminate, giving better performance in sulfate environments. The inclusion of limestone to the slag concrete specimens makes them much more durable to sulfate degradation than concretes specimens without limestone because the formation of carboaluminate phases stabilizes ettringite formation and reduces monosulfoaluminate content [16]. However, the overabundance of $CaCO_3$ powder has no beneficial effect on sulfate

29

protection. An earlier study found that introducing 7% of $CaCO_3$ to the concrete mixture diminished the pore size and improved sulfate attach performance, but adding 25% of calcium carbonate enhanced pore size and lessened sulfate tolerance. The hydraulic conductivity of a concrete or cement mixture has a significant impact on its ability to thwart sulfate damage [116]. By incorporating slag cement, the mixture's penetrability is diminished, and the passage of the sulfates is blocked by the production of C-S-H in porous medium [117].
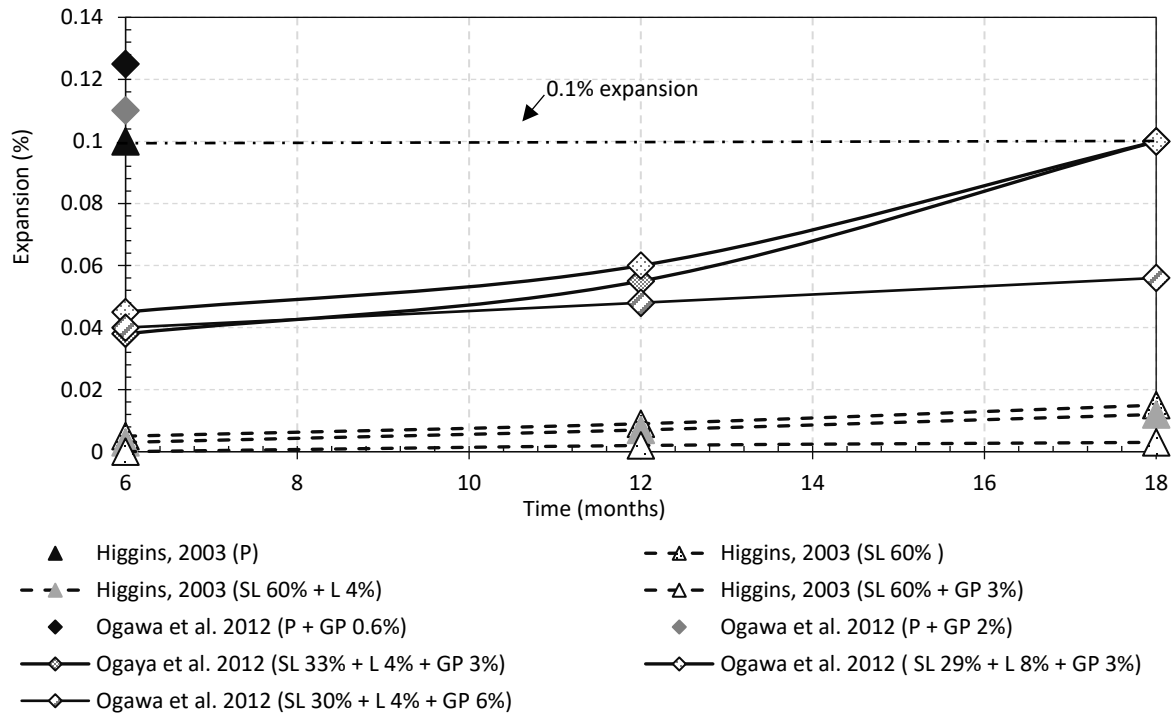
*P= plain concrete, SL= slag, GP= gypsum, L= limestone

Figure 21: Concrete expansion due to sulfate attack with the addition of slag cement, limestone and gypsum [16], [118]

Figure 22 clearly depicts that the sulfate resistance of concrete is enhanced by partially substituting slag cement for portland cement. Greater impedance of sulfate ingress usually can be found when the slag cement supplement surpasses 50% of the total cementitious materials [119]. When slag cement is utilized with portland cement that has a C_3A composition of up to 12%, the threshold proportion of slag cement would be $\geq$ 50% if the slag cement alumina level is less than 11%. Slag substitutions of 60-70% can be necessary whenever the slag cement has an alumina composition over 11% [18]. This high of a replacement level can be helpful because in large amounts the C-S-H gel bonds with the alumina component to form C-A-S-H with a smaller CaO/SiO_2 ratio [120].

30
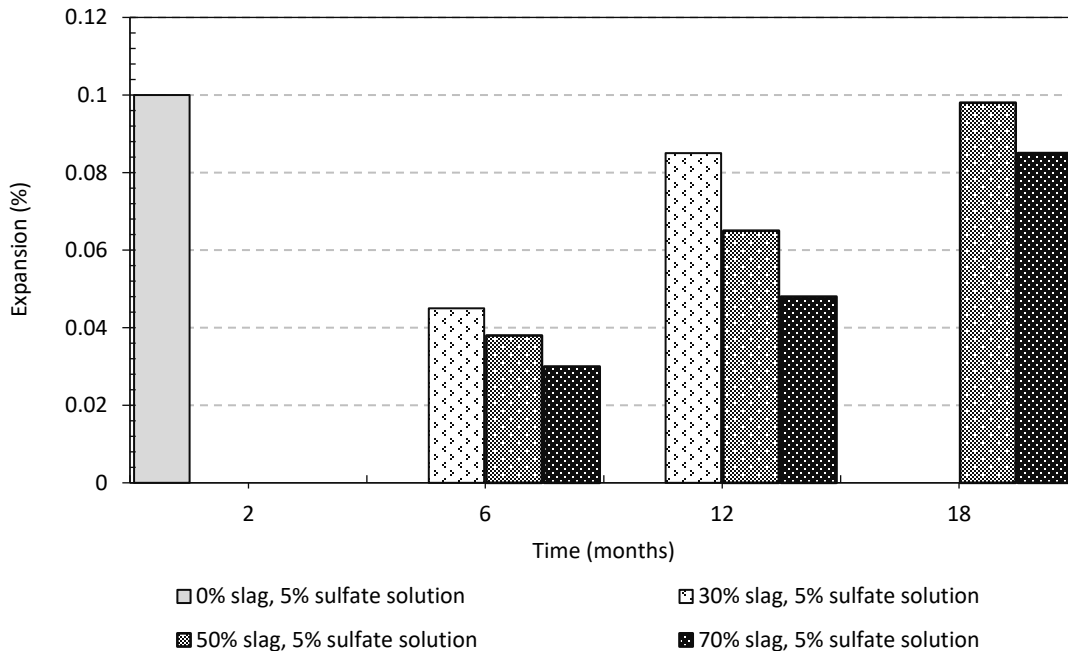
Figure 22: Sulfate expansion of concrete with different proportion of slag cement [121]

Slag cement with high Mg contents may assist in augmenting the sulfate resistivity and tying Al up to form hydrotalcite (Ht) [122]. This curtails the quantity of reactive aluminum that could interact with sulfates directly. According to previous studies, the hydrates of the alumina that is coupled to C-S-H and the hydrotalcite (Ht) are solidly connected, which reduces ettringite content [122], [123].

Slag cement seems to help concrete resist against thaumasite sulfate degradation. This can be ascribed to the reduction of calcium hydroxide content in the cementitious matrix from the addition of slag cement [8]. In addition to the slag proportion, w/cm ratio has a great influence on the sulfate penetrability. An increase in the w/cm leads to an increase in susceptibility to sulfate damage [115]. This is due to the fact that mortar gets weaker and more porous as the w/cm rises, which opens up more passageways for sulfate ion transportation. Consequently, higher production of expansive products (secondary ettringite and gypsum) to facilitate sulfate damage occurs [15]. Giving slag cement more time to cure or by exposing it to higher temperatures to increase degree of hydration can decrease sulphate degradation. In addition, slag cement shows smaller resistance to magnesium sulfate solution compared to sodium sulfate solution [124]. This can be ascribed to the fact sodium does not react with the same hydration products magnesium reacts with. The effect of magnesium substituting for calcium to generate M-S-H is primarily responsible for the durability impairment that can be observed in the samples that are exposed to magnesium sulfate rich solutions [125]. On the other hand, when subjected to sodium sulfate waters, the C-S-H composition of the cementitious matrix is mostly unaltered with only a little amount of deleterious ettringite and gypsum precipitating [126].

31

2.6. Summary

Concrete compressive strength and durability is enhanced by incorporating slag cement as a partial substitution of portland cement in concrete. While slag cement provides high later age strengths, strengths at one day needed for precast concrete manufacturing decrease as the slag replacement level increases. Early-age strengths are particularly low at replacement levels above 50%. Generally, the strength of slag cement concrete is substantially enhanced by high temperatures at early age because slag cement is much more temperature sensitive than portland cement. Slag cement significantly improves concrete durability, with replacement levels above 50% especially providing high durability against chloride ingress. The slag chemical compositions, however, have quite an impact on how much sulfate attack durability have improved. Adding slag with an alumina content > 11% at a cement replacement level >50% boosts the sulfate durability of concrete if it is properly sulfated. Concrete made with slag at cement replacement levels below 50% may still provide acceptable performance if used at a low w/cm.

3. MATERIAL CHARACTERIZATIONS

3.1. Background

The objective of this current study is to determine the durability and strength of concrete containing less than 50% slag cement. Recommendations will be made on minimum slag cement replacement levels required to give equivalent sulfate and chloride durability as concrete made with 20% class F fly ash and still meet early-age strength requirements for precast concrete construction. In order to achieve these objectives, concrete constituent materials were acquired and characterized. A local natural sand and an ASTM C33 [127] #67 coarse aggregate were acquired for this work. An ASTM C595 [4] Type IL cement, an ASTM C618 [2] class F fly ash, an ASTM C1240 [6] silica fume, and three ASTM C989[5] slag cements were obtained from three different sources. Slag cement concrete durability performance is affected by Al_2O_3 content in cement and slag chemical composition [1]. Therefore, slag cement Al_2O_3 was chosen as a variable in this study. Cement-slag blends with low-alumina slags (Al_2O_3 <11%) are expected to have improved sulfate durability, while those with high-alumina slags (Al_2O_3 >18%) are expected to be less effective in mitigating sulfate durability [85]. In this study, slag cement with Al_2O_3 contents of 8.8%, 13.4%, and 17.6% were selected. Furthermore, the amount of silica fume required to provide reliable early-age strength as well as resistance to chloride and sulfate attack will be determined by preparing ternary blends containing different proportions of slag and silica fume. Concrete constituent materials were characterized for use in this study. The aggregate gradation (sieve analysis), bulk specific gravity (SSD), and absorption capacity (AC) were measured for both aggregates. The dry rodded unit weight of coarse aggregate (DRUW) was measured for the coarse aggregate according to ASTM C29[128]. Cementitious materials were characterized using x-ray fluorescence (XRF), X-ray diffraction (XRD) coupled with Rietveld refinement, gas pycnometry for density, laser particle size distribution (PSD), and thermogravimetric analysis (TGA).

3.2. Aggregate Characterization

Prior to performing sand characterization tests, fine aggregate samples were obtained in accordance with ASTM D75 [129]. To measure the aggregate particle size distribution according to ASTM C136 [130], the aggregates were first dried at $110 \pm 5°C$. They were then sieved using a mechanical sieve shaker, with the amount of material retained on each sieve weighed. Figure 23 shows the coarse and fine aggregate measured particle size distributions. The fine aggregate fineness modulus was calculated to be 2.32.
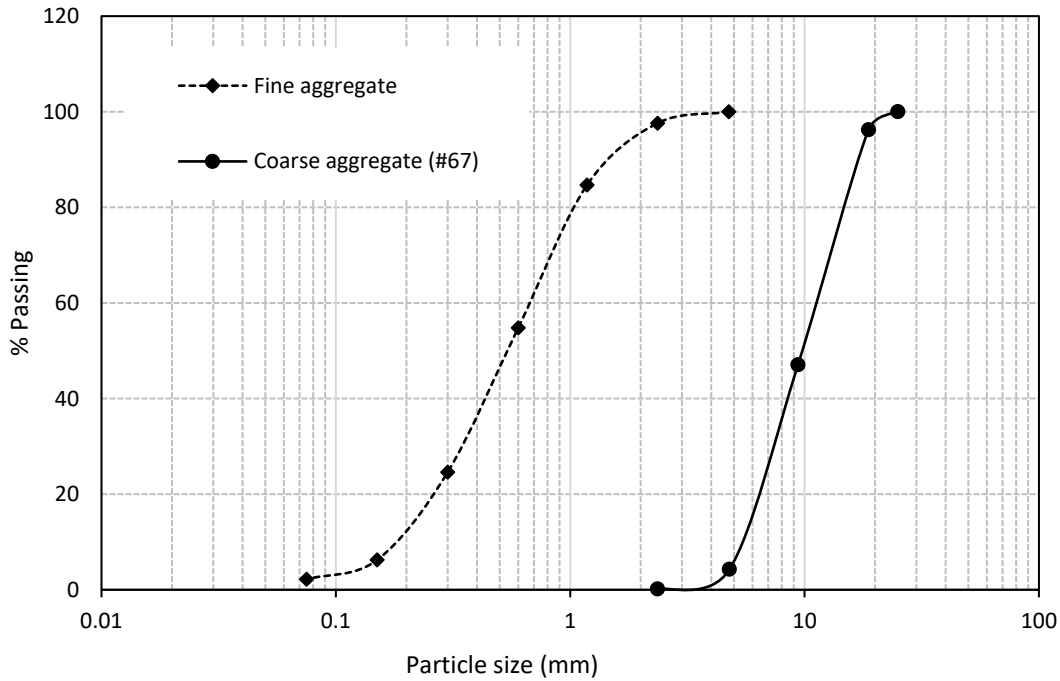
Figure 23: Cumulative particle size distribution or fine and coarse aggregates

The fine aggregate specific gravity and absorption were measured according to ASTM C128 [131]. Following drying at $110 \pm 5°C$ and weighing, the fine aggregates were immersed in water for 24 hours. To achieve the saturated surface-dry condition, the wet sand was spread on a flat nonabsorbent pan and exposed to a gentle moving current of warm air. After that, a cone test was performed to determine whether saturated surface dry conditions were achieved**.** The fine aggregate weight was measured at SSD condition to determine the absorption capacity. The fine aggregate specific gravity was measured using a pycnometer. The coarse aggregate specific gravity and absorption were measured according to ASTM C127 [132]. Coarse aggregates were submerged in water for a period of at least 48 hours after being dried and cooled before the specific gravity measurement was performed. Upon removing aggregate from water after 48 hours of soaking, the aggregates were rolled on an absorbent cloth until visible liquid films on the aggregates were removed to achieve a saturated surface-dry condition. The coarse aggregates were weighed after removing the free moisture to determine their absorption capacity. Upon reaching the saturated surface-dry condition, the SSD sample was placed in a container and weighed in water to determine its specific gravity. A summary of the measured aggregate properties are shown in Table 3. Bulk density and specific gravity tests of coarse aggregate were performed to determine the amount of void space between aggregate particles. The coarse aggregate dry-rodded unit weight was measured using ASTM C29 [128]. The dry-rodded unit weight was found to be 81.7 lb/ft^3.

Table 3: Aggregate physical properties

Property	Fine Aggregate	Coarse Aggregate
Bulk Specific Gravity (OD)	2.59	2.32
Bulk Specific Gravity (SSD)	2.60	2.41
Apparent Specific Gravity	2.62	2.56
Absorption Capacity (%)	0.44	4.10

3.3. Elemental Oxide Composition of Cementitious Materials

The elemental oxide compositions of cement, fly ash, silica fume, and slag cements used in this study were determined using x-ray fluorescence spectroscopy (XRF) on prepared glass beads. The measured results are listed in Table 4. The loss-on-ignition (LOI) for each sample is also given in Table 4. Al_2O_3 content has been reported to have a large effect on slag reactivity as well as the durability of cementitious systems containing slag [85], [16], [105]. Hence, slag cements with varying Al_2O_3 content of the slag were procured to obtain a different range of reactivity characteristics. As shown in Table 4, there is a wide range of Al_2O_3 contents in the slags from approximately 8.77% to 17.60%, and a range of MgO contents from 6.05% to 12.45%. Moreover, according to Table 4, the slags have CaO/SiO_2 ratios ranging from 1.09 to 1.30. It has been reported that the effects of increasing Al_2O_3 and MgO contents on slag reactivity are favorable [122]. In contrast, the negative effects of decreasing the CaO/SiO_2 ratio are offset by higher Al_2O_3 and/or MgO contents[30] [133]. The negative LOI values measured for the slags are because the sulfides present in the slag cements oxidize during heating, increasing the sample mass.

Table 4: Cementitious material oxide chemical composition (wt.%) measured using XRF

Analyte	Cement Type IL	Fly Ash (Class F)	Silica Fume	Slag 9	Slag 13	Slag 18
SiO_2	19.3	59.0	85.4	36.7	33.4	27.7
Al_2O_3	4.8	23.2	0.5	8.8	13.4	17.6
Fe_2O_3	3.2	7.0	4.1	0.5	1.2	0.6
CaO	65.8	3.5	0.8	40.1	42.6	36.1
MgO	1.0	2.1	8.0	11.7	6.1	12.5
SO_3	2.9	0.5	0.4	3.1	2.7	3.9
Na_2O	0.12	0.56	0.17	0.18	0.14	0.31
K_2O	0.25	2.34	0.71	0.33	0.32	0.28
TiO_2	0.4	1.06	0.01	0.39	0.59	1.94
P_2O_5	0.36	0.25	0.02	0.03	0.04	0.04
Mn_2O_3	0.09	0.06	0.32	0.14	0.18	0.4
L.O.I. (950°C)	6.1	2.0	3.1	-1.4	0.0	-0.8
Total	98.3	99.5	100.3	101.9	100.5	101.2
Na_2O_{eq}	0.29	2.1	0.64	0.4	0.35	0.49

35

3.4. Cement Composition

An X-ray diffraction (XRD) pattern is generated when crystalline material diffracts X-rays at specific angles, producing peaks of varied intensities[134]. In this study, XRD measurements were carried out according to ASTM C1365 [135] to determine the mineral composition of the as-received cement. A 20% by mass of corundum internal standard was mixed evenly into the cement sample to enable amorphous content quantification. Intergrinding the sample and internal standard (corundum) was carefully controlled to avoid overgrinding, which could cause widening of the peak [136]. After blending, the sample was mounted on a sample holder using a backloading approach and then carefully inserted into the X-ray diffractometer. A CuKα (λ = 1.5408 Å) radiation source with a nickel foil filter was used operating at 45 mV and 40 mA with a step size of 0.008°2θ and with angular range of 5-70°2θ. After the sample had been scanned, Rietveld refinement analysis for phase quantification was carried out using the Panalytical HighScore plus 4.5 software. The identified phases are summarized in Table 5. The XRD analysis of cement revealed that it was primarily crystalline, with only a small amorphous content.

Table 5 : Cement composition measured using XRD with Rietveld refinement

Analyte	Type IL Cement
Alite	44.3
Belite	19.1
Aluminate	5.4
Ferrite	9.7
Gypsum	1.5
Hemihydrate	3.6
Anhydrite	0.0
Calcite	12.3
Portlandite	1.5
Quartz	0.6
Amorphous/ unidentified	1.9

Thermogravimetric analysis (TGA) was used to measure the cement $CaCO_3$ and $Ca(OH)_2$ contents to validate the values measured using XRD [134]. In this study, ASTM C1872 [137] was followed to quantify the cement portlandite and calcite content using TGA. The system was heated at a rate of 20°C/min with a gas flow rate of 30 mL/min from 50 to 950°C. Cement weight loss at temperatures between 50 and 950°C is shown in Figure 24. Figure 24 shows that portlandite decomposed between 400°C and 500°C. Furthermore, Figure 24 also indicates that calcite decomposition occurred above 700°C. The tangential method was used to quantify the portlandite and calcite content from thermal mass loss curves (Figure 24).
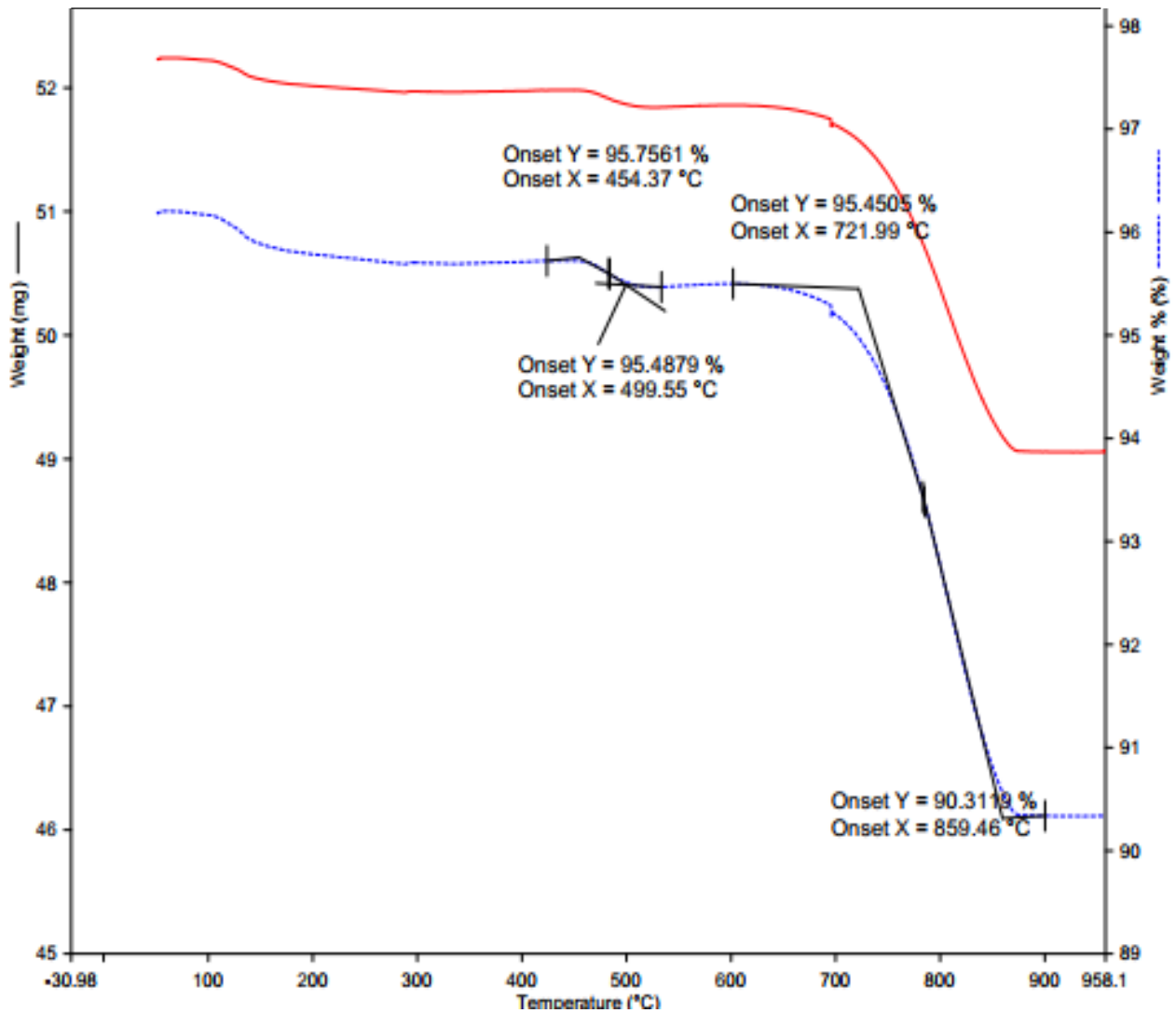
Figure 24: Mass loss measured using TGA and tangent method for Type IL

The cement calcite and portlandite contents as measured using XRD and TG are compared in Table 6. The two techniques are in excellent agreement, giving confidence in the measurements made of the cement composition.

Table 6: Calcite and portlandite content of type IL cement determined by TGA and XRD

Phase	TGA	XRD	Difference between TGA and XRD
Calcite	11.8%	12.3%	-0.5%
Portlandite	1.2%	1.5%	-0.3%

37

3.5. Cementitious Materials Physical Properties

Density and particle size distribution were determined for the as-received cementitious materials. ASTM C188 [138] was used to determine the density of cements, fly ash, silica fume and three different kinds of slags, respectively, as shown in Table 7. As specified by ASTM C188, standard deviations were within the ASTM C188 limit while measurements were taken five times. Helium pycnometry was used to determine the density of cementitious materials, as shown in Table 7.

Table 7: Cementitious material density and particle size distribution

Physical properties	Type IL cement	Fly ash (Class F)	Silica fume	Slag 9	Slag 13	Slag 18
Average density (g/cm^3)	3.16	2.32	2.39	3.01	2.97	2.99
D_{10} (μm)	1.9	8.7	12.1	2.2	2.8	2.3
D_{50} (μm)	10.1	19.6	27.5	10.7	12.1	10.6
D_{90} (μm)	23.3	87.0	68.9	22.3	27.7	21.8
Mean size (μm)	11.8	35.7	35.6	11.9	14.4	11.6

Laser diffraction analysis was used to measure the particle size distribution of cementitious materials. Isopropanol was used as the carrier fluid in this study. Results of the laser particle size analysis are shown in Table 7 as well as Figure 25. In this study, silica fume was found to be agglomerated even after ultrasonic treatment, giving the highest particle sizes measured even though silica fume particles are known to be typically smaller than a micrometer.
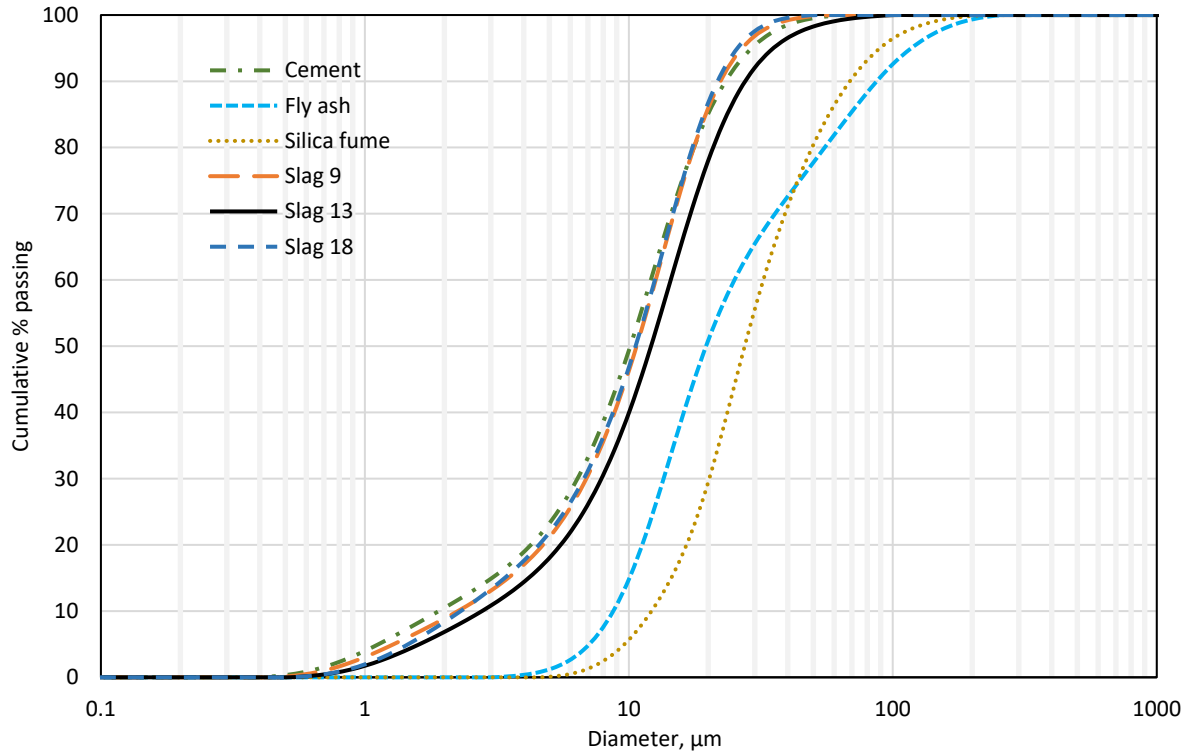
Figure 25 : Cumulative volume size distributions for cement, fly ash, silica fume and slag

3.6. Conclusions

In this chapter, the chemical, mineralogical and physical properties of the as-received cement, silica fume, fly ash and slag were measured along with the physical properties of the as-received aggregate. The slags procured for this study have Al_2O_3 contents of 8.8%, 13.4%, and 17.6%, giving a wide range of compositions.

4. METHODOLOGY AND TEST RESULTS

4.1. Background

Although concrete containing slag obtains a higher ultimate strength for a given water-cementitious material ratio (w/cm), its strength development at early ages can be slower than portland cement concrete under standard curing conditions [133], [139]. Curing temperature has a substantial effect on slag cement hydration and strength gain rates. The strength of slag concrete at early ages is significantly enhanced when cured at elevated temperatures [93], [133]. This is because slag hydration is much more sensitive to temperature than portland cement [133]. This study evaluated concrete compressive strength development with time to determine if mixtures made with slag cement could meet precast concrete strength requirements for release at 18 hours at laboratory and elevated temperatures. The chloride and sulfate durability development of slag cement concrete in binary and ternary blends under different curing regimes was also evaluated.

4.2. Methodology

4.2.1. Mixture Proportions

Concrete mixtures were designed to meet FDOT requirements for self-consolidating concrete. High-range water reducer additions were adjusted to adjust the concrete slump flow. Mortar bars were made to measure the mixture sulfate durability using the same fly ash, slag, and silica fume replacement levels as the concrete mixtures.

Table 8 shows the mixture proportions used for each concrete mixture made. In order to determine how the composition of the slag influences the development of compressive strength, Type IL(12) cement [4] and three different slags with alumina contents of S9 (8.8% alumina), S13 (13.4% alumina), and S18 (17.6% alumina) [5] were used in concrete mixtures at cement replacement levels of 0, 30, 40, and 50 as shown in Table 8. A mixture containing 20% Class F fly ash [2] was also made as a benchmark to compare the the slag mixture strength and durability against. Moreover, two different proportions of slag (30% and 50%), as well as silica fume (4% and 6%) in ternary concrete blends, were also prepared to determine the amount of silica fume necessary for reliable early-age strength as well as chloride and sulfate attack durability. All concrete mixtures were designed to produce self-consolidating concrete (SCC) with a fine-to-total aggregate content of no more than 50% [140]. Considering this study was focused on precast concrete, the concrete mixtures were made at a water-cementitious ratio of 0.27. The w/cm content was selected to ensure that the fly ash mixture had a compressive strength exceeding 5200 psi at 18 hr when cured at elevated temperatures.

Table 8: Concrete mixture proportions

Mixture	Water (lbs/yd³)	Type IL(12) Cement (lbs/yd³)	Class F Flyash (lbs/yd³)	Slag 9 (lbs/yd³)	Slag 13 (lbs/yd³)	Slag 18 (lbs/yd³)	Silica fume (lbs/yd³)	Coarse Aggregate (lbs/yd³)	Fine Aggregate (lbs/yd³)	High-Range Water Reducing Admixture (oz/cwt)
Control	210.6	780	--	--	--	--	--	1480	1505	23.5
20FA	210.6	624	156	--	--	--	--	1455	1485	19.0
S9(30%)	210.6	546	--	234	--	--	--	1475	1502	26.5
S9(40%)	210.6	468	--	312	--	--	--	1474	1500	24.0
S9(50%)	210.6	390	--	390	--	--	--	1475	1497	22.0
S13(30%)	210.6	546	--	--	234	--	--	1474	1501	25.5
S13(40%)	210.6	468	--	--	312	--	--	1473	1498	23.0
S13(50%)	210.6	390	--	--	390	--	--	1470	1497	20.5
S18(30%)	210.6	546	--	--	--	234	--	1475	1501	25.0
S18(40%)	210.6	468	--	--	--	312	--	1475	1497	22.0
S18(50%)	210.6	390	--	--	--	390	--	1474	1495	19.5
S13(30%)_4SF	210.6	514.8	--	--	234	--	31.2	1472	1495	36.0
S13(30%)_6SF	210.6	499.2	--	--	234	--	46.8	1472	1491	40.0
S13(50%)_4SF	210.6	358.8	--	--	390	--	31.2	1470	1490	33.0
S13(50%)_6SF	210.6	343.2	--	--	390	--	46.8	1470	1485	37.5

4.2.2. Fresh Properties

Each concrete mixture was repeated (mix A and mix B) to ensure the validity of results, giving a total of 30 batches made in this study. In order to obtain the desired workability (26 $\pm$ 2.5 inch), an ASTM C494 Type F [141] high-range water-reducing admixture (MasterGlenium 7920) was used with the dosage adjusted as necessary. Fresh property tests were performed to measure concrete flowability and stability. In all batches, slump flow, air content, unit weight, and temperature were measured. A J-Ring test according to ASTM C1621 [142] was used to assess the mixture's passing ability, which satisfied the FDOT criteria (Δflow $\leq$ 2 in.) for all SCC mixtures. The concrete stability was measured using the rapid assessment of static segregation resistance according to ASTM C1712 [143]. All SCC mixtures exhibited a static segregation value $\leq$ 25 mm, which satisfied the FDOT requirement. Additionally, ASTM C1610 [144] was used to measure the static column segregation resistance of the concrete on mixtures with 20% and 50% cement replacement with fly ash and slag 13, respectively, to compare with the ASTM C1712 results. In the column segregation test, both mixtures showed zero column segregation, satisfying FDOT requirements (S$\leq$ 15%). The relative viscosity (T50) was measured using ASTM C1611 [145], which met FDOT requirements of 2 to 7 seconds for all SCC mixtures.

4.2.3. Compressive Strength

4 $\times$ 8 in. concrete cylinders were made to measure the concrete strength development according to ASTM C192 [146] and tested at the concrete laboratories at the University of Florida (UF). Immediately after mixing and finishing the concrete cylinders, the samples were cured in two different ways, elevated temperature and lab temperature, to determine the concrete compressive strength development. Curing at elevated temperatures was carried out by keeping samples in their molds with the lids tightly fixed and placing them in an oven at 120°F as soon as the molding was complete. As soon as the samples reached the desired age (18 hrs. and 24 hrs.) for testing, they were demolded, the ends ground flat, and tested. For laboratory temperature curing, samples were cured in molds at laboratory temperature (73±3°F) until they were ready for testing, or until 24 hours had passed. Following demolding, samples were placed into buckets filled with 3.25±0.25 gallons of saturated limewater. Saturated limewater was prepared by adding 3 grams of calcium hydroxide per liter of deionized water (DI). To ensure that the samples were kept between 70 and 76°F during curing, the buckets were sealed and placed in the UF moist room. Three concrete cylinders were stored in each 5-gallon bucket. The compressive strengths of concrete cylinders were measured under lab temperature curing at 18 hr, 24 hr, 7 days, and 28 days.

4.2.4. Resistivity Measurements

Surface resistivity testing was performed in accordance with AASHTO T 358 [147] as a measure of the concrete resistance to aggressive ion penetration. The concrete electrical impendence was measured using a four-point Wenner probe on 4 in. $\times$ 8 in. cylinders. Concrete cylinders were cured using two different methods. Resistivity measurements were made for samples cured at laboratory temperature (73±3°F) at 28, 56, and 91 days using the same limewater curing method as the samples cured at laboratory temperature for compressive strength. Aside from the

42

laboratory temperature curing, an accelerated curing technique was also implemented following ASTM C1202 [3] to determine if the period required to evaluate long-term durability could be shortened. In this technique, concrete specimens were cured for 7 days in the same way as the lab temperature-cured specimens. At 7 days, the samples were placed in an oven at 100°F and left there until tested. Tests were conducted on the accelerated concrete cured specimen by using AASHTO T 358 at 28 days. Using a laser thermometer, the concrete temperature was also measured according to AASHTO T 358 to ensure it was within the specified range. Moreover, as electrical conductivity can vary with the moisture content of concrete's pores, all concrete specimens were tested in a saturated surface dry condition.

As part of this study, bulk resistivity was measured according to AASHTO TP 119 [148] on the same samples used to measure concrete surface resistivity at the same ages. The uniaxial impedance was determined by placing steel plates on each end of the specimen that were connected to a Resipod concrete resistivity meter. Before every measurement, sponge inserts were soaked in limewater and squeezed lightly by hand to drain excess water, such that the sponge inserts were saturated but not dripping. Limewater-soaked sponges were then placed between the plates and the concrete specimens. The temperature of the specimen during the experiment was recorded along with the resistance of the concrete. Furthermore, the resistivity of the sponges was also measured.

In both cases (surface and bulk resistivity), the electrical resistivity of the concrete cylinders was calculated by applying necessary geometric corrections.

4.2.5. Sulfate Durability

Three test methods were used to measure slag cement resistance to sulfate attack, 1) an electrochemical method for assessing sulfate intrusion into concrete in terms of coulombs, 2) ASTM C1012, and 3) an accelerated version of ASTM C1012.

4.2.5.1. Sulfate Permeability Measurements

An electrochemical test similar to ASTM C1202 [3] was used in the current study to assess sulfate attack durability. Essentially, the purpose was to determine whether this test method provided information on concrete sulfate resistance. Samples for the rapid electrochemical sulfate test were prepared using similar procedures as for ASTM C1202 test. Three concrete cylinders were cured in saturated limewater at $73\pm3°F$ until the samples were 27 days old. 2 in. thick by 4 in. diameter concrete samples were cut from the cylinders. The concrete samples were coated with epoxy and placed under vacuum for 3hr and then submerged in deaired water under vacuum for one hour. The vacuum was then released, and the samples were kept submerged for an additional $18 \pm 2hr$ without vacuum. At 28 days, a 60V electrical potential was applied to the sample for 6 hr using the same apparatus used for ASTM C1202 except that a 5% Na_2SO_4 solution was used instead of the chloride solution. The cumulative charge passed through the sample during the 6 hr period was recorded.

43

4.2.5.2. Sulfate Mortar Bar Length Change Measurements

The effect of slag characteristics on sulfate durability was assessed by measuring the length change of mortar bars stored in 5% sodium sulfate solution. In this study, the resistance of the cementitious material against sulfate attack was measured in accordance with ASTM C1012 [149] "Standard Test Method for Length Change of Hydraulic-Cement Mortars Exposed to a Sulfate Solution." Mortar bars were produced using the same cementitious material combinations as the concrete mixtures made in this study, except that the w/cm ratio for each combination was fixed at 0.485. Initial curing was conducted in an oven maintained at 35°C ± 3°C (95°F ± 5°F) for 23.5 hr ± 0.5 hr. In accordance with the specification, mortar bars were exposed to sulfate solution when the companion cube strength reached 2850 psi (20 MPa). For all mortar bars, length change measurements and sulfate solution renewal were carried out at 1, 2, 3, 4, 8, 13, and 15 weeks, and also at 4, 6 months after immersion in the sulfate solution [149]. Whenever the solution was changed, a pH strip was used to measure the pH of the solution to make sure it was between 6 and 8.

An accelerated version of ASTM C1012 was used to measure whether the test time could be shortened [14]. Before beginning the accelerated test, mortar cubes were measured for strength after demolding to determine whether they achieved 2,850 psi. If the mortar cubes had not reached 2,850 psi, the bars and cubes were placed in limewater at 73°F until they reached 2,850 psi. Upon reaching strength, mortar bars were placed in a sealed container above a saturated NaOH solution in the bottom in an oven at at 100°F for 14 days to dry. The saturated NaOH solution was used to maintain a relative humidity in the air of the container of 6.5%. Care was taken to ensure that the mortar bars did not touch the sodium hydroxide solution. After drying, the bars were subjected to a high vacuum of 6.7 kPa for 4 hours in a large desiccator. While under vacuum, a 5% sodium sulfate solution was introduced into the desiccator to completely cover the samples. Following 20 hours of immersion, the vacuum was released and the bars were measured for their initial length ("zero-measurement"). The bars were then stored at 23°C ± 2°C (73°F ± 4°F) in a 5% sodium sulfate solution. Mortar bar expansion was monitored at the same frequency as indicated in ASTM C1012.

4.3. Test Results

4.3.1. Fresh Properties

Table 9 presents the results of all fresh concrete properties tests. No segregation was noted in any of the column segregation tests. All of the concrete batches met FDOT self-consolidating concrete requirements.

Table 9: Fresh SCC properties of all mixtures

Mix ID	Date of mixing	Batch #	Fresh SCC Properties				
			Slump flow (inch)	J-ring (inc.)	Relative viscosity (s)	Static segregation Pd (mm)	Column static segregation(%)
20FA	4/13/2023	A	27	27	3	2.5	0
	4/18/2023	B	26	25.5	4	1.5	0
Slag 13(50%)	4/27/2023	A	26.5	25.5	4	1	0
		B	26	25.5	4	0.5	0
Control	5/2/2023	A	26.5	25	3	2	
		B	26	25.5	4	1.5	
Slag 13(40%)	5/4/2023	A	26.75	25	3	2.5	
		B	26	24.5	4	1.5	
Slag 13(30%)	5/9/2023	A	27	25.5	4	2.2	
		B	27	25	4	2	
Slag 13 (30%)-4SF	5/11/2023	A	26.5	24.5	5	1	
		B	27	25.5	3	2.5	
Slag 18 (30%)	5/16/2023	A	26.5	25	4	1.5	
		B	25.5	24	5	1	
Slag 18 (40%)	5/18/2023	A	28	26.5	2	2.5	
		B	27	25	3	1.5	
Slag 18 (50%)	5/23/2023	A	27	26.75	4	1	
		B	27.5	27	3	2	
Slag 13 (30%)-6SF	5/25/2023	A	25.5	24	6	0.5	
		B	26.25	25	4	1.5	
Slag 9 (50%)	5/30/2023	A	27	25.25	5	2	
		B	27.5	26	3	2	
Slag 13 (50%)-4SF	6/6/2023	A	26.5	26	4	1.5	
		B	25.5	24	5	1	
Slag 13 (50%)-6SF	6/8/2023	A	27.25	26.5	3	1.5	
		B	27.5	26.25	2	2	
Slag 9 (30%)	6/13/2023	A	28	26.5	2	3	
		B	27.75	26	3	2	
Slag 9 (40%)	6/15/2023	A	27.5	27.25	2	1.5	
		B	28	27.25	2	1.5	

4.3.2. Compressive Strength

Table 10 presents the concrete compressive strength measurements. All of the mixtures that contained slag 13 or 18 met the 5200 psi requirement at 18 hr for detensioning prestressing reinforcement and were above that of the 20% fly ash at elevated temperature curing. None of the slag 9 mixtures were able to meet that requirement at 18 hr. None of the ternary mixtures met the requirement because the high admixture dosages retarded the mixtures. None of the mixtures cured at lab temperature met the 5200 psi requirement at 18 hr, not even the control mixture.

Table 10: Results of average compressive strength of SCC mixtures at different curing ages

Mixing type	w/cm	Curing Temperature	Average Compressive Strength (psi)			
			18 hr.	24 hr.	7 day	28 day
Control	0.27	Elevated	6312	7111	--	
		Lab	3410	5015	7901	9003
20FA		Elevated	5299	5855	--	
		Lab	3268	3994	6079	7880
Slag 9 (30%)		Elevated	4898	6369	--	
		Lab	1327	2476	7782	8674
Slag 9 (40%)		Elevated	4626	6097	--	
		Lab	1173	2185	7248	8880
Slag 9 (50%)		Elevated	4366	5935	--	
		Lab	1022	1897	6882	9256
Slag 13 (30%)		Elevated	6012	6983	--	
		Lab	2625	3748	8504	8980
Slag 13 (40%)		Elevated	5570	6716	--	
		Lab	2286	3192	7827	9057
Slag 13 (50%)		Elevated	5363	6590	--	
		Lab	1857	2831	7051	9544
Slag 18 (30%)		Elevated	5937	6970	--	
		Lab	1394	3388	8470	8748
Slag 18 (40%)		Elevated	5547	6660	--	
		Lab	1271	3142	7770	8899
Slag 18 (50%)		Elevated	5340	6601	--	
		Lab	732	2424	7280	9328
Slag 13 (30%)-4SF		Elevated	4903	5994	--	
		Lab	1560	2616	8052	8631
Slag 13 (30%)-6SF		Elevated	3429	4817	--	
		Lab	513	1694	6517	8581
Slag 13 (50%)-4SF		Elevated	4051	4858	--	
		Lab	428	1370	7082	8938
Slag 13 (50%)-6SF		Elevated	2388	3815	--	
		Lab	99	683	6520	8699

4.3.3. Resistivity Measurements

Table 11 summarizes the surface and bulk resistivity results after applying geometric correction factors.

Table 11: Results of concrete surface and bulk resistivity under accelerated and lab curing

Mix ID	Curing	Resistivity (k.ohm.cm)					
		28-Day Surface	28-Day Bulk	56-Day Surface	56-Day Bulk	91-Day Surface	91-Day Bulk
Control	Accelerated	4.72	4.38	--	--	--	--
	Laboratory	5.59	5.31	6.27	6.05	6.97	6.52
20FA	Accelerated	10.98	10.34	--	--	--	--
	Laboratory	5.18	5.07	7.34	7.84	10.41	11.20
Slag 9 (30%)	Accelerated	7.28	7.93	--	--	--	--
	Laboratory	7.26	7.81	9.05	9.35	10.77	11.23
Slag 9 (40%)	Accelerated	8.25	8.79	--	--	--	--
	Laboratory	8.05	8.52	10.03	11.24	12.35	12.86
Slag 9 (50%)	Accelerated	15.83	16.6	--	--	--	--
	Laboratory	13.30	12.83	14.82	15.06	17.17	17.31
Slag 13 (30%)	Accelerated	8.33	9.24	--	--	--	--
	Laboratory	8.63	9.04	9.62	10.66	11.50	11.87
Slag 13 (40%)	Accelerated	9.83	10.95	--	--	--	--
	Laboratory	9.48	10.54	12.12	12.51	14.59	14.35
Slag 13 (50%)	Accelerated	14.28	15.15	--	--	--	--
	Laboratory	13.17	13.57	14.49	14.45	16.63	17.03
Slag 18 (30%)	Accelerated	7.94	8.17	--	--	--	--
	Laboratory	8.33	8.32	9.05	9.31	10.17	10.15
Slag 18 (40%)	Accelerated	8.33	9.60	--	--	--	--
	Laboratory	8.23	8.72	9.48	9.83	11.44	11.09
Slag 18 (50%)	Accelerated	10.68	12.57	--	--	--	--
	Laboratory	10.01	10.7	11.01	11.18	12.6	13.73
Slag 13 (30%)_4SF	Accelerated	20.28	22.52	--	--	--	--
	Laboratory	11.21	12.4	16.82	16.97	20.29	21.40
Slag 13 (30%)_6SF	Accelerated	18.56	19.64	--	--	--	--
	Laboratory	11.23	11.99	16.97	17.39	22.14	22.79
Slag 13 (50%)_4SF	Accelerated	22.50	21.75	--	--	--	--
	Laboratory	14.82	15.86	20.10	20.32	25.81	26.72
Slag 13 (50%)_6SF	Accelerated	23.59	23.34	--	--	--	--
	Laboratory	14.75	14.35	20.34	21.63	27.67	28.35

4.3.4.   Sulfate Durability

4.3.4.1.   Sulfate Permeability Measurements

The data for the rapid sulfate permeability test is presented in Table 12**.**

Table 12: Results of rapid sulfate permeability of SCC (Binary mixtures)

Mix ID	% of replacement	Average rapid sulfate permeability (Coulombs)
Control	0	2577
FA	20	1916
Slag 9	30	1319
	40	1232
	50	798
Slag 13	30	1257
	40	997
	50	812
Slag 18	30	1275
	40	1192
	50	908
Slag 13_4SF	30	1084
	50	659
Slag 13_6SF	30	1082
	50	611

4.3.4.2.   Sulfate Mortar Bar Length Change Measurements

The sulfate expansion of mortar bars prepared with as-received cementitious materials is displayed in Figure 26 to Figure 31. For all mixtures, the rate of expansion of mortar bars was measured until 180 days. In both the standard and accelerated exposure methods, none of the mixtures exceeded 0.1% expansion at 6 months. In all slag cement binary mixtures as shown in Figure 27 to Figure 29, the expansion under standard exposure followed the alumina content for low, moderate, and high expansion rate with slag 9, slag 13, and slag 18 respectively, whereas the trend demonstrated a reversed pattern under accelerated exposure with low to high expansion rate for slag 18, slag 13 and slag 9 mixtures.

48
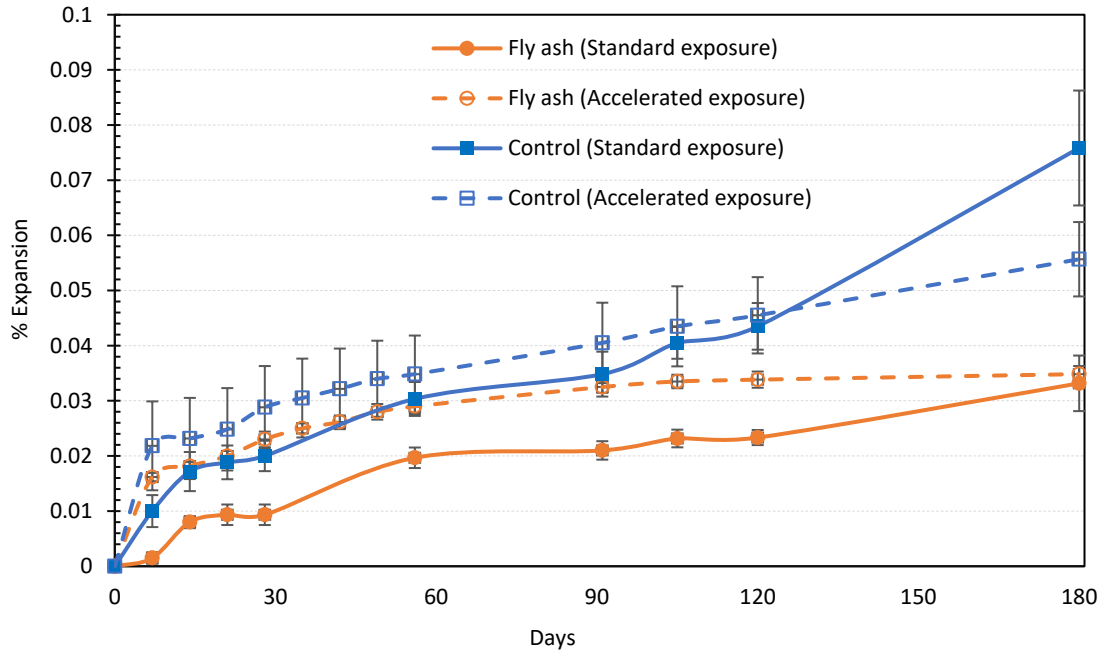
Figure 26: Comparison of the expansion behavior of control and fly ash specimens under standard and accelerated exposure

Figure 27: Comparison of the expansion behavior of slag 9, slag 13 and slag 18 with 30% cement replacement under standard and accelerated exposure

49
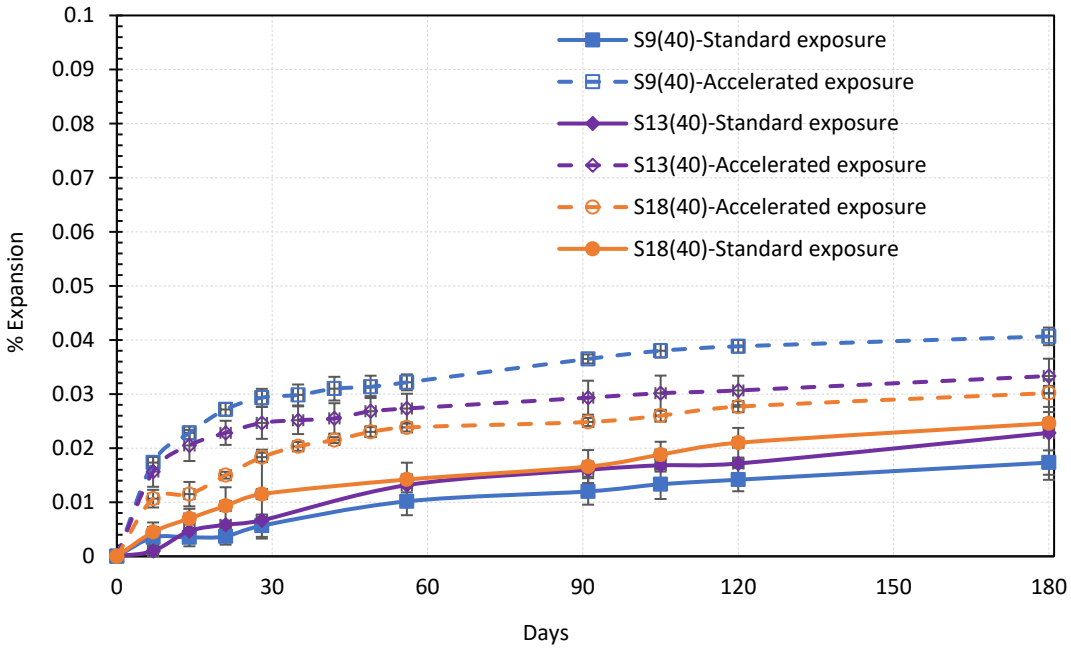
Figure 28: Comparison of the expansion behavior of slag 9, slag 13 and slag 18 with 40% cement replacement under standard and accelerated exposure
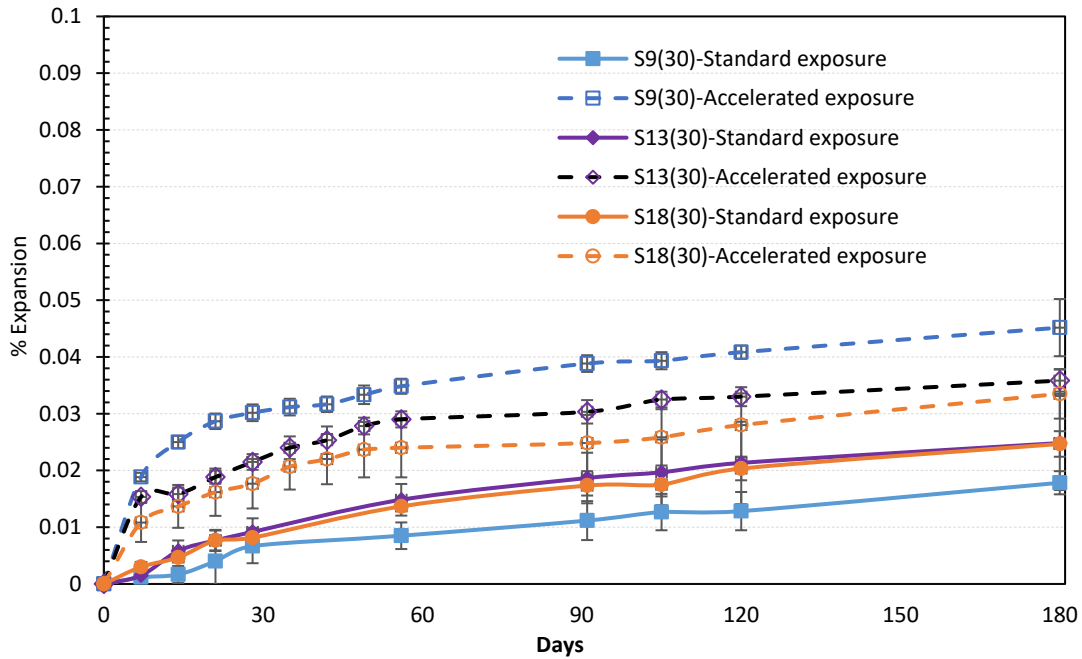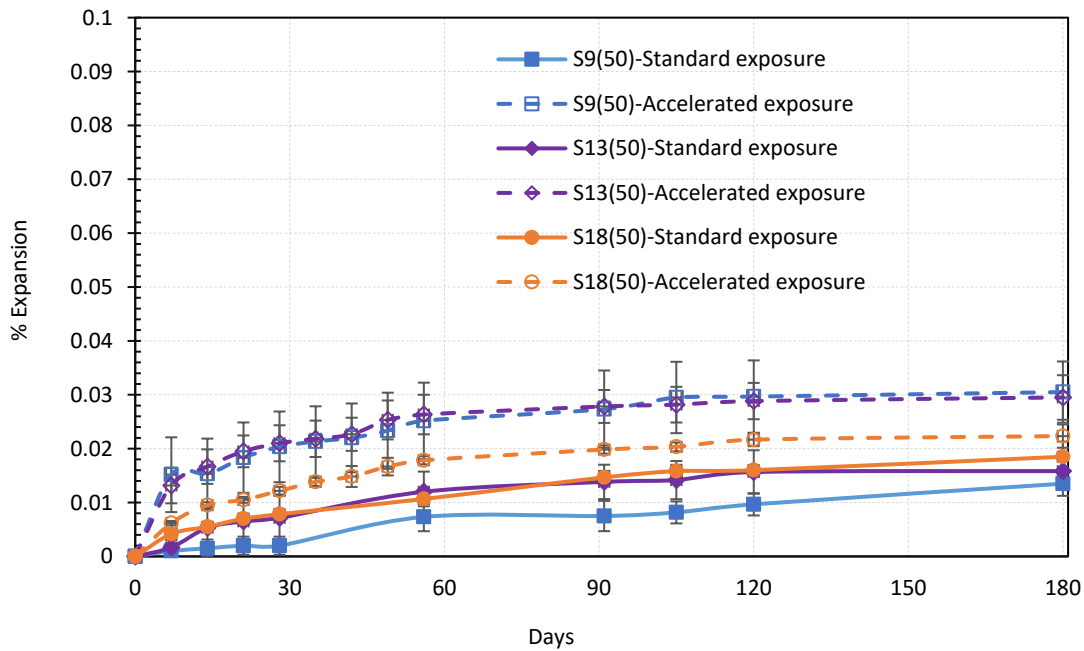

Figure 29: Comparison of the expansion behavior of slag 9, slag 13 and slag 18 with 50% cement replacement under standard and accelerated exposure

50
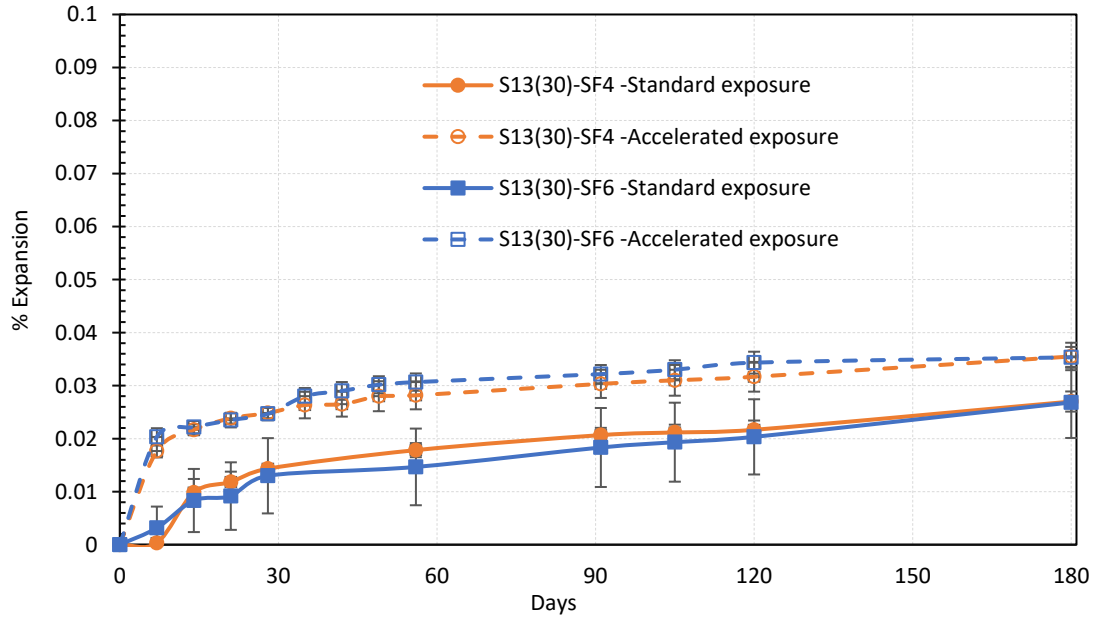
Figure 30: Comparison of the expansion behavior of ternary blended mixture of 30% cement replacement with slag 13 and 4% and 6% silica fume under standard and accelerated exposure
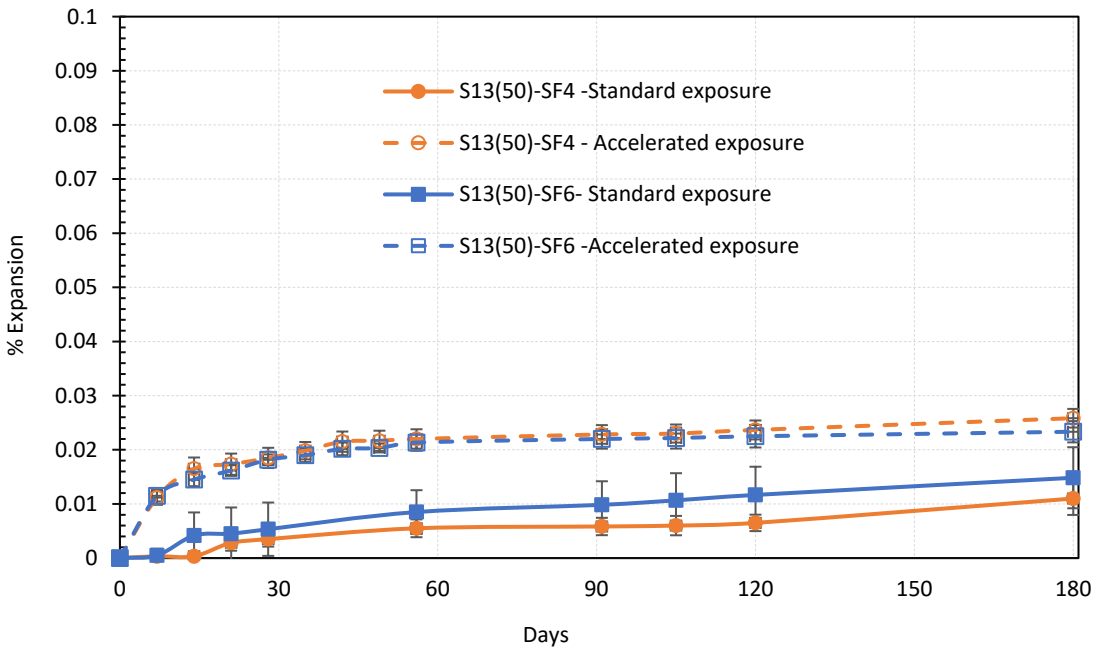
Figure 31: Comparison of the expansion behavior of ternary blended mixture of 50% cement replacement with slag 13 and 4% and 6% silica fume under standard and accelerated exposure

51

4.4. Conclusions

This study examined the compressive strength and durability of concrete with a w/cm ratio of 0.27 containing fly ash, three different slag cements, and slag with silica fume in ternary blends. All mixtures made with slags S13 and S18 had compressive strengths above 5200 psi at 18 hr when cured using the elevated curing method. Mixtures with SCM combinations performed better in all cases when compared to control mixtures resistivity and expansion.

5.   DISCUSSION OF TEST RESULTS

5.1. Background

Slag cement has a positive effect on the durability of concrete mixtures, but can reduce the early-age strength development rate that is critical for precast concrete productivity. Experiments were performed to determine the slag replacement level necessary to maintain durability at least equivalent to that provided by concrete containing 20% Class F fly ash, and the maximum replacement level that can be used while still providing adequate strength for detensioning prestressing steel strand at 18 hr. The three slag cements used in this study were selected to represent variations in Al_2O_3, CaO, SiO_2, and MgO contents.

5.2. Results and Discussions

5.2.1.   Compressive Strength

Measurements of concrete compressive strength were performed using ASTM C39 [150]. Figure 32 and Figure 33 shows the concrete compression strength measured at 18 and 24 hours after mixing and cured at elevated temperatures (120°F) to determine if the concrete could reach 5200-psi (80% of 28-day compressive strength of FDOT Class V concrete) strength at 18 hours to allow for detensioning. Figure 32 shows that the concrete mixture that contained 20% fly ash was able to meet the 5200 psi requirement at 18 hr required for detensioning prestressing reinforcement. As expected, increasing replacement levels of slag reduced the early-age strength gain development of concrete. Nevertheless, the slag cements with Al_2O_3 contents of 13% and 18% had compressive strengths above that of the 20% fly ash mixture for all mixtures containing up to 50% slag replacement levels at 18 hours. The slag with an Al_2O_3 content of 9% had equivalent strength at 18 hr to the mixture containing 20% fly ash with a replacement level of 24%. All slag mixtures tested had compressive strengths above that of the 20% fly ash mixture at 24 hr with elevated temperature curing.
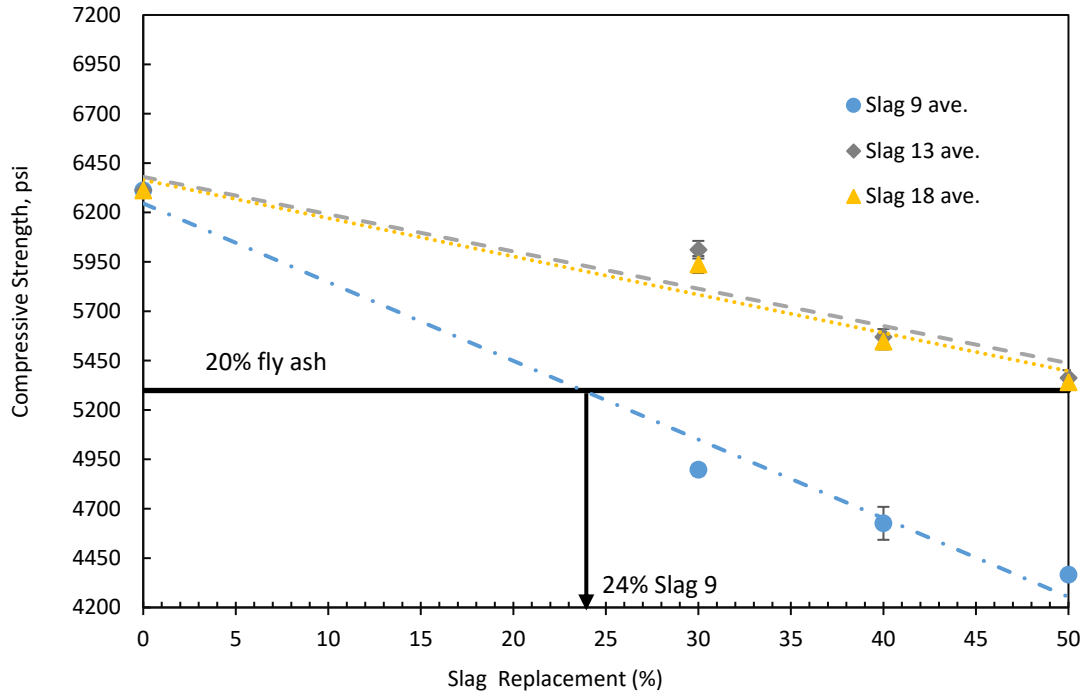
53

Figure 32: Compressive strength of concrete containing fly ash, slag 9, slag 13 and slag 18 at 18 hr under elevated temperature curing (120°F)
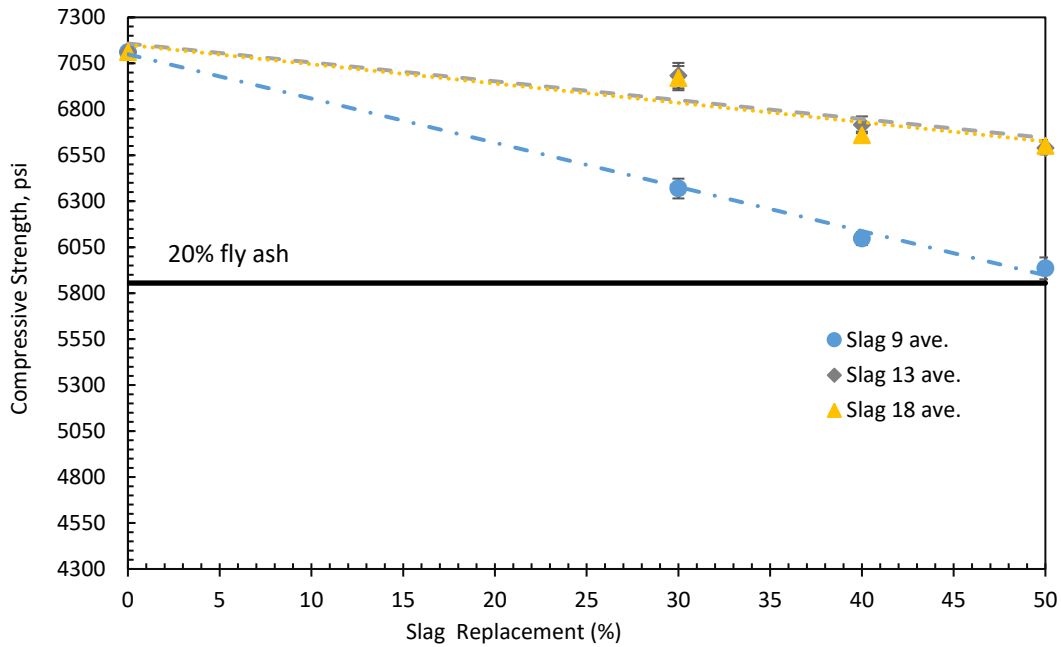

Figure 33: Compressive strength of concrete containing fly ash, slag 9, slag 13 and slag 18 at 24 hr under elevated temperature curing (120°F)

54

The elevated temperature significantly accelerates the concrete strength development rate and Figure 35 shows that the strength development rate of slag cement concrete is significantly lower at early ages (18 and 24 hr) under lab temperature curing conditions compared to control and fly ash concrete. Slag is known to have a high activation energy, meaning that its reaction rate at early ages is much more temperature sensitive than portland cement [2], [3]. It is well established that high MgO/Al_2O_3 ratios negatively affect slag activation energy. According to Zhan et al., the activation energy of low aluminum slag decreased with increases in MgO/Al_2O_3 ratio in low-aluminum slag systems, and the polymerization degree of slag was also reduced, which affects the strength development [151]. As a result of the increase in MgO/Al_2O_3, the slag will be less sensitive to temperature, indicating that the increasing MgO/Al_2O_3 ratio will enhance thermal stability of slag. Zhan et.al also reported that the MgO/Al_2O_3 ratio of low-aluminum slag should be at about 0.60 to 0.75 to give high-temperature sensitivity. In the current study, slag 9 had the lowest Al_2O_3 (8.8%) and the highest MgO/Al_2O_3 ratio (1.33), compared to slag 13 and slag 18, which had MgO/Al_2O_3 ratios of 0.46 and 0.71, respectively. Thus, it is not surprising that slag 13 and slag 18 concrete had similar and higher compressive strength than concrete made with slag 9 at elevated temperature curing. Overall, slag cement use in hot weather with concrete can provide good strength development, however adding slag to concrete in cold weather without externally applied heat can cause difficulty in achieving the desired strength at early ages.

Figure 34: Compressive strength of concrete containing fly ash, slag 9, slag 13 and slag 18 at 18 hr under lab temperature curing (73°F)

55

Figure 35: Compressive strength of concrete containing fly ash, slag 9, slag 13 and slag 18 at 24 hr under lab temperature curing (73°F)

Figure 36 and Figure 37 show that even after 7 days and 28 days, 20% fly ash showed 23% and 12% respectively lower compressive strength than the control. On the other hand, all cement replacements with all three slags used exhibited higher compressive strength than that of the 20% fly ash concrete at both 7 and 28 days. This is likely due to the presence of a higher amount of CaO in the slag that contributes to slag hydraulic reactivity [67]. The strength of all three slags with 50% cement replacement was greater than the strength of the control at 28 days, as illustrated in Figure. The compressive strength of slag 13 with 50% cement substitution was highest at 28 days.
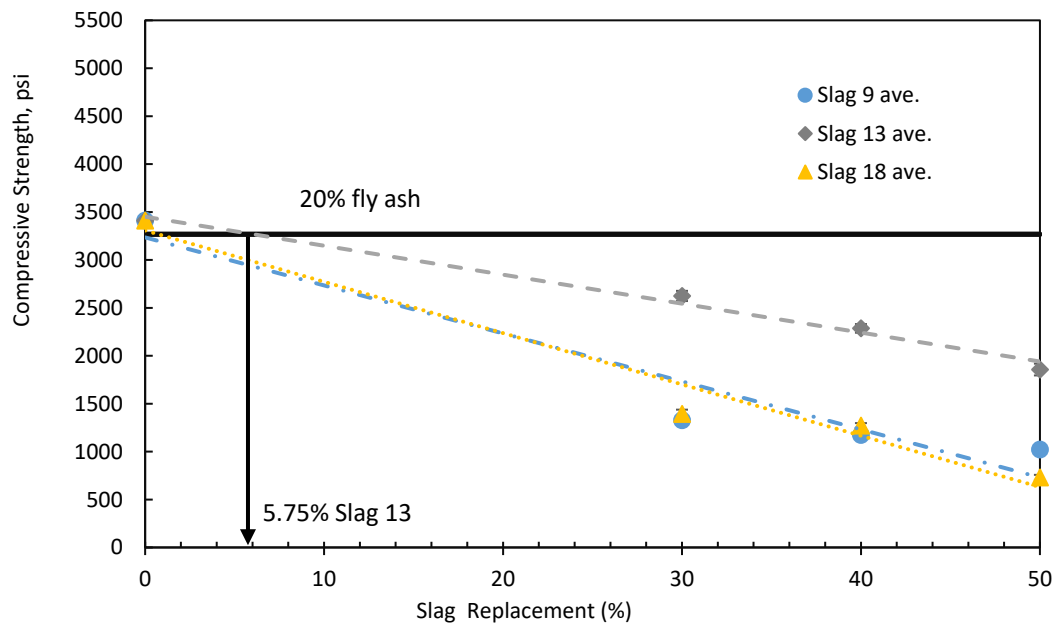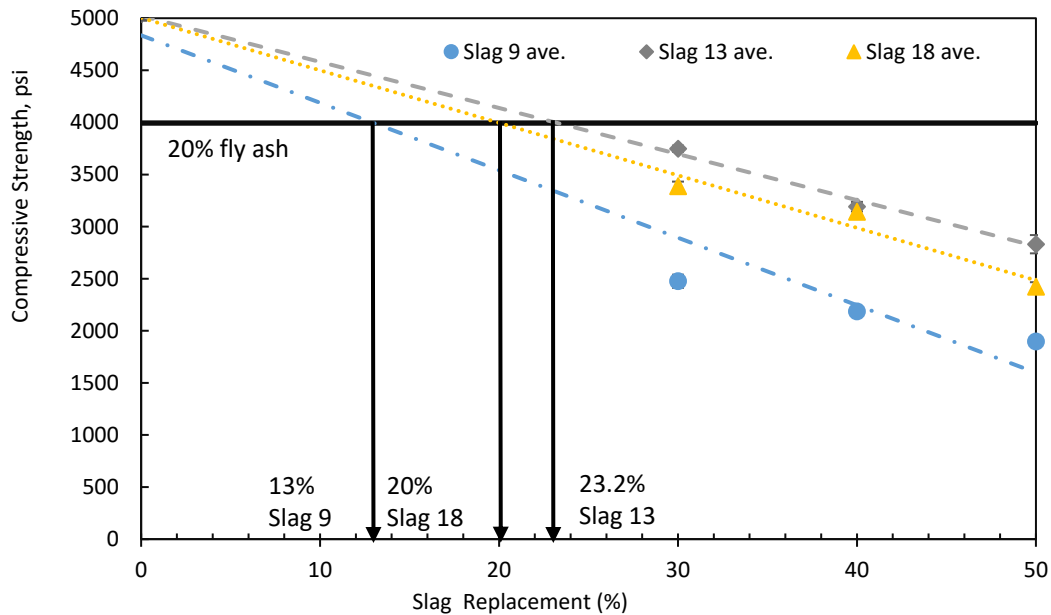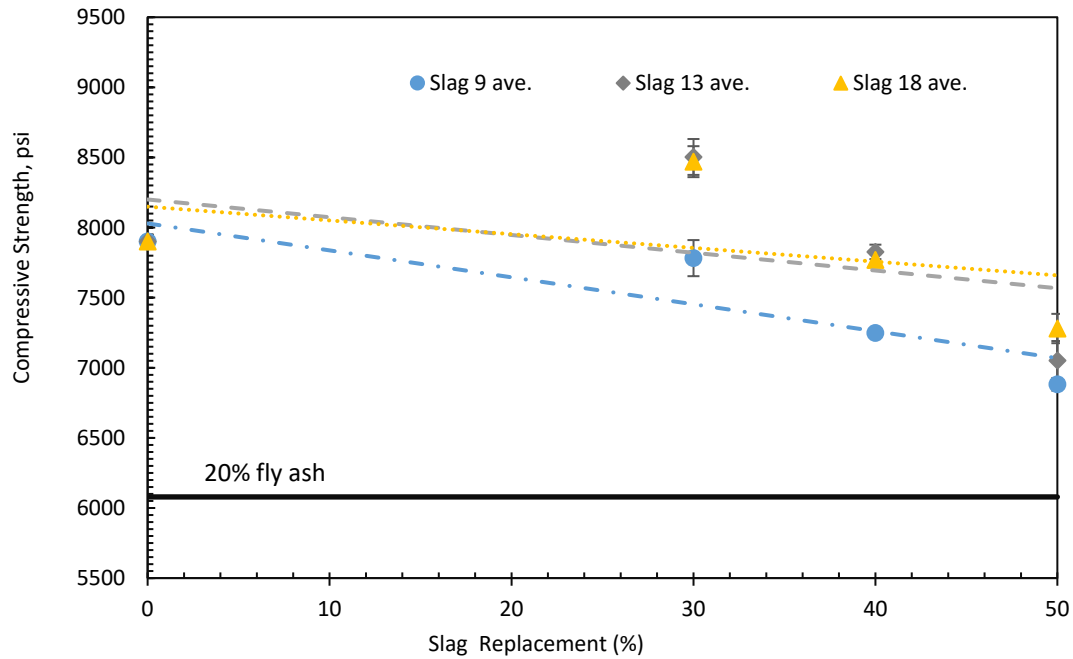
Figure 36: Compressive strength of concrete containing fly ash, slag 9, slag 13 and slag 18 at 7 days under lab temperature curing (73°F)
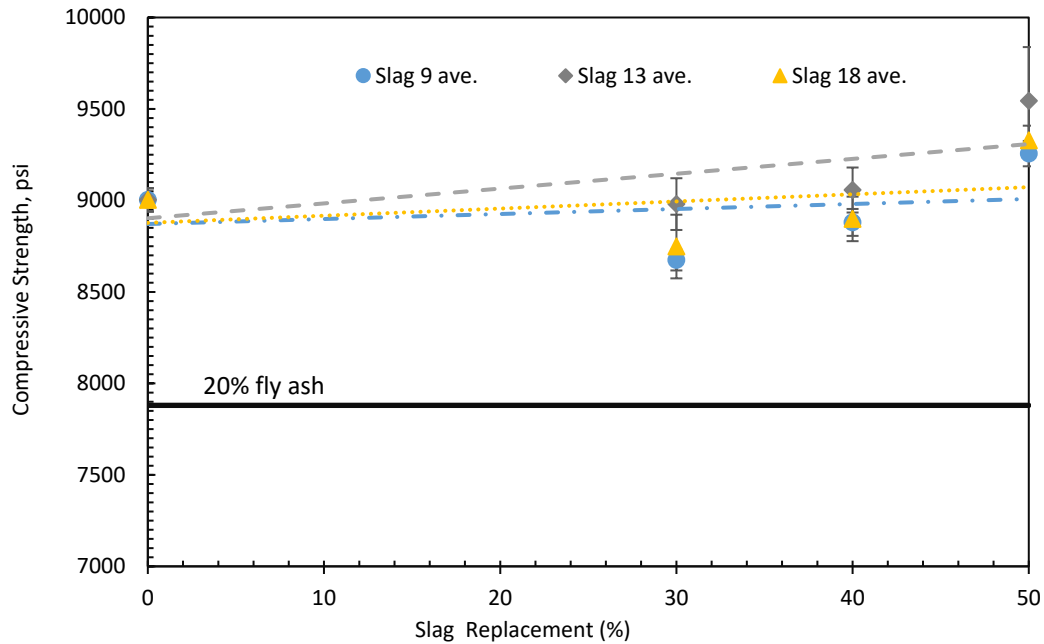
Figure 37: Compressive strength of concrete containing fly ash, slag 9, slag 13 and slag 18 at 28 days under lab temperature curing (73°F)

57

The early age compressive strengths of ternary-blend samples at elevated and lab temperatures are shown in Figure 38. It was found that the mixtures that contained 4% and 6% silica fume had lower compressive strengths compared to the binary concrete mixtures. In addition, the elevated temperature curing did not accelerate the strength gain sufficiently to meet the desired 5200 psi at 18 hr for mixtures with slag and silica fume. As shown in Figure 38, the ternary blended concrete mixtures with 50% slag 13 and silica fume had lower compressive strength at early ages when compared to other mixes. The retardation appears to have been even more significant at room temperature. The higher the cement replacement with silica fume, the greater the superplasticizer needed to achieve the desired slump flow. Consequently, the retardation effect was higher, and the concrete compressive strength was less likely to develop by 18 hr.
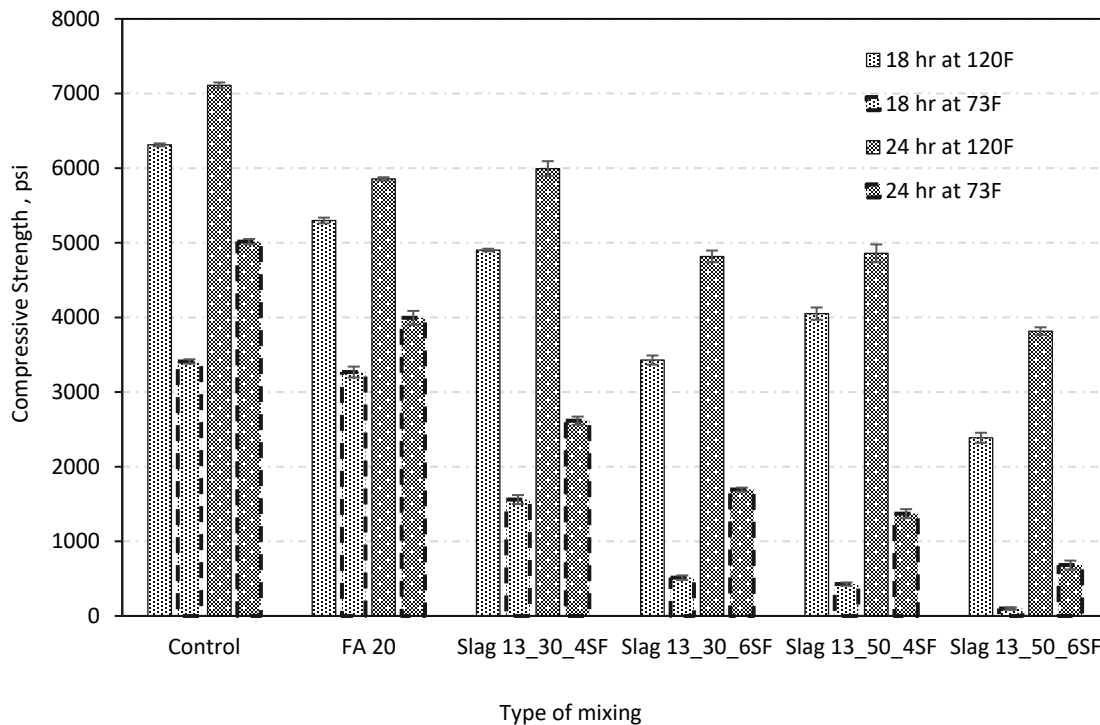
Figure 38: Comparison of compressive strength of concrete containing fly ash, slag 13 with 30% and 50% cement replacement with having 4% and 6% silica fume at 18 and 24 hr under lab temperature (73°F) and elevated temperature (120°F) curing

As illustrated in Figure 39, among the ternary blended mixings, only the mixture with slag 13 with 30% slag and 4% silica fume surpassed the control strength at 7 days. However, all the ternary blended mixtures showed higher strength than the mixture containing fly ash at 7 and 28 days.
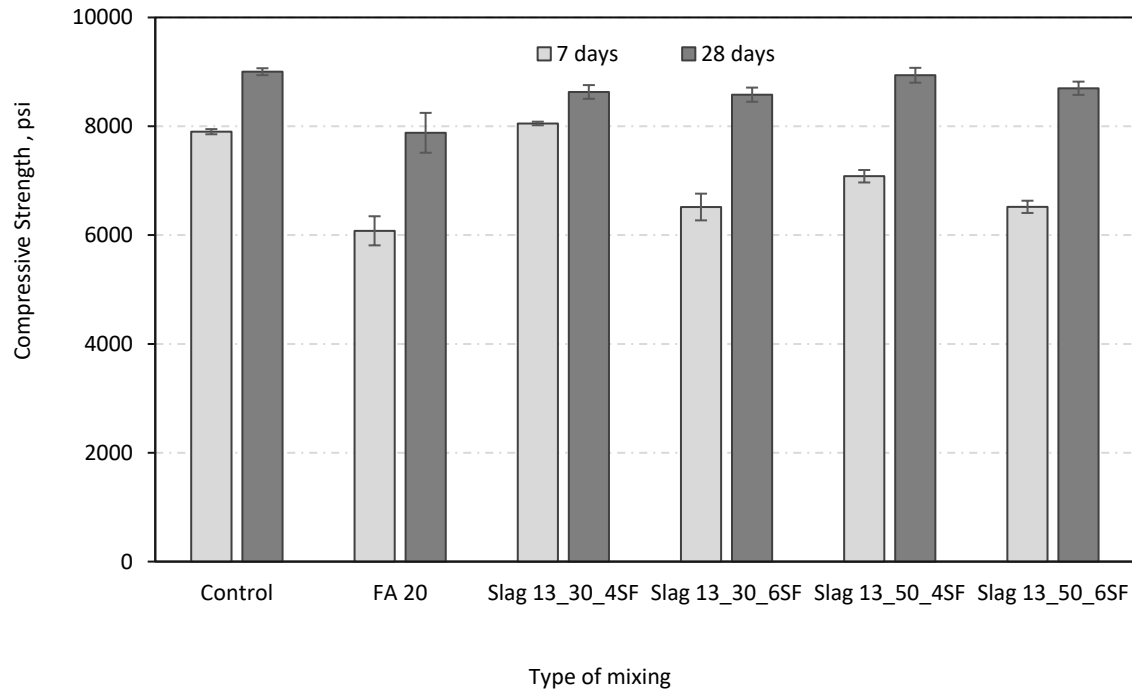
Figure 39: Comparison of compressive strength of concrete containing fly ash, slag 13 with 30% and 50% cement replacement with having 4% and 6% silica fume at 7 and 28 days under lab temperature (73°F) curing

5.2.2.   Resistivity

5.2.2.1.   Surface Resistivity

Figure 40 and Figure 41 show the surface resistivity of concrete mixtures with 20% fly ash and three different slags (slag 9, slag 13, and slag 18), each with at varying cement replacement levels (30%, 40% and 50%) under accelerated curing. The samples were cured in limewater either using the accelerated curing procedure described in ASTM C1202, or lab curing (73°F). Among the samples that experienced accelerated curing (Figure 40), the control mixture without fly ash or slag had the lowest surface electrical resistivity compared to the fly ash and slag mixtures. This was expected; as many SCMs refine the pore structure and increase the resistivity of the pore solution by binding alkalis [152]. All of the mixtures made with slag exhibited higher surface resistivity under accelerated curing than the control mixture. As shown in Figure 40, a trendline was fit to the resistivity measured for with each type of slag. The slag replacement level required to give equivalent performance to the 20% fly ash mixture was found by setting the trendline equal to the resistivity measured on the 20% fly ash mixture. The slag replacement levels required to give equivalent performance were found to be 40.5% and 39.5% for slag 9 and 13, while the slag 18 replacement level required for equivalent performance was higher than 50%.

59

Figure 40: Electrical surface resistivity of concrete containing fly ash, slag 9, slag 13 and slag 18 mixtures at 28 days under accelerated curing (100°F)

Figure 41 illustrates the surface resistivity of the binary mixtures at 28 days under lab temperature curing. From Figure 41 it can be seen that, fly ash mixtures had similar surface resistivity values as the control at 28 days when cured at lab temperature curing. This can be attributed to the slower rate at which pozzolanic reactions occur between the fly ash and calcium hydroxide generated by OPC hydration at lab temperature at early ages [153]. However, all slag mixtures demonstrated higher surface resistivity under lab temperature curing compared to control and fly ash mixtures. As shown in Figure 41, all of the concrete mixtures made with slag had higher resistivity values at 28 days than the control or mixture made with 20% fly ash. The same methodology used to find the slag replacement levels required to achieve equivalent resistivity values as the mixture containing 20% fly ash for the accelerated curing samples was used on the samples cured at room temperature. At 28 days, replacement levels greater than 9% were shown to give surface resistivity values greater than that of the 20% fly ash mixture.

Figure 41: Electrical surface resistivity of concrete containing fly ash, slag 9, slag 13 and slag 18 mixtures at 28 days under lab temperature curing (73°F)

In the Figure 42 and Figure 43, surface resistivity is shown for concrete mixtures containing fly ash and all three slags at 56 days and 91 days lab temperature curing. The results show that all of the concrete mixtures studied showed an increase in surface resistivity with age. This behavior is consistent with increased hydration with time, which directly affects the electrical resistivity. Lab temperature-cured samples containing slag showed small increases in resistivity between 28 and 56 days, and 56 and 91 days. As shown in Figure 42, at 56 days mixtures made with at least 12% slag would be expected to have surface resistivity values equaling or exceeding that of the 20% fly ash mixture. As shown in Figure 43, 30.9% slag would be required to produce concrete with equivalent surface resistivity to that of 20% fly ash at 91 days.
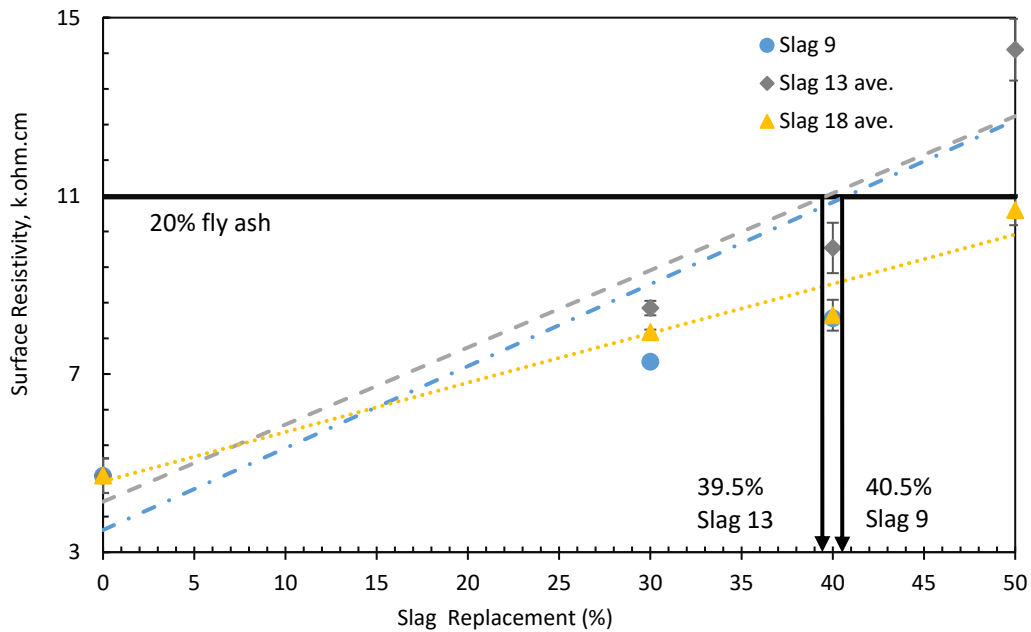
Figure 42: Electrical surface resistivity of concrete containing fly ash, slag 9, slag 13, and slag 18 mixtures at 56 days under lab temperature curing (73°F)
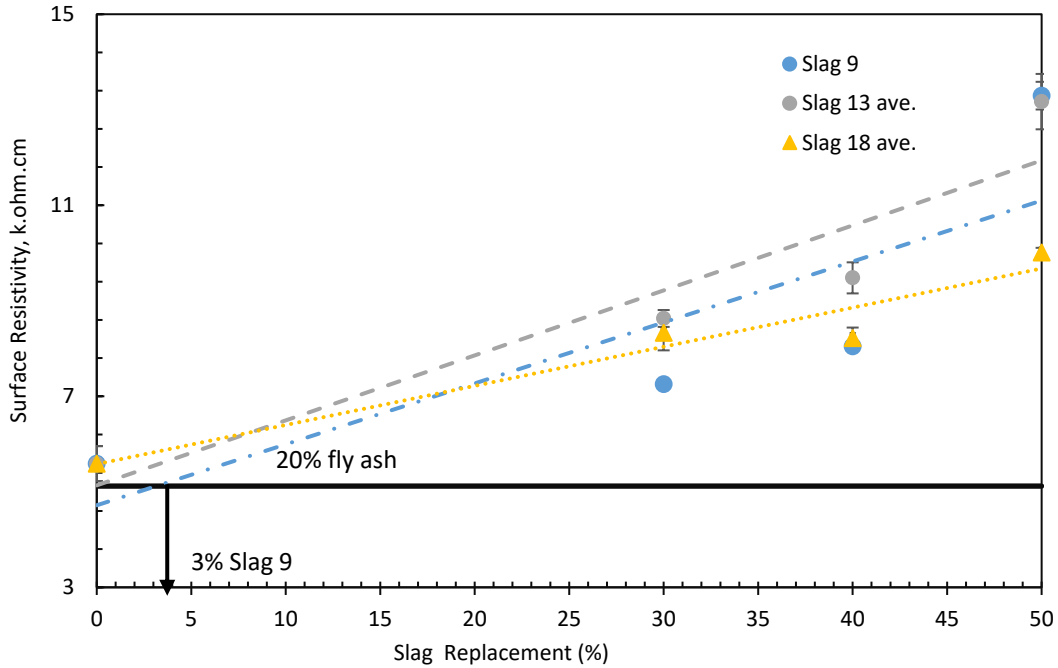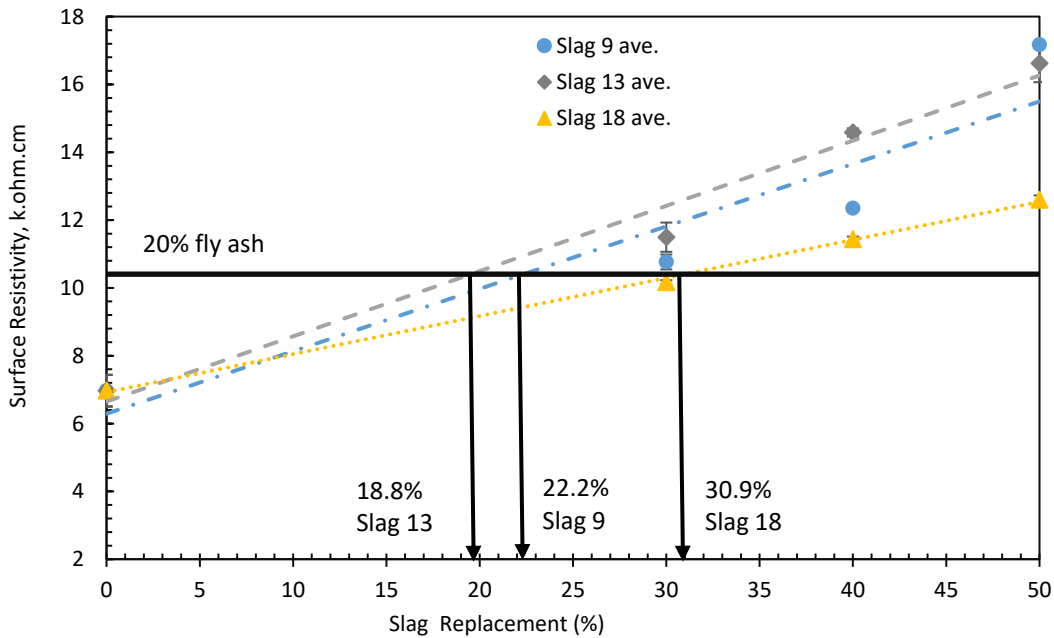

Figure 43: Electrical surface resistivity of concrete containing fly ash, slag 9, slag 13, and slag 18 at 91 days under lab temperature curing (73°F)

62

Figure 44 illustrates the surface electrical resistivity of concrete with ternary blended mixtures containing 4% and 6% silica fume with cement slag replacements of 30% and 50% with accelerated and lab curing at different ages. Figure 44 shows that the addition of silica fume greatly enhanced the concrete surface resistivity and above that measured for the 20% fly ash mixture in all ternary mixtures tested. In all cases, it is observed that ternary blended mixtures with 4% and 6% silica fume showed similar surface resistivity values, with the highest difference of 1.85 kΩ-cm observed between slag 13_30% with 4 and 6% silica fume at 91 days lab temperature curing. This shows the diminishing return of increased silica fume replacement levels on durability.
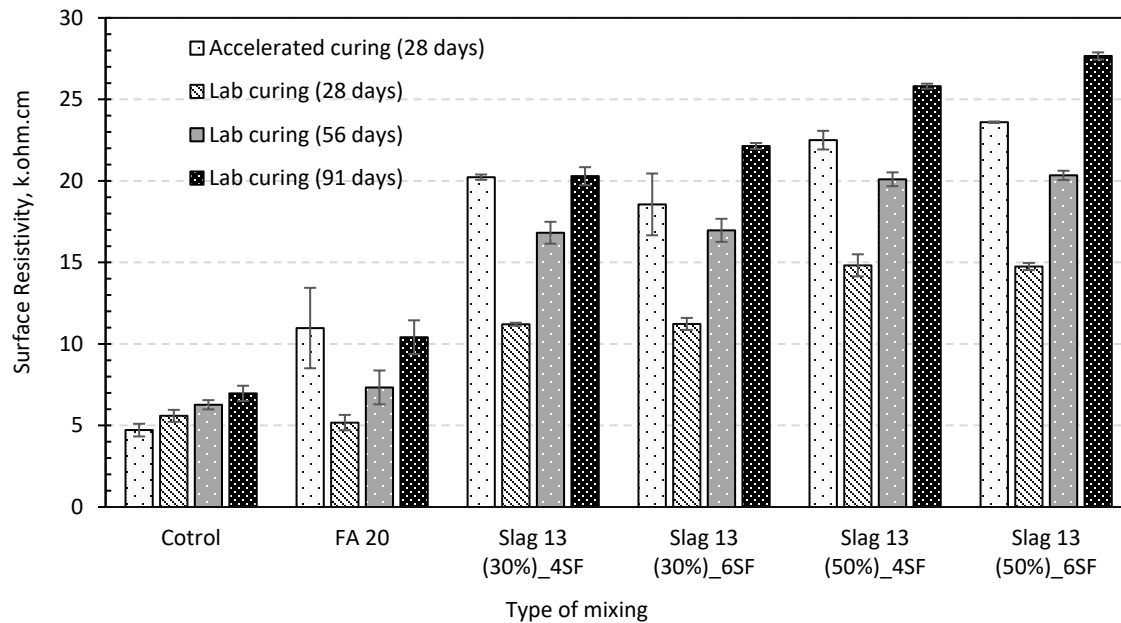
Figure 44: Electrical surface resistivity of ternary blended concrete containing slag with 4% and 6% silica fume under accelerated (100°F) and lab curing (73°F) with different ages (28, 56, 91)

5.2.2.2. Bulk Resistivity

The bulk electrical resistivity results under accelerated curing and lab curing at 28 days are shown in Figure 45 and Figure 46. It is evident from the results that surface electrical resistivity and bulk electrical resistivity exhibit similar trends. Trendlines of the bulk resistivity for samples cured using the accelerated method (Figure 45), a 40.8% replacement of cement with slag 9 or slag 18 and a 32% replacement of cement with slag 13 would produce concrete with a similar bulk resistivity to 20% fly ash.

Figure 45: Bulk electrical resistivity of concrete containing fly ash, slag 9, slag 13, and slag 18 mixtures at 28 days under accelerated curing (100°F)
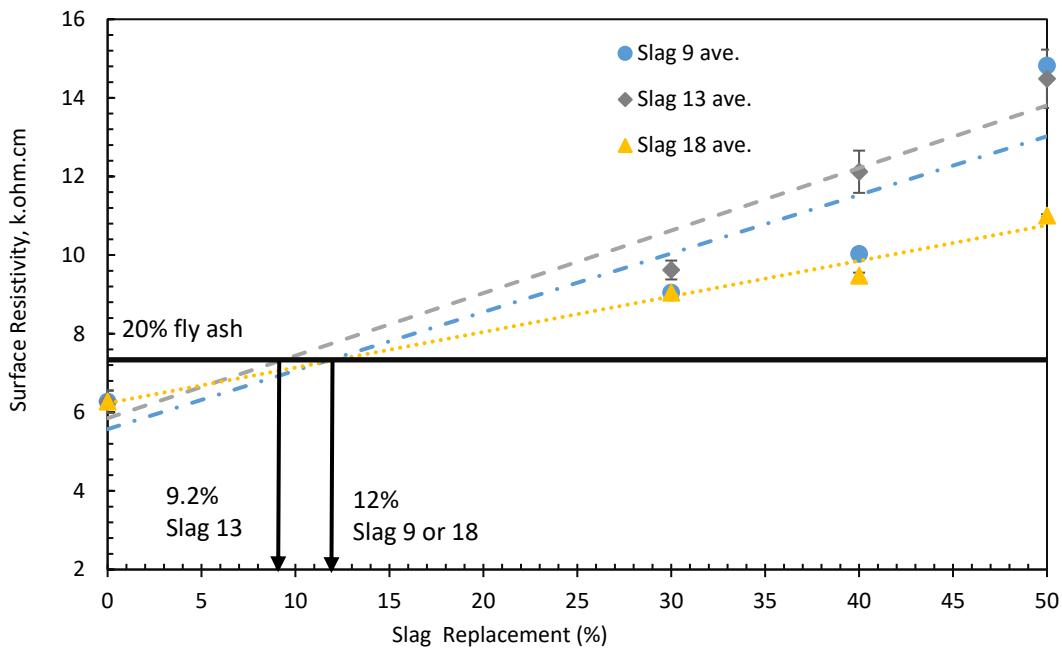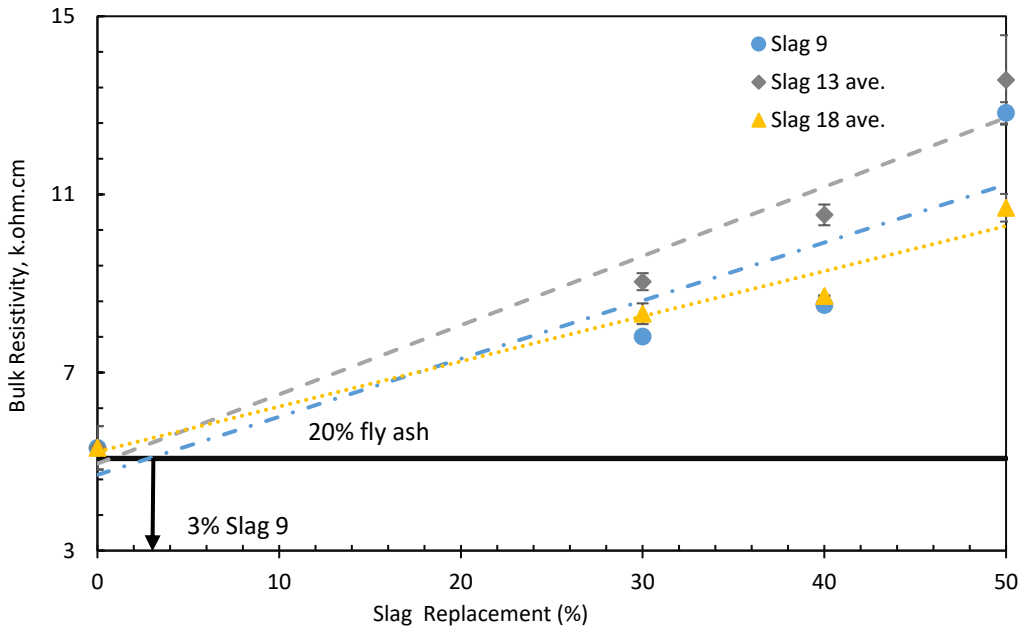

Figure 46: Bulk electrical resistivity of concrete containing fly ash, slag 9, slag 13 and slag 18 mixtures at 28 days under lab curing (73°F)

64

As illustrated in Figure 46, the bulk resistivity of all slag mixtures was higher than that of the control mix as well as the mixture with fly ash. Bulk resistivity values shown in Figure 47 at 56 days showed a similar trend to surface resistivity with the slag mixtures (slag 9, slag 13, and slag 18). As expected, concrete resistivity increased with age. There was little improvement in the resistance of concrete containing slag from 28 days to 56 days, whereas the resistance was much higher for the 20% fly ash mixture from 28 days to 56 days. Concrete resistivity significantly improved when slag replacement levels were > 40% in all types of slag mixtures. In order to achieve concrete bulk resistance equivalent to 20% fly ash at 56 days, 14.2% replacement of cement with slag 9 was necessary, whereas, for slag 13 and slag 18, 11.7% and 17.7% were needed, respectively.
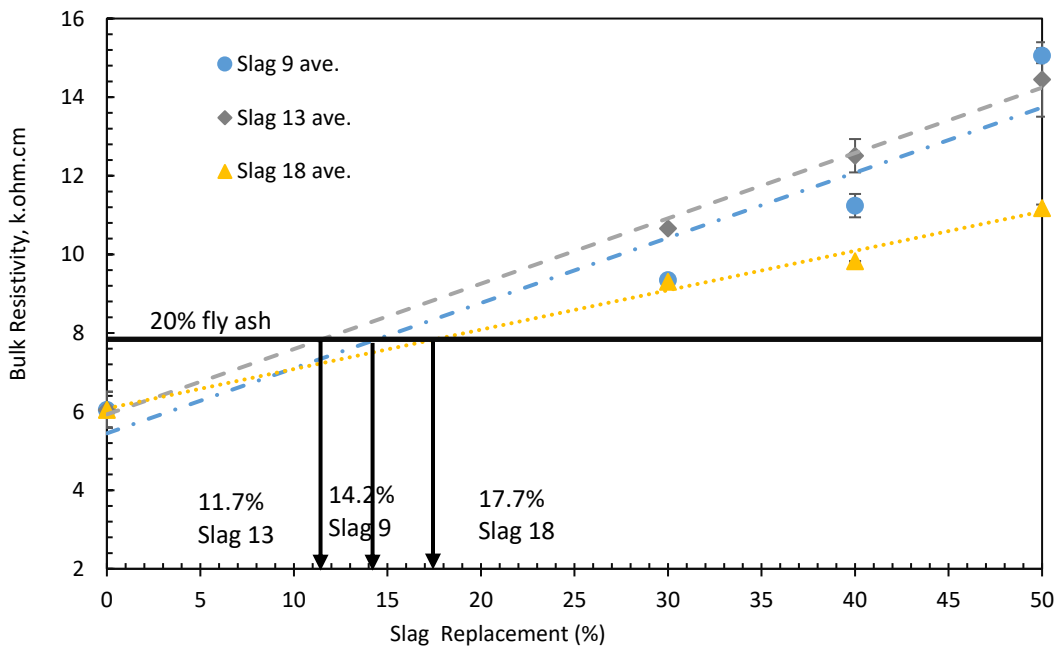
Figure 47: Bulk electrical bulk resistivity of concrete containing fly ash, slag 9, slag 13 and slag 18 mixtures at 56 days under lab curing (73°F)

Figure 48 shows an increase in electrical resistivity in concrete samples tested following 91 days of hydration. The fly ash mixture performance improved by 121% between 28 and 91 days, showing the slower reactivity but eventual excellent performance. An analysis of the bulk resistivity trendlines for each slag by replacement level showed that slag 9 should be substituted for 26% of cement to achieve concrete bulk resistance equivalent to 20% fly ash, while slag 13 and slag 18 require replacements of 24.1% and 36.2%, respectively.
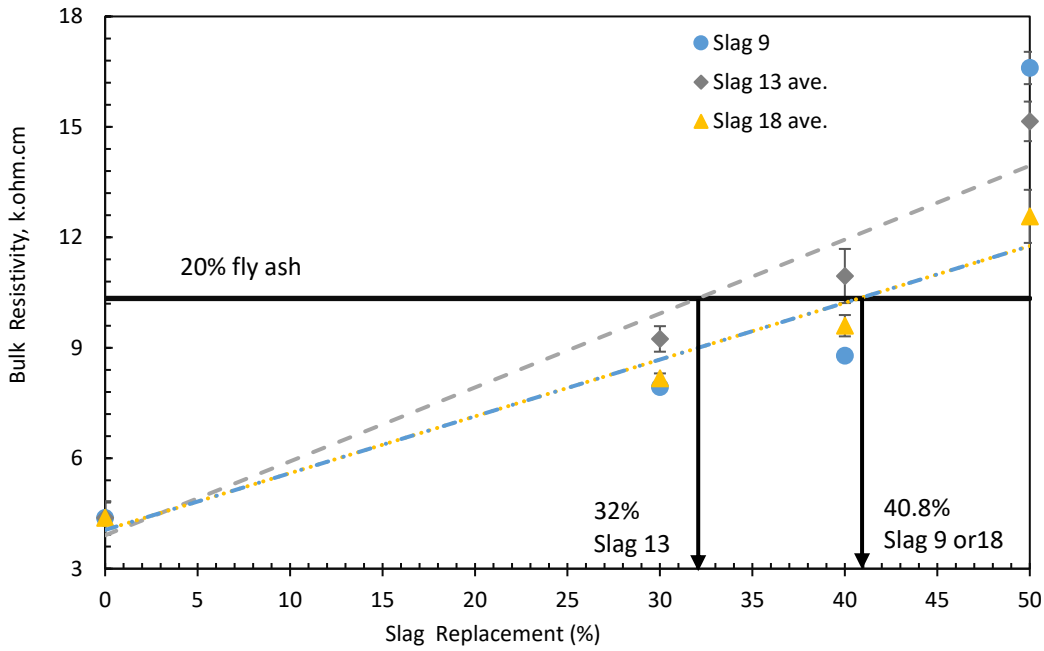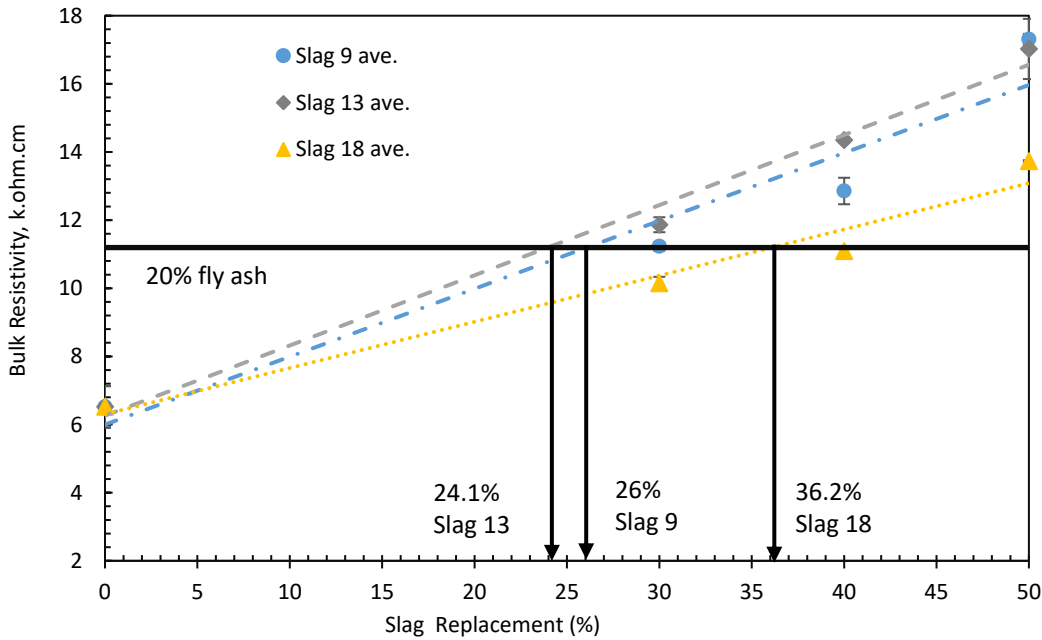
Figure 48: Bulk electrical resistivity of concrete containing fly ash, slag 9, slag 13, and slag 18 mixtures at 91 days under lab curing (73°F)

A comparison of ternary blend bulk electrical resistivity under accelerated curing and lab temperature curing at 28, 56, and 91 days is shown in Figure 49. Like surface resistivity, ternary blended mixtures exhibited greater bulk resistivity than control and fly ash mixtures in all ages.
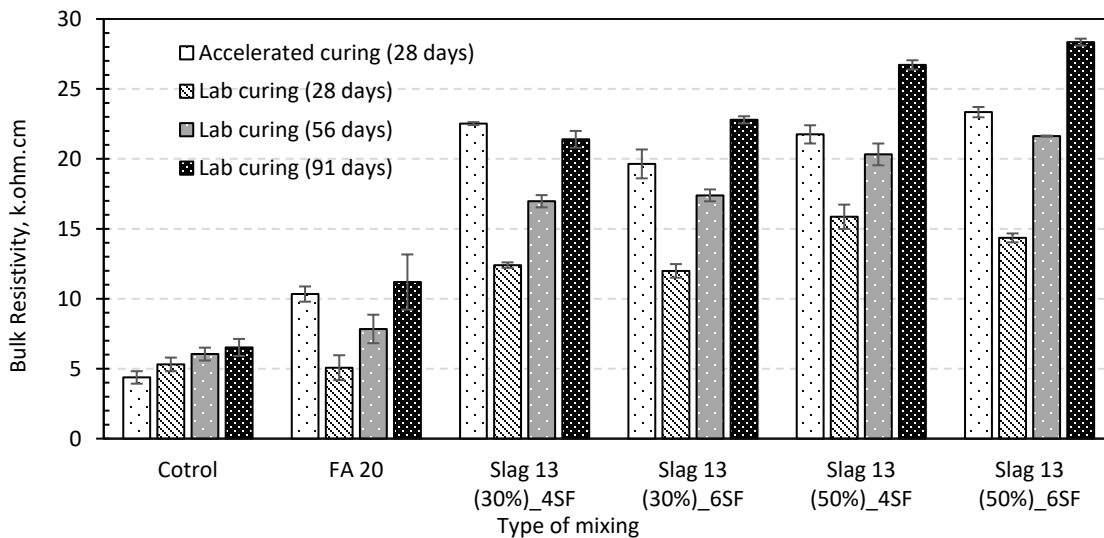
Figure 49: Electrical bulk resistivity of ternary blended concrete containing slag with 4% and 6% silica fume under accelerated (100°F) and lab curing (73°F) at different ages (28, 56, 91)

5.2.2.3. Comparison of Standard and Accelerated Curing

A comparison of surface and bulk resistivity of standard curing specimens for all ages with respect to accelerated curing specimens at 28 days is illustrated in Figure 50 and Figure 51. The results of accelerated curing for surface resistivity are similar to those of lab curing for 56 days (Figure 50). Some variations in material activation energy and temperature dependence may be expected depending on the cementitious material used and chemical composition. This method appears to be effective for accelerating durability testing and should be further examined.
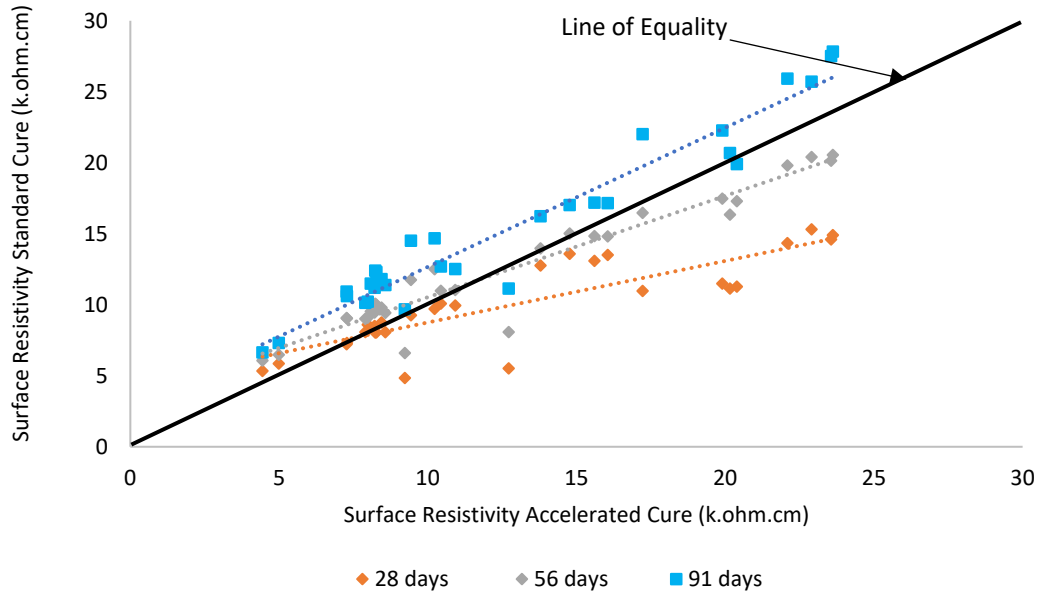
Figure 50: Comparison of surface resistivity between standard (73°F) and accelerated curing (100°F)

In Figure 51, accelerated curing results for bulk resistivity show values between 56 and 91 days of lab cure, demonstrating the effectiveness of accelerated curing tests to speed up long-term durability testing.
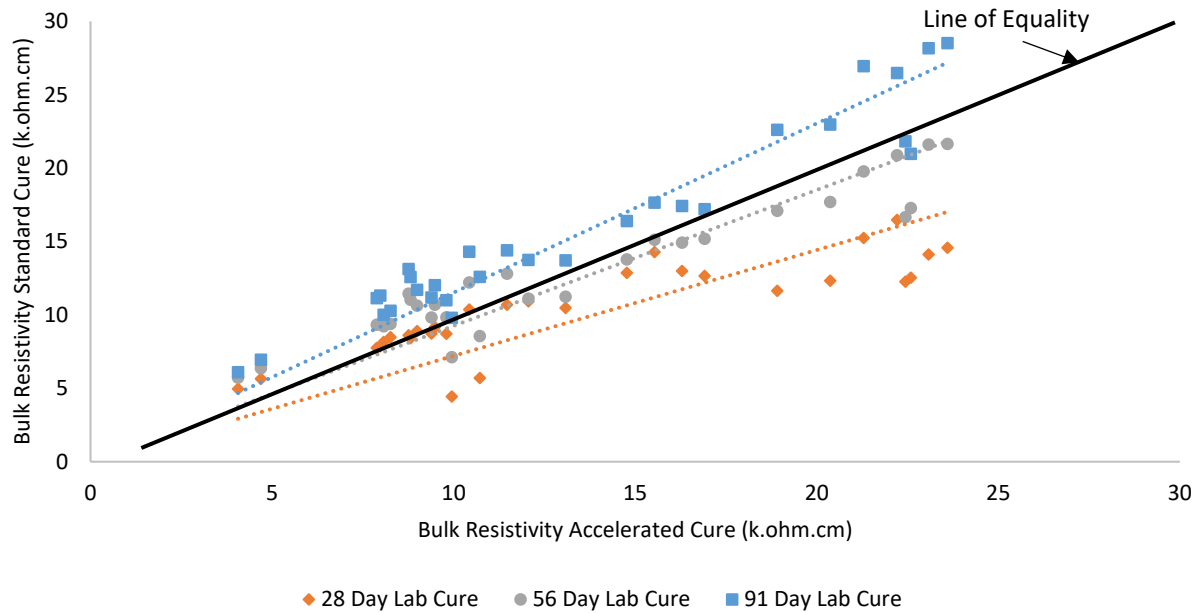
Figure 51: Comparison of bulk resistivity between standard (73°F) and accelerated curing (100°F)

5.2.3. Sulfate Durability

5.2.3.1. Sulfate Mortar Bar Length Change Measurements

Figure 52 shows the 6-month expansion results for the standard ASTM C1012 [149] tests and accelerated sulfate attack test results for the control and 20% Class F fly ash mixtures. In general, the accelerated exposure method showed faster rates of expansion during the first month of exposure when compared to standard ASTM C1012. As expected, the control mixture (100% Type IL cement) exhibited the highest expansion with the standard ASTM C1012 and accelerated exposure method. However, the expansion at 6 months was below 0.1% under both test methods and would be considered a moderate sulfate resisting cement. When compared to standard exposure, the results for the control mixture under the accelerated method showed a slight increase in expansion during the first month, but did not show a significant increase in expansion at 6 months. Although the control mixture with the accelerated method displayed a slightly faster expansion rate until 4 months of 0.0455% than the standard method of 0.0435%, at 6 months the control mixture with standard measurements (0.0758%) outpaced the accelerated mixture (0.0557%). It is possible that the maturity of the mortar may be influenced when subjected to the drying regime at 100°F. The mortar bars tested according to ASTM C1012 were immersed immediately in a sulfate solution as soon as they reached the specified strength (20 MPa). This means that the standard-cured samples could have had a lower degree of hydration when exposed to sulfates compared to the accelerated mortar bars that could have continued to hydrate for a period of time during the beginning of the drying period at 38°C (100°F). Further, the Type 1L cement used in this study, which contained 12.3% calcium carbonate and 5.4% aluminate content, may have bound some of the aluminate compounds in monocarboaluminate

68

and stabilized ettringite, leaving less alumina available to form monosulfoaluminate during curing. This would give less potential for monosulfoaluminate conversion to ettringite when exposed to external sulfates [118] . On the other hand, the results for the 20% Class F fly ash mortars subjected to the drying regime to accelerate sulfate ingress exhibited similar trends to the standard ASTM C1012 method but with a slightly higher rate of expansion early on because of the vacuum saturation with sulfate solution. Compared to the Type 1L cement samples, the mixture containing 20% Class F fly ash exhibited better performance with an expansion rate below 0.05% after 6 months of measurements at both standard exposure (0.0332%) and accelerated exposure (0.0348%).
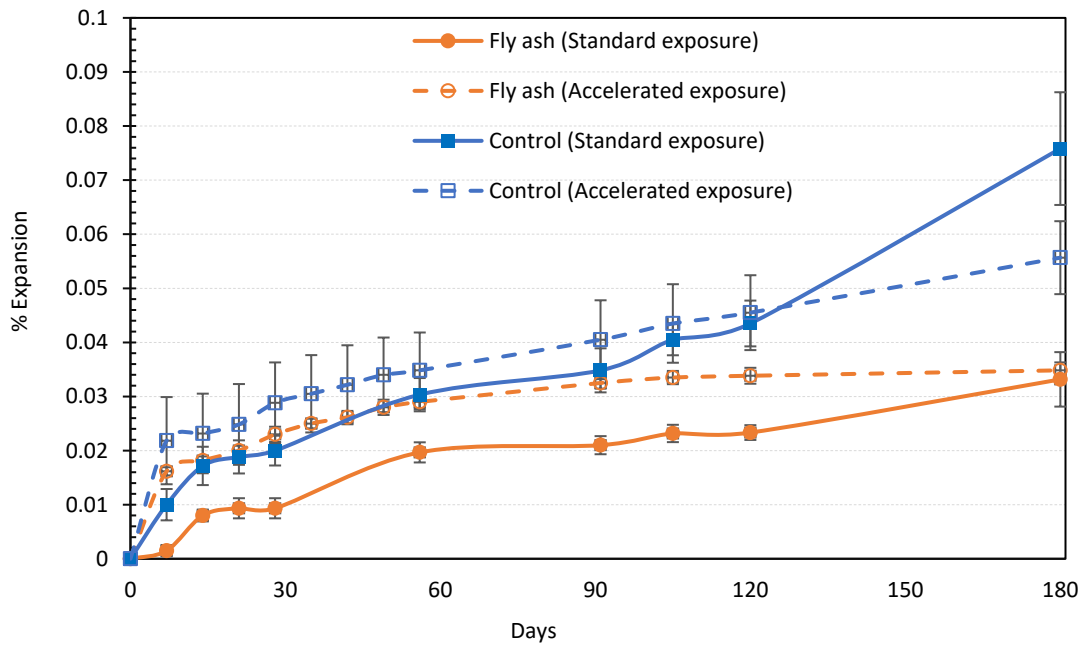
Figure 52: Comparison of the expansion behavior of control and fly ash specimens under standard and accelerated exposure

With the exception of the control mixture, all binary mixtures demonstrated expansion rates below 0.05% under both the standard ASTM C1012 and accelerated exposure method. Figure 53 shows the expansion rate of the three different slags tested with 30% cement replacement under standard ASTM C1012 and accelerated exposure.
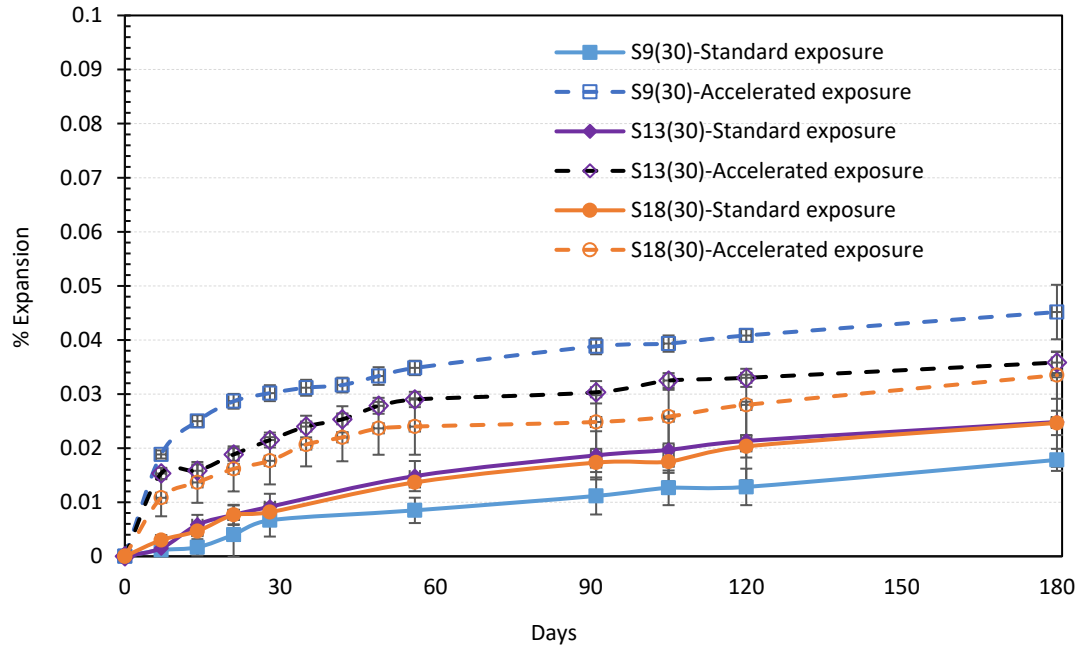
Figure 53: Comparison of the expansion behavior of slag 9, slag 13 and slag 18 with 30% cement replacement under standard and accelerated exposure

The sulfate expansion rate of three different slags with 40% cement replacement under ASTM C1012 and accelerated exposure is illustrated in Figure 54. At standard ASTM C1012 exposure, one mortar bar from slag 18 with 40% replacement completely deteriorated after 8 weeks, with the remaining five mortar bars available for testing. Moreover, those remaining mortar bars had fine hairline cracks along the length with significant deterioration around the corner; however, the mortar bars were still intact and measurable at 6 months. It is likely that the abrupt expansion observed in mortar bars is attributed to a differential volume change from high sulfate concentration gradients caused by the low mortar permeability that led to fine hairline cracks on the surface, causing significant deterioration in the corners. Interestingly, similar mortar bars under accelerated exposure showed no deterioration and hairline cracks after 6 months with an expansion of 0.0302%. The driving of the sodium sulfate solution into the mortar bars through the vacuum impregnation technique is thought to cause more uniform sulfate penetration into the specimen [14], which results in less differential volume change between the surface and core of the mortar bar.
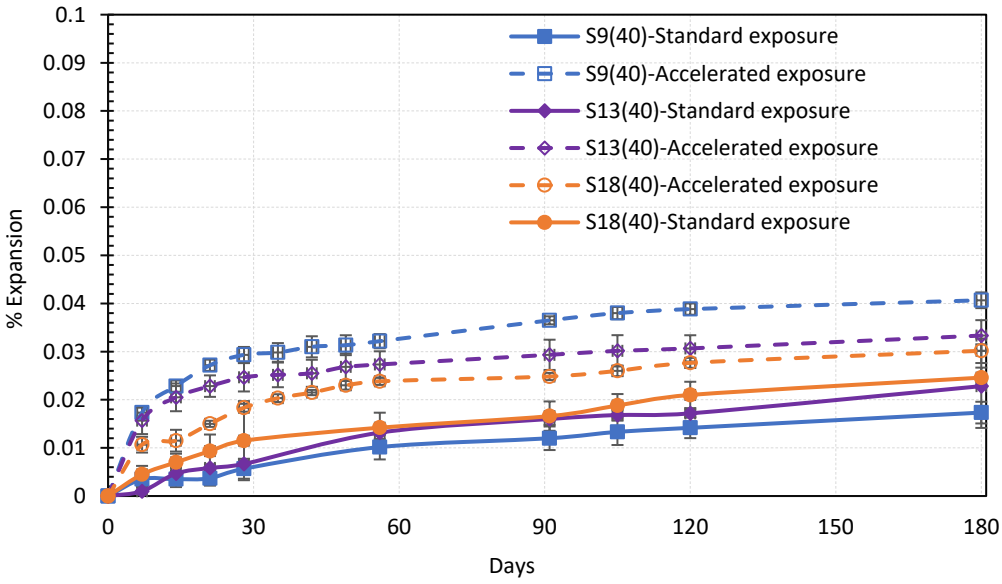
Figure 54: Comparison of the expansion behavior of slag 9, slag 13 and slag 18 with 40% cement replacement under standard and accelerated exposure

Figure 55 shows the expansion of the mortar bars made with 50% slag replacement through 6 months of exposure. All mixtures showed excellent performance, with all qualifying as high sulfate resisting cementitious systems.
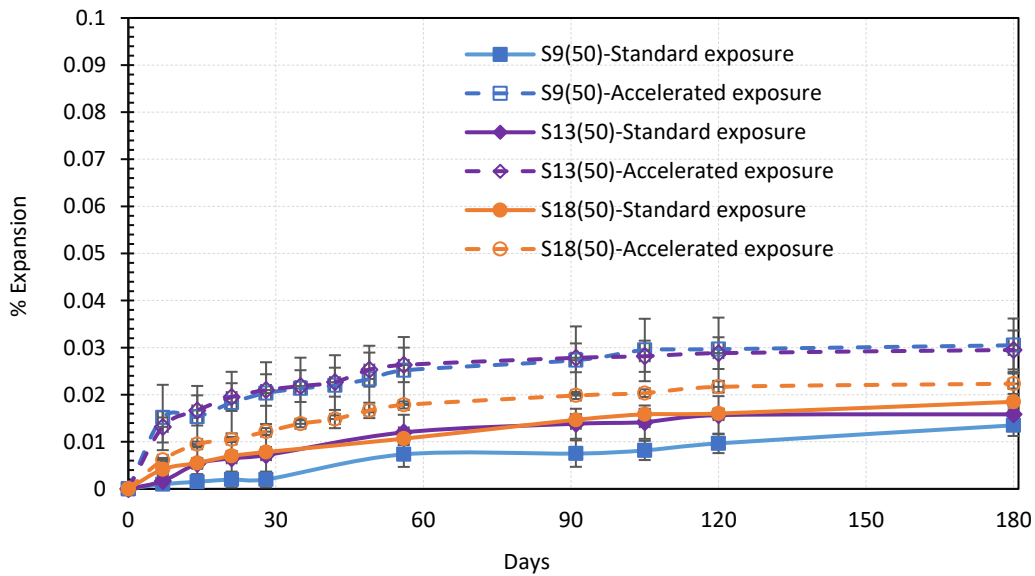
Figure 55: Comparison of the expansion behavior of slag 9, slag 13 and slag 18 with 50% cement replacement under standard and accelerated exposure

In Figure 56 and Figure 57, the expansion rates of ternary blended mixtures are shown under standard and accelerated conditions. As expected, in all ternary mixtures, the expansion rate during the first month was higher under accelerated exposure. All ternary mixtures showed low expansion and would be classified as high sulfate resisting cementitious systems.
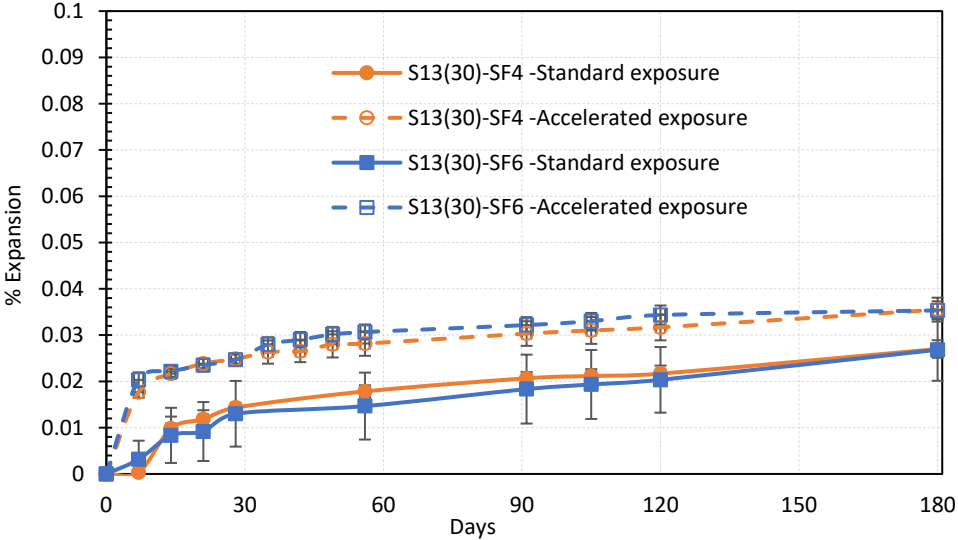
Figure 56: Comparison of the expansion behavior of ternary blended mixture of 30% cement replacement with slag 13 and having 4% and 6% silica fume under standard and accelerated exposure
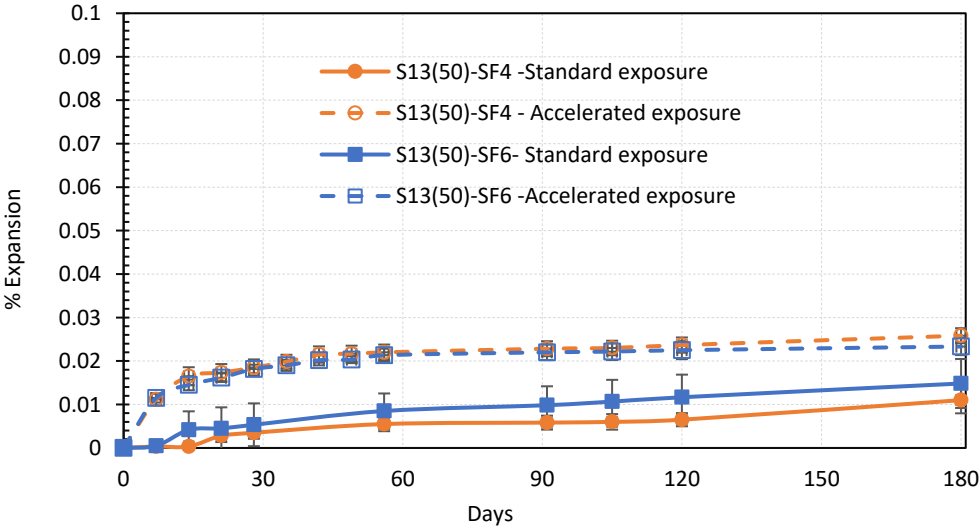
Figure 57: Comparison of the expansion behavior of ternary blended mixture of 50% cement replacement with slag 13 and having 4% and 6% silica fume under standard and accelerated exposure

72

5.2.3.2.   Rapid Sulfate Permeability Measurements

A version of ASTM C1202 [3] with a 5% sodium sulfate used instead of the sodium chloride solution was run to see if this test method could be used as a performance test for concrete sulfate durability. As shown in Figure 58, the limits of ASTM C1202 are shown along with the measured data. Concrete containing slag cement had lower charge passed during the 6 hr test than concrete containing 20% fly ash. This can be attributed to the slower rate at which the pozzolanic reaction occurs between fly ash and the lime produced by OPC hydration, giving higher permeability for the mixture containing fly ash [153].
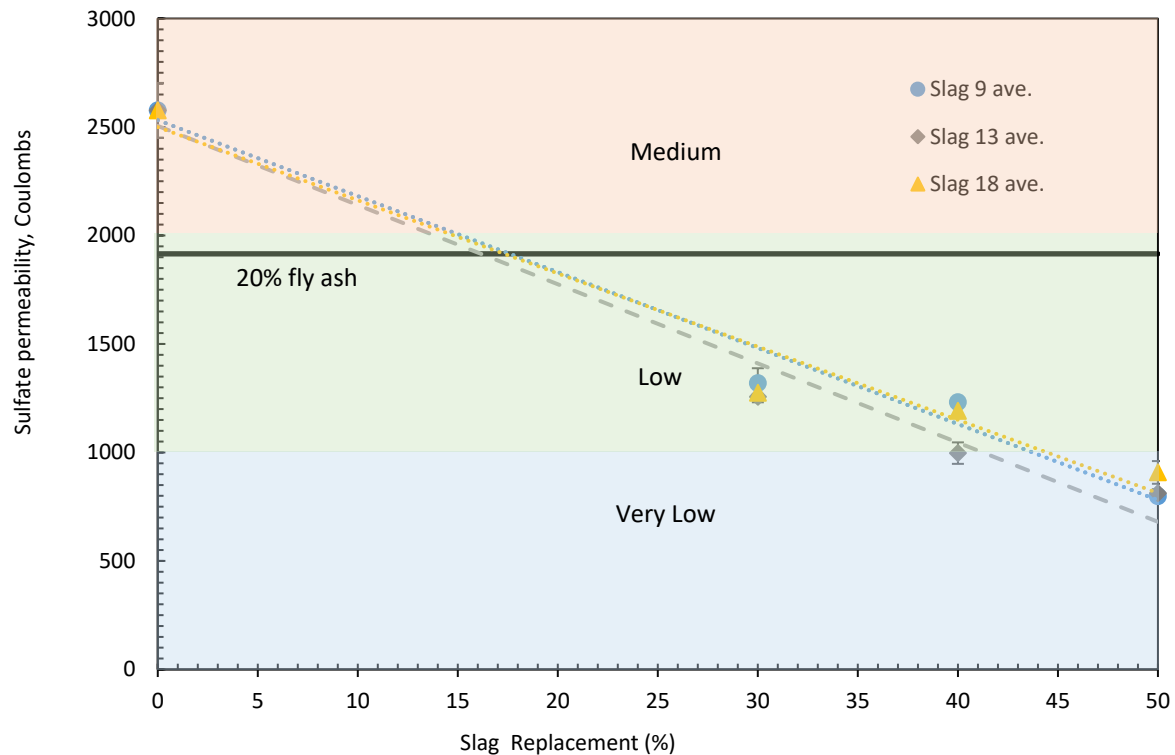
Figure 58: Rapid sulfate permeability of binary blended concrete containing fly ash, slag 9, slag 13 and slag 18

As illustrated in Figure 58, a 26% decrease in charge passed was observed by adding 20% fly ash to concrete. Compared to control mixtures, all binary mixtures of slag with 30% cement replacement exhibited an approximately 50% decrease in charge passed. In all cases, results showed that a lower charge was passed through concrete mixtures with larger slag replacement levels. This is not surprising since it is expected that secondary hydration interactions will increase with the increasing proportion of slag cement, which will stimulate the production of calcium silicate hydrate gel. A greater amount of slag cement supplementation will have a greater effect on modifying macro pores and depleting porosity. An earlier study by Megat et.al.

73

[153] found that replacing cement with 40% slag led to a significant decrease in macropore volume (>50 nm), and an increase in mesopore volume (15-30 nm) compared to control at 28 days. These effects were attributed to the pozzolanic activity and the filler effect of the slag cement. As a result of the pozzolanic reaction, calcium hydroxide ($Ca(OH)_2$) undergoes a transformation into secondary C–S–H gel, refining the pore structure by transforming coarser pores into finer ones [153].

Figure 59 displays the penetrability of sulfate ions through concrete using ternary mixtures containing slag 13 and silica fume according to the modified ASTM 1202 test. The results show that increasing slag and silica fume replacement levels improved the permeability as expected. According to Megat et.al. the SF particles serve as nucleation sites for calcium silicate hydrate, C–S–H, and $Ca(OH)_2$ [153]. A further advantage of SF particles is that they act as microfillers, densifying the transition zone, and thus improving matrix-aggregate bond formation and microstructural development [65].
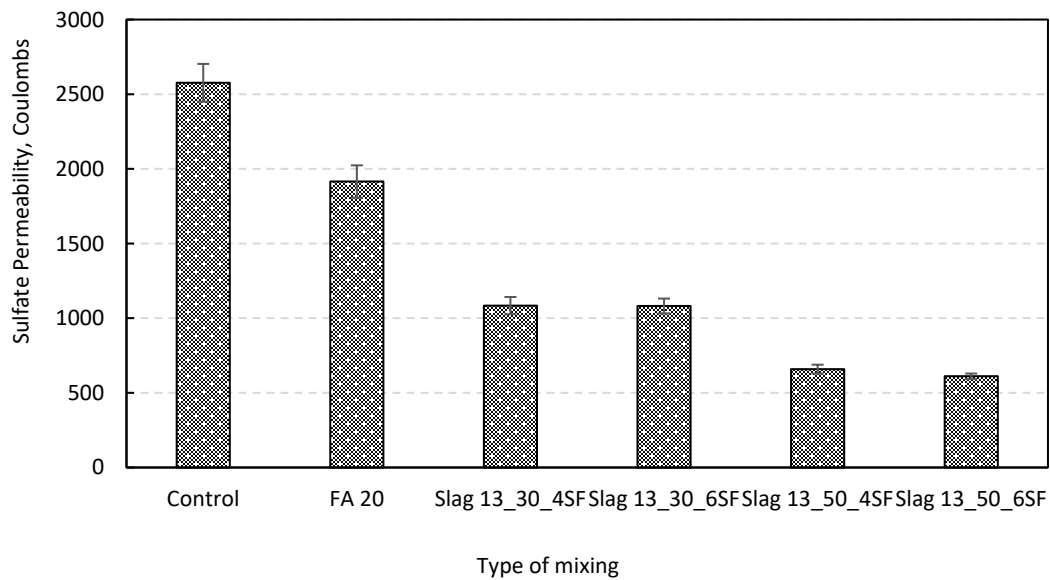
Figure 59: Rapid sulfate permeability of ternary blended concrete with 30% and 50% cement replacement with slag 13 containing 4% and 6% silica fume

5.3. Recommendations

The following recommendations can be drawn from the experimental results of this study:

1. Precast concrete producers want to achieve a compressive strength of 5200-psi (80% of 28-day compressive strength of FDOT Class V concrete) at 18 hours in order to detension prestressing. At elevated temperature curing, all mixtures tested containing slag with an alumina content $\geq$ 13% (slag 13 and slag 18) were capable of reaching the 5200 psi target strength at 18 hr and were above that of the 20% fly ash mixes. However, the low alumina slag had slightly lower strength. These results show that it is possible to achieve early-age

74

strengths needed for precast concrete production, however some slags may require additional heat or accelerators to achieve such strengths.

2. Accelerated curing of concrete gave bulk and surface resistivity results in between that measured for 56 and 91 days of curing at lab temperature. Accelerated curing of concrete samples should be considered by FDOT for future acceptance testing.

3. The worst performing slag for resistivity, slag 18, required 30.9% slag to achieve equivalent surface resistivity as 20% fly ash at 91 days, and 36.2% slag to achieve equivalent bulk resistivity as 20% fly ash at 91 days.

4. All mortar mixtures made with slag cement had a 6 month expansion in ASTM C1012 less than 0.05% when used with a Type IL cement and would be classified as having a high sulfate resistance. According to the ACI 201 Guide to Durable Concrete [154], these materials would qualify to be used in very severe sulfate environments (S3) when used with a w/cm at or below 0.40. Because FDOT class V, VI, and VII concrete limits the w/cm to 0.37, all of the slags studied could be used in these classes with replacement levels of 30% or greater.

5. Based on the resistivity and sulfate attack test results, it is recommended that the minimum slag replacement level required for chloride durability in Class V, VI, and VII concrete be changed to allow slag cement replacement levels of 35% when used with Type IL cement.

6.   CONCLUSIONS

A literature review and experimental study was conducted to assess the strength development and durability of concrete made with slag replacement levels up to 50%. The findings from compressive strength, resistivity, and external sulfate durability testing of binary and ternary blended concrete mixtures can be summarized as follows:

- At elevated temperature curing, all mixtures tested containing slag with an alumina content $\geq$ 13% (slag 13 and slag 18) were capable of reaching the 5200 psi target strength at 18 hr and were above that of the 20% fly ash mixes. However, the low alumina slag had slightly lower strength. These results show that it is possible to achieve early-age strengths needed for precast concrete production, however some slags may require additional heat or accelerators to achieve such strengths.

- Accelerated curing of concrete gave bulk and surface resistivity results in between that measured for 56 and 91 days of curing at lab temperature.

- The worst performing slag for resistivity, slag 18, required 30.9% slag to achieve equivalent surface resistivity as 20% fly ash at 91 days, and 36.2% slag to achieve equivalent bulk resistivity as 20% fly ash at 91 days.

- All mortar mixtures made with slag cement had a 6 month expansion in ASTM C1012 less than 0.05% when used with a Type IL cement and would be classified as having a high sulfate resistance. According to the ACI 201 Guide to Durable Concrete, these materials would qualify to be used in very severe sulfate environments (S3) when used with a w/cm at or below 0.40. Because FDOT class V, VI, and VII concrete limits the w/cm to 0.37, all the slags studied could be used in these classes with replacement levels of 30% or greater.

6.1. Recommendations

Based on the project findings, the following recommendations can be made:

- Accelerated curing of concrete samples should be considered by FDOT for future acceptance testing.

- Based on the resistivity and sulfate attack test results, it is recommended that the minimum slag replacement level required for chloride durability in Class V, VI, and VII concrete be changed to allow slag cement replacement levels of 35% when used with Type IL cement.

6.2. Recommendations for Future Work

This study recommends the following future studies based on its findings:

76

- Measure the slag activation energy at elevated temperatures for slag-blended concrete, including the effects of slag fineness and composition.

- Conduct a study on the effect of high-temperature exposure on high alumina slag-blended specimens to improve durability under sulfate attack.

- Develop an accelerated concrete sulfate attack test.

REFERENCES

[1]   F. Nosouhian, M. Fincan, N. Shanahan, Y. P. Stetsko, K. A. Riding, and A. Zayed, "Effects of slag characteristics on sulfate durability of Portland cement-slag blended systems," *Constr Build Mater*, vol. 229, p. 116882, 2019, doi: 10.1016/j.conbuildmat.2019.116882.

[2]   ASTM C618-22, "Standard Specification for Coal Fly Ash and Raw or Calcined Natural Pozzolan for Use in Concrete 1," *ASTM*, pp. 1–5, 2022, doi: 10.1520/C0618-22.

[3]   ASTM C1202-22, "Standard Test Method for Electrical Indication of Concrete's Ability to Resist Chloride Ion Penetration," *ASTM*, pp. 1–8, 2022, doi: 10.1520/C1202-22E01.

[4]   ASTM C595-21, "Standard Specification for Blended Hydraulic Cements," *ASTM* , pp. 1–10, 2021, doi: 10.1520/C0595_C0595M-21.

[5]   ASTM C989-22, "Standard Specification for Slag Cement for Use in Concrete and Mortars," *ASTM*, pp. 1–7, 2022, doi: 10.1520/C0989_C0989M-22.

[6]   ASTM C1240-20, "Standard Specification for Silica Fume Used in Cementitious Mixtures," *ASTM* , pp. 1–7, 2020, doi: 10.1520/C1240-20.

[7]   R. Alyousef, W. Abbass, F. Aslam, and S. A. A. Gillani, "Characterization of high-performance concrete using limestone powder and supplementary fillers in binary and ternary blends under different curing regimes," *Case Studies in Construction Materials*, vol. 18, Jul. 2023, doi: 10.1016/j.cscm.2023.e02058.

[8]   ACI 233, "233R-17 Guide to use of slag cement in concrete and mortar," *American Concrete Institute*, pp. 1–37, 2017.

[9]   Y. Zhou *et al.*, "The effect of temperature rise inhibitor on the hydration and strength development of slag/fly ash blended cement paste," *Constr Build Mater*, vol. 395, p. 132307, Sep. 2023, doi: 10.1016/j.conbuildmat.2023.132307.

[10]   S. H. Han, J. K. Kim, and Y. D. Park, "Prediction of compressive strength of fly ash concrete by new apparent activation energy function," *Cem Concr Res*, vol. 33, no. 7, pp. 965–971, Jul. 2003, doi: 10.1016/S0008-8846(03)00007-3.

[11]   F. Deschner, B. Lothenbach, F. Winnefeld, and J. Neubauer, "Effect of temperature on the hydration of Portland cement blended with siliceous fly ash," *Cem Concr Res*, vol. 52, pp. 169–181, 2013, doi: 10.1016/j.cemconres.2013.07.006.

[12]   M. Jabbour, O. O. Metalssi, M. Quiertant, and V. Baroghel-Bouny, "A Critical Review of Existing Test-Methods for External Sulfate Attack," *Materials*, vol. 15, no. 21. MDPI, Nov. 01, 2022. doi: 10.3390/ma15217554.

78

[13]   X. Lv, L. Yang, J. Li, and F. Wang, "Roles of fly ash, granulated blast-furnace slag, and silica fume in long-term resistance to external sulfate attacks at atmospheric temperature," *Cem Concr Compos*, vol. 133, Oct. 2022, doi: 10.1016/j.cemconcomp.2022.104696.

[14]   F. Aguayo, "External Sulfate Attack of Concrete: An Accelerated Test Method, Mechanism, and Mitigation Techniques," University of Texas at Austin, 2016.

[15]   Y. Yang, B. Zhan, J. Wang, Y. Zhang, and W. Duan, "Damage evolution of cement mortar with high volume slag exposed to sulfate attack," *Constr Build Mater*, vol. 247, p. 118626, 2020, doi: 10.1016/j.conbuildmat.2020.118626.

[16]   S. Ogawa, T. Nozaki, K. Yamada, H. Hirao, and R. D. Hooton, "Improvement on sulfate resistance of blended cement with high alumina slag," *Cem Concr Res*, vol. 42, no. 2, pp. 244–251, 2012, doi: 10.1016/j.cemconres.2011.09.008.

[17]   ACI 130, "Report on the Role of Materials in Sustainable Concrete Construction," *American Concrete Institute*, pp. 1–41, 2019, [Online]. Available: www.concrete.org

[18]   ACI 201.2, "Guide to Durable Concrete," *American Concrete Institute*, pp. 1–87, 2016.

[19]   ACI 231, "Report on early-age cracking : causes, measurement, and mitigation," *American Concrete Institute*, pp. 1–51, 2010.

[20]   ITG 10, "Practitioner's guide for alternative cements," *American Concrete Institute*, pp. 1–21, 2018.

[21]   ACI 211.4, "Guide for selecting proportions for high-strength concrete using portland cement and other cementitious materials," *American Concrete Institute*, pp. 1–30, 2008.

[22]   ACI 329.1, "Minimum Cementitious Materials Content in specifications," *American Concrete Institute*, pp. 1–5, 2018, [Online]. Available: www.concrete.org

[23]   M. A. Megat Johari, J. J. Brooks, S. Kabir, and P. Rivard, "Influence of supplementary cementitious materials on engineering properties of high strength concrete," *Constr Build Mater*, vol. 25, no. 5, pp. 2639–2648, 2011, doi: 10.1016/j.conbuildmat.2010.12.013.

[24]   L. Wang, H. Quan, and Q. Li, "Evaluation of slag reaction efficiency in slag-cement mortars under different curing temperature," *Materials*, vol. 12, no. 18, Sep. 2019, doi: 10.3390/ma12182875.

[25]   P. Taylor, S. Tritsch, T. van Dam, Sutter Larry, and Fick Gary, *Integrated Materials and Construction Practices for Concrete Pavement: A State-of-the-Practice Manual*, no. 2. 2019.

[26]   Kosmatka, S.H., and J. A. Farny, "Design and control of concrete mixtures," *Portland cement association*, 2016.

[27]   J. Lizarazo-Marriaga, P. Claisse, and E. Ganjian, "Effect of Steel Slag and Portland Cement in the Rate of Hydration and Strength of Blast Furnace Slag Pastes," *Journal of Materials in Civil Engineering*, pp. 153–160, 2011, doi: 10.1061/ASCEMT.1943-5533.0000149.

[28]   Slag Cement Association (SCA), "Compressive and flexural strength," *Farmington Hills, MI 48331*, no. 14, 2013.

[29]   E. Özbay, M. Erdemir, and H. I. Durmuş, "Utilization and efficiency of ground granulated blast furnace slag on concrete properties - A review," *Constr Build Mater*, vol. 105, pp. 423–434, 2016, doi: 10.1016/j.conbuildmat.2015.12.153.

[30]   S. C. Pal, A. Mukherjee, and S. R. Pathak, "Investigation of hydraulic activity of ground granulated blast furnace slag in concrete," *Cem Concr Res*, vol. 33, no. 9, pp. 1481–1486, 2003, doi: 10.1016/S0008-8846(03)00062-0.

[31]   S. U. Khan, M. F. Nuruddin, T. Ayub, and N. Shafiq, "Effects of different mineral admixtures on the properties of fresh concrete," *The Scientific World Journal*. ScientificWorld Ltd., 2014. doi: 10.1155/2014/986567.

[32]   R. K. Patra and B. B. Mukharjee, "Fresh and hardened properties of concrete incorporating ground granulated blast furnace slag-A review," *Advances in concrete construction*, vol. 4, no. 4, pp. 283–303, 2016, doi: 10.12989/acc.2016.4.4.283.

[33]   Q. Q. Zhang, J. Z. Liu, and J. P. Liu, "Influence of ground slag on the rheology of mortar," *Applied Mechanics and Materials*, vol. 438–439, pp. 67–71, 2013, doi: 10.4028/www.scientific.net/AMM.438-439.67.

[34]   R. A. T. Cahyani and Y. Rusdianto, "An Overview of Behaviour of Concrete with Granulated Blast Furnace Slag as Partial Cement Replacement," *IOP Conf Ser Earth Environ Sci*, vol. 933, no. 1, 2021, doi: 10.1088/1755-1315/933/1/012006.

[35]   D. K. Panesar, "Supplementary cementing materials," *Developments in the Formulation and Reinforcement of Concrete*, pp. 55–85, Jan. 2019, doi: 10.1016/B978-0-08-102616-8.00003-4.

[36]   S. Choi and S. Pyo, "Fresh and hardened properties of portland cement-slag concrete activated using the by-product of the liquid crystal display manufacturing process," *Materials*, vol. 13, no. 19, pp. 1–15, 2020, doi: 10.3390/ma13194354.

[37]   ASTM C403, "Standard Test Method for Time of Setting of Concrete Mixtures by Penetration Resistance," 1999.

80

[38] M. D. Luther and W. J. Mikols, "Effect of Ground Granulated Blast-Furnace Slag Fineness on High-Strength Concrete Properties," *Proceedings of the Utilization of High-Strength Concrete Symposium*, vol. 2, pp. 822–829, 1993.

[39] S. Dai, H. Zhu, D. Zhang, Z. Liu, S. Cheng, and J. Zhao, "Insights to compressive strength, impermeability and microstructure of micro-expansion steel slag cement under constraint conditions," *Constr Build Mater*, vol. 326, no. October 2021, p. 126540, 2022, doi: 10.1016/j.conbuildmat.2022.126540.

[40] F. J. Hogan and J. W. Meusel, "Evaluation for Durability and Strength Development of a Ground Granulated Blast-Furnace Slag," *Cement, Concrete and Aggregates*, vol. 3, no. 1, pp. 40–52, 1981.

[41] L. Ting, W. Qiang, and Z. Shiyu, "Effects of ultra-fine ground granulated blast-furnace slag on initial setting time, fluidity and rheological properties of cement pastes," *Powder Technol*, vol. 345, pp. 54–63, 2019, doi: 10.1016/j.powtec.2018.12.094.

[42] S. Siddiqui and K. A. Riding, "Effect of Calculation Methods on Cement Paste and Mortar Apparent Activation Energy," *Adv Civ Eng Mater*, vol. 1, no. 1, Sep. 2012, doi: 10.1520/acem20120011.

[43] S. A. Wade, J. M. Nixon, A. K. Schindler, and R. W. Barnes, "Effect of temperature on the setting behaviour of concrete," *Journal of Materials in Civil Engineering*, vol. 22, no. 3, pp. 214–222, 2010, doi: 10.6028/jres.018.007.

[44] H.-M. Yang, S.-J. Kwon, N. V. Myung, J. K. Singh, H.-S. Lee, and S. Mandal, "Evaluation of strength development in concrete with ground granulated blast furnace slag using apparant activation energy," *Materials*, vol. 13, pp. 1–14, 2020.

[45] A. Sedaghat, N. Shanahan, and A. Zayed, "Predicting One-Day, Three-Day, and Seven-Day Heat of Hydration of Portland Cement," *Journal of Materials in Civil Engineering*, vol. 27, no. 9, pp. 1–12, 2015, doi: 10.1061/(asce)mt.1943-5533.0001220.

[46] N. Nakamura, M. Sakai, and R. N. Swamy, "Effect of Slag Fineness on the Development of Concrete Strength and Microstructure," *American Concrete Institute*, vol. 132, pp. 1343–1366, 1992.

[47] K. Yang *et al.*, "Investigation of effects of Portland cement fineness and alkali content on concrete plastic shrinkage cracking," *Constr Build Mater*, vol. 144, no. July, pp. 279–290, 2017, doi: 10.1016/j.conbuildmat.2017.03.130.

[48] S. J. Barnett, M. N. Soutsos, S. G. Millard, and J. H. Bungey, "Strength development of mortars containing ground granulated blast-furnace slag: Effect of curing temperature and determination of apparent activation energies," *Cem Concr Res*, vol. 36, no. 3, pp. 434–440, 2006, doi: 10.1016/j.cemconres.2005.11.002.

81

[49] J. L. Poole, K. A. Riding, K. J. Folliard, M. C. G. Juenger, and A. K. Schindler, "Methods for Calculating Activation Energy for Portland Cement," *ACI Mater J*, vol. 104, no. 1, pp. 303–311, 2007.

[50] C. C. Castellano, V. L. Bonavetti, H. A. Donza, and E. F. Irassar, "The effect of w/b and temperature on the hydration and strength of blastfurnace slag cements," *Construction and Building Materials*, vol. 111. Elsevier Ltd, pp. 679–688, May 15, 2016. doi: 10.1016/j.conbuildmat.2015.11.001.

[51] K. A. Riding, J. L. Poole, K. J. Folliard, M. C. G. Juenger, and A. K. Schindler, "New Model for Estimating Apparent Activation Energy of Cementitious Systems," *ACI Mater J*, vol. 108, no. 5, pp. 550–557, 2011, [Online]. Available: www.concrete.org

[52] Slag Cement Association (SCA), "Producing Precast and Prestressed Concrete with Slag Cement." [Online]. Available: www.slagcement.org

[53] A. Vollpracht, M. Soutsos, and F. Kanavaris, "Strength development of GGBS and fly ash concretes and applicability of fib model code's maturity function – A critical review," *Constr Build Mater*, vol. 162, pp. 830–846, Feb. 2018, doi: 10.1016/j.conbuildmat.2017.12.054.

[54] M. Soutsos, A. Hatzitheodorou, J. Kwasny, and F. Kanavaris, "Effect of in situ temperature on the early age strength development of concretes with supplementary cementitious materials," *Constr Build Mater*, vol. 103, pp. 105–116, Jan. 2016, doi: 10.1016/j.conbuildmat.2015.11.034.

[55] Y. Sumra, S. Payam, Z. Ibrahim, H. Hashim, and M. Panjehpour, "Crossover E ff ect in Cement-Based Materials: A Review," *applied sciences*, vol. 9, pp. 1–18, 2019.

[56] X. Zhang, "Quantitative Microstructural Characterisation of Concrete Cured under Realistic Temperature Conditions," *EPFL*, 2007.

[57] H. S. Lee, X. Y. Wang, L. N. Zhang, and K. T. Koh, "Analysis of the optimum usage of slag for the compressive strength of concrete," *Materials*, vol. 8, no. 3, pp. 1213–1229, 2015, doi: 10.3390/ma8031213.

[58] J. Backus, D. McPolin, M. Basheer, A. Long, and N. Holmes, "Exposure of mortars to cyclic chloride ingress and carbonation," *Advances in Cement Research*, vol. 25, no. 1, pp. 3–11, 2013.

[59] O. R. Ogirigbo and L. Black, "Chloride binding and diffusion in slag blends: Influence of slag composition and temperature," *Constr Build Mater*, vol. 149, pp. 816–825, 2017, doi: 10.1016/j.conbuildmat.2017.05.184.

[60] H. Peng, J. Yin, and W. Song, "Mechanical and hydraulic behaviors of eco-friendly pervious concrete incorporating fly ash and blast furnace slag," *Applied Sciences (Switzerland)*, vol. 8, no. 6, 2018, doi: 10.3390/app8060859.

[61] J. Nakamoto, K. Togawa, T. Miyagawa, and M. Fujii, "Water permeability of high slag content concrete," *American Concrete Institute, ACI Special Publication*, vol. SP178, pp. 779–795, 1998, doi: 10.14359/6008.

[62] J. Valdez, "Bio-friendly slag cement benefit to the drainage systems for the city of Houston," *Slag cement association*, no. 246, 2017.

[63] M. Otieno, H. Beushausen, and M. Alexander, "Effect of chemical composition of slag on chloride penetration resistance of concrete," *Cem Concr Compos*, vol. 46, pp. 56–64, 2014, doi: 10.1016/j.cemconcomp.2013.11.003.

[64] H. Jin *et al.*, "Iodide and chloride ions diffusivity, pore characterization and microstructures of concrete incorporating ground granulated blast furnace slag," *Journal of Materials Research and Technology*, vol. 16, pp. 302–321, 2022, doi: 10.1016/j.jmrt.2021.11.155.

[65] M. Gesoğlu, E. Güneyisi, and E. Özbay, "Properties of self-compacting concretes made with binary, ternary, and quaternary cementitious blends of fly ash, blast furnace slag, and silica fume," *Constr Build Mater*, vol. 23, no. 5, pp. 1847–1854, 2009, doi: 10.1016/j.conbuildmat.2008.09.015.

[66] Z. Shi *et al.*, "Role of calcium on chloride binding in hydrated Portland cement–metakaolin–limestone blends," *Cem Concr Res*, vol. 95, pp. 205–216, 2017, doi: 10.1016/j.cemconres.2017.02.003.

[67] A. Mehta, R. Siddique, T. Ozbakkaloglu, F. Uddin Ahmed Shaikh, and R. Belarbi, "Fly ash and ground granulated blast furnace slag-based alkali-activated concrete: Mechanical, transport and microstructural properties," *Constr Build Mater*, vol. 257, p. 119548, 2020, doi: 10.1016/j.conbuildmat.2020.119548.

[68] O. Kayali, M. S. H. Khan, and M. Sharfuddin Ahmed, "The role of hydrotalcite in chloride binding and corrosion protection in concretes with ground granulated blast furnace slag," *Cem Concr Compos*, vol. 34, no. 8, pp. 936–945, 2012, doi: 10.1016/j.cemconcomp.2012.04.009.

[69] K. Garg and K. Kapoor, "A review on ground granulated blast furnace slag as a cement replacing material," *International Journal of Engineering Research and Management (IJERM)*, vol. 03, no. 07, pp. 214–217, 2016.

[70] R. G. Pillai, R. Gettu, and M. Santhanam, "Use of supplementary cementitious materials (SCM) in reinforced concrete system-Benefits and limitation," *Revista ALCONPAT*, vol. 10, no. 2, pp. 147–164, 2020.

[71] J. L. Marriaga and P. Claisse, "The influence of the blast furnace slag replacement on chloride penetration in concrete," *Ingenieria e Investigacion*, vol. 31, no. 2, 2011.

[72] M. Amran *et al.*, "Slag uses in making an ecofriendly and sustainable concrete: A review," *Constr Build Mater*, vol. 272, p. 121942, 2021, doi: 10.1016/j.conbuildmat.2020.121942.

[73] T. Huyen Vu, L. C. Dang, G. Kang, and V. Sirivivatnanon, "Chloride induced corrosion of steel reinforcement in alkali activated slag concretes: A critical review," *Case Studies in Construction Materials*, vol. 16, no. April, p. e01112, 2022, doi: 10.1016/j.cscm.2022.e01112.

[74] X. Han, J. Feng, Y. Shao, and R. Hong, "Influence of a steel slag powder-ground fly ash composite supplementary cementitious material on the chloride and sulphate resistance of mass concrete," *Powder Technol*, vol. 370, pp. 176–183, 2020, doi: 10.1016/j.powtec.2020.05.015.

[75] S. Yoo and S. J. Kwon, "Effects of cold joint and loading conditions on chloride diffusion in concrete containing GGBFS," *Constr Build Mater*, vol. 115, pp. 247–255, 2016.

[76] J. Zhang *et al.*, "Chloride diffusion in alkali-activated fly ash/slag concretes: Role of slag content, water/binder ratio, alkali content and sand-aggregate ratio," *Constr Build Mater*, vol. 261, p. 119940, 2020, doi: 10.1016/j.conbuildmat.2020.119940.

[77] F. Qu, W. Li, Y. Guo, S. Zhang, J. L. Zhou, and K. Wang, "Chloride-binding capacity of cement-GGBFS-nanosilica composites under seawater chloride-rich environment," *Constr Build Mater*, vol. 342, no. PB, p. 127890, 2022, doi: 10.1016/j.conbuildmat.2022.127890.

[78] H. A. F. Dehwah, "Effect of sulphate contamination on chloride binding capacity of plain and blended cements," *Advances in Cement Research*, vol. 18, no. 1, pp. 7–15, 2006.

[79] A. Ipavec, T. Vuk, R. Gabrovšek, and V. Kaučič, "Chloride binding into hydrated blended cements: The influence of limestone and alkalinity," *Cem Concr Res*, vol. 48, pp. 74–85, 2013, doi: 10.1016/j.cemconres.2013.02.010.

[80] F. Leng, N. Feng, and X. Lu, "An experimental study on the properties of resistance to diffusion of chloride ions of fly ash and blast furnace slag concrete," *Cem Concr Res*, vol. 30, pp. 989–992, 2000.

[81] K. de Weerdt and H. Justnes, "The effect of sea water on the phase assemblage of hydrated cement paste," *Cem Concr Compos*, vol. 55, pp. 215–222, 2015, doi: 10.1016/j.cemconcomp.2014.09.006.

[82] R. Loser, B. Lothenbach, A. Leemann, and M. Tuchschmid, "Chloride resistance of concrete and its binding capacity- Comparison between experimental results and thermodynamic modelling," *Cem Concr Compos*, vol. 32, pp. 34–42, 2010.

[83] Q. Yuan, C. Shi, G. de Schutter, D. Audenaert, and D. Deng, "Chloride binding of cement-based materials subjected to external chloride environment- A review," *Construction and Building Materials*, vol. 23, no. 1, pp. 1–13, 2009.

[84] M. V. A. Florea and H. J. H. Brouwers, "Modelling of chloride binding related to hydration products in slag-blended cements," *Constr Build Mater*, vol. 64, pp. 421–430, 2014, doi: 10.1016/j.conbuildmat.2014.04.038.

[85] A. Zayed *et al.*, "Correlation of Slag Cement Composition with Durability of Portland Cement-Slag Concrete," *FDOT Report*, pp. 1–335, 2021.

[86] S. Caijun, H. Xiang, W. Xiaogang, W. Zemei, and D. S. Geert, "Effects of chloride ion binding on microstructure of cement pastes," *Journal of Materials in Civil Engineering*, vol. 29, no. 1, pp. 1–7, 2017.

[87] J. O. Ukpata, P. A. M. Basheer, and L. Black, "Performance of plain and slag-blended cements and mortars exposed to combined chloride-sulfate solution," *Advances in Cement Research*, vol. 30, no. 8, pp. 371–386, 2018.

[88] X. Chen, Y. He, L. Lu, F. Wang, and S. Hu, "Effects of curing regimes on the chloride binding capacity of cementitious materials," *Constr Build Mater*, vol. 342, no. PB, p. 127929, 2022, doi: 10.1016/j.conbuildmat.2022.127929.

[89] Y. Wang, Z. Shui, X. Gao, Y. Huang, R. Yu, and Q. Song, "Chloride binding capacity and phase modification of alumina compound blended cement paste under chloride attack," *Cem Concr Compos*, vol. 108, no. March 2019, p. 103537, 2020, doi: 10.1016/j.cemconcomp.2020.103537.

[90] Y. Wang, Z. Shui, X. Gao, R. Yu, Y. Huang, and S. Cheng, "Understanding the chloride binding and diffusion behaviors of marine concrete based on Portland limestone cement-alumina enriched pozzolans," *Constr Build Mater*, vol. 198, pp. 207–217, 2019, doi: 10.1016/j.conbuildmat.2018.11.270.

[91] Y. Chen, J. Gao, L. Tang, and X. Li, "Resistance of concrete against combined attack of chloride and sulfate under drying-wetting cycles," *Constr Build Mater*, vol. 106, pp. 650–658, 2016, doi: 10.1016/j.conbuildmat.2015.12.151.

[92] Y. Wang, Z. Shui, X. Gao, Y. Huang, R. Yu, and G. Ling, "Chloride binding behaviors of metakaolin-lime hydrated blends: Influence of gypsum and atmospheric carbonation," *Constr Build Mater*, vol. 201, pp. 380–390, Mar. 2019, doi: 10.1016/j.conbuildmat.2018.12.162.

[93] Y. Cao, L. Guo, B. Chen, and X. Fei, "Modeling early age hydration kinetics and the hydrated phase of cement paste blended with chloride and sulfate," *Constr Build Mater*, vol. 261, Nov. 2020, doi: 10.1016/j.conbuildmat.2020.120537.

[94] D. A. Kilcoyne, P. J. M. Monterio, S. Yoon, J. Ha, and S. R. Chae, "X-ray spectromicroscopic study of interactions between NaCl and Calcium silicate hydrates," *Magazine of Concrete Research*, vol. 66, no. 3, pp. 141–149, 2013.

[95] G. Plusquellec and A. Nonat, "Interactions between calcium silicate hydrate (C-S-H) and calcium chloride, bromide and nitrate," *Cem Concr Res*, vol. 90, pp. 89–96, 2016.

[96] Z. Yang *et al.*, "Improving the chloride binding capacity of cement paste by adding nano-Al2O3: The cases of blended cement pastes," *Constr Build Mater*, vol. 232, p. 117219, 2020, doi: 10.1016/j.conbuildmat.2019.117219.

[97] C. Arya, N. R. Buenfeld, and J. B. Newman, "Factors influencing chloride-binding in concrete," *Cem Concr Res*, vol. 20, no. 2, pp. 291–300, 1990, doi: 10.1016/0008-8846(90)90083-A.

[98] J. O. Ukpata, P. A. M. Basheer, and L. Black, "Slag hydration and chloride binding in slag cements exposed to a combined chloride-sulphate solution," *Constr Build Mater*, vol. 195, pp. 238–248, 2019, doi: 10.1016/j.conbuildmat.2018.11.055.

[99] J. O. Ukpata, P. A. M. Basheer, and L. Black, "Influence of temperature on the chloride binding of slag-blended cements in the presence of external sulphate," in *37th Cement and Cocrete Science Conference*, 2017, pp. 191–194.

[100] A. Dousti and M. Shekarchi, "Effect of exposure temperature on chloride-binding capacity of cementing materials," *Magazine of Concrete Research*, vol. 67, no. 15, pp. 821–832, 2015.

[101] K. de Weerdt, D. Orsáková, and M. R. Geiker, "The impact of sulphate and magnesium on chloride binding in Portland cement paste," *Cem Concr Res*, vol. 65, pp. 30–40, 2014, doi: 10.1016/j.cemconres.2014.07.007.

[102] M. Maes and N. de Belie, "Resistance of concrete and mortar against combined attack of chloride and sodium sulphate," *Cem Concr Compos*, vol. 53, pp. 59–72, 2014, doi: 10.1016/j.cemconcomp.2014.06.013.

[103] J. O. Ukpata, "Durability of slag-blended cements in composite chloride-sulphate environments," 2018, [Online]. Available: http://etheses.whiterose.ac.uk/20968/

[104] T. H. Wee, A. K. Suryavanshi, S. F. Wong, and A. K. M. A. Rahman, "Sulfate resistance of concrete containing mineral admixtures," *ACI Mater J*, vol. 97, pp. 536–549, 2000.

[105] R. D. Hooton and J. Emery, "Sulfate resistance of a canadian slag cement," *ACI Materials Journal* , vol. 87, pp. 547–555, 1990.

[106] M. Komljenović, Z. Baščarević, N. Marjanović, and V. Nikolić, "External sulfate attack on alkali-activated slag," *Constr Build Mater*, vol. 49, pp. 31–39, 2013, doi: 10.1016/j.conbuildmat.2013.08.013.

[107] Y. Ballim and P. C. Graham, "The effects of supplementary cementing materials in modifying the heat of hydration of concrete," *Materials and Strcutures*, vol. 42, no. 6, pp. 803–811, 2009.

[108] G. Zhang, C. Wu, D. Hou, J. Yang, D. Sun, and X. Zhang, "Effect of environmental pH values on phase composition and microstructure of Portland cement paste under sulfate attack," *Compos B Eng*, vol. 216, Jul. 2021, doi: 10.1016/j.compositesb.2021.108862.

[109] X. Zhu *et al.*, "Effect of Ca(OH)2 on shrinkage characteristics and microstructures of alkali-activated slag concrete," *Constr Build Mater*, vol. 175, pp. 467–482, Jun. 2018, doi: 10.1016/j.conbuildmat.2018.04.180.

[110] T. Zhang, T. Li, Z. Zhou, M. Li, Y. Jia, and C. Cheeseman, "A novel magnesium hydroxide sulfate hydrate whisker-reinforced magnesium silicate hydrate composites," *Compos B Eng*, vol. 198, Oct. 2020, doi: 10.1016/j.compositesb.2020.108203.

[111] Y. Wang, Y. Cao, L. Cui, Z. Si, and H. Wang, "Effect of external sulfate attack on the mechanical behavior of cemented paste backfill," *Constr Build Mater*, vol. 263, Dec. 2020, doi: 10.1016/j.conbuildmat.2020.120968.

[112] A. Bouikni, R. N. Swamy, and A. Bali, "Durability properties of concrete containing 50% and 65% slag," *Constr Build Mater*, vol. 23, no. 8, pp. 2836–2845, Aug. 2009, doi: 10.1016/j.conbuildmat.2009.02.040.

[113] Y. Thiebaut *et al.*, "Effects of stress on concrete expansion due to delayed ettringite formation," *Constr Build Mater*, vol. 183, pp. 626–641, Sep. 2018, doi: 10.1016/j.conbuildmat.2018.06.172.

[114] Y. Jeong, H. Park, Y. Jun, J. H. Jeong, and J. E. Oh, "Influence of slag characteristics on strength development and reaction products in a CaO-activated slag system," *Cem Concr Compos*, vol. 72, pp. 155–167, Sep. 2016, doi: 10.1016/j.cemconcomp.2016.06.005.

[115] M. H. Alyami, H. Mosavi, R. S. Alrashidi, M. A. Almarshoud, C. C. Ferraro, and K. A. Riding, "Lab and Field Study of Physical Sulfate Attack on Concrete Mixtures with Supplementary Cementitious Materials," *Journal of Materials in Civil Engineering*, vol. 33, no. 1, p. 04020397, 2021, doi: 10.1061/(asce)mt.1943-5533.0003500.

[116] J. Fu *et al.*, "Mechanisms of enhancement in early hydration by sodium sulfate in a slag-cement blend – Insights from pore solution chemistry," *Cem Concr Res*, vol. 135, Sep. 2020, doi: 10.1016/j.cemconres.2020.106110.

[117] S. Zheng, L. Qi, R. He, J. Wu, and Z. Wang, "Erosion damage and expansion evolution of interfacial transition zone in concrete under dry-wet cycles and sulfate erosion," *Constr Build Mater*, vol. 307, Nov. 2021, doi: 10.1016/j.conbuildmat.2021.124954.

[118] D. D. Higgins, "Increased sulfate resistance of ggbs concrete in the presence of carbonate," *Cem Concr Compos*, vol. 25, no. 8, pp. 913–919, 2003, doi: 10.1016/S0958-9465(03)00148-3.

[119] Z. Guo, P. Hou, Z. Xu, J. Gao, and Y. Zhao, "Sulfate attack resistance of tricalcium silicate modified with nano-silica and supplementary cementitious materials," *Constr Build Mater*, vol. 321, Feb. 2022, doi: 10.1016/j.conbuildmat.2022.126332.

[120] M. M. A. Elahi *et al.*, "Improving the sulfate attack resistance of concrete by using supplementary cementitious materials (SCMs): A review," *Constr Build Mater*, vol. 281, p. 122628, 2021, doi: 10.1016/j.conbuildmat.2021.122628.

[121] A.Zayed *et al.*, "Effect of blast furnace slag characteristics on durability of cementitious system for Florida concrete structures," *FDOT Report*, pp. 1–164, 2019.

[122] M. Whittaker, M. Zajac, M. Ben Haha, and L. Black, "The impact of alumina availability on sulfate resistance of slag composite cements," *Constr Build Mater*, vol. 119, pp. 356–369, 2016, doi: 10.1016/j.conbuildmat.2016.05.015.

[123] H. M. Yang *et al.*, "High-ferrite Portland cement with slag: Hydration, microstructure, and resistance to sulfate attack at elevated temperature," *Cem Concr Compos*, vol. 130, no. April, 2022, doi: 10.1016/j.cemconcomp.2022.104560.

[124] A. Hadjsadok, S. Kenai, L. Courard, F. Michel, and J. Khatib, "Durability of mortar and concretes containing slag with low hydraulic activity," *Cem Concr Compos*, vol. 34, no. 5, pp. 671–677, 2012, doi: 10.1016/j.cemconcomp.2012.02.011.

[125] S. Boudache, E. Rozière, A. Loukili, and L. Izoret, "Towards common specifications for low- and high-expansion cement-based materials exposed to external sulphate attacks," *Constr Build Mater*, vol. 294, p. 123586, 2021, doi: 10.1016/j.conbuildmat.2021.123586.

[126] M. Dener, M. Karatas, and M. Mohabbi, "Sulfate resistance of alkali-activated slag/Portland cement mortar produced with lightweight pumice aggregate," *Constr Build Mater*, vol. 304, no. March, p. 124671, 2021, doi: 10.1016/j.conbuildmat.2021.124671.

[127] ASTM C33-18, "Standard Specification for Concrete Aggregates," *ASTM*, pp. 1–8, 2018, doi: 10.1520/C0033_C0033M-18.

[128] ASTM C29-17, "Standard Test Method for Bulk Density ('Unit Weight') and Voids in Aggregate," *ASTM*, pp. 1–5, 2017, doi: 10.1520/C0029_C0029M-17a.

[129] ASTM D75-19, "Standard Practice for Sampling Aggregates," *ASTM*, pp. 1–7, 2019, doi: 10.1520/D0075_D0075M-19.

[130] ASTM C136-19, "Standard Test Method for Sieve Analysis of Fine and Coarse Aggregates," *ASTM*, pp. 1–5, 2019, doi: 10.1520/C0136_C0136M-19.

[131] ASTM C128-15, "Standard Test Method for Relative Density (Specific Gravity) and Absorption of Fine Aggregate," *ASTM*, pp. 1–6, 2015, doi: 10.1520/C0128-15.

[132] ASTM C127-15, "Standard Test Method for Relative Density (Specific Gravity) and Absorption of Coarse Aggregate," *ASTM*, pp. 1–5, 2015, doi: 10.1520/C0127-15.

[133] Y. Zhang, S. Zhang, Y. Chen, and O. Çopuroğlu, "The effect of slag chemistry on the reactivity of synthetic and commercial slags," *Constr Build Mater*, vol. 335, Jun. 2022, doi: 10.1016/j.conbuildmat.2022.127493.

[134] K. L. Scrivener, T. Füllmann, E. Gallucci, G. Walenta, and E. Bermejo, "Quantitative study of Portland cement hydration by X-ray diffraction/Rietveld analysis and independent methods," *Cem Concr Res*, vol. 34, no. 9, pp. 1541–1547, Sep. 2004, doi: 10.1016/j.cemconres.2004.04.014.

[135] ASTM C1365-18, "Standard Test Method for Determination of the Proportion of Phases in Portland Cement and Portland-Cement Clinker Using X-Ray Powder Diffraction Analysis," *ASTM*, pp. 1–11, 2018, doi: 10.1520/C1365-18.

[136] K. Scrivener, R. Snellings, and B. Lothenbach, *A practical guide to microstructural analysis of cementitious materials*. 2016.

[137] ASTM C1872-18, "Standard Test Method for Thermogravimetric Analysis of Hydraulic Cement," *ASTM*, pp. 1–7, 2018, doi: 10.1520/C1872-18E02.

[138] ASTM C188-17, "Standard Test Method for Density of Hydraulic Cement," *ASTM*, pp. 1–3, 2017, doi: 10.1520/C0188-17.

[139] J. Stroh, B. Meng, and F. Emmerling, "Monitoring of sulphate attack on hardened cement paste studied by synchrotron XRD," *Solid State Sci*, vol. 48, pp. 278–285, Oct. 2015, doi: 10.1016/j.solidstatesciences.2015.08.006.

[140] Materials Manual, "Self-Consolidating Concrete (SCC) for Precast/ Prestressed Concrete Products," in *Precast/Prestressed Concrete Products*, vol. II, 2022, pp. 1–12.

[141] ASTM C494-19, "Standard Specification for Chemical Admixtures for Concrete," *ASTM*, pp. 1–15, 2019, doi: 10.1520/C0494_C0494M-19.

[142] ASTM C1621-17, "Standard Test Method for Passing Ability of Self-Consolidating Concrete by J-Ring," *ASTM*, pp. 1–4, 2017, doi: 10.1520/C1621_C1621M-17.

[143] ASTM C1712-20, "Standard Test Method for Rapid Assessment of Static Segregation Resistance of Self-Consolidating Concrete Using Penetration Test," *ASTM*, pp. 1–5, 2020, doi: 10.1520/C1712-20.

[144] ASTM C1610-21, "Standard Test Method for Static Segregation of Self-Consolidating Concrete Using Column Technique," *ASTM*, pp. 1–4, 2021, doi: 10.1520/C1610_C1610M-21.

[145] ASTM C1611-21, "Standard Test Method for Slump Flow of Self-Consolidating Concrete," *ASTM*, pp. 1–6, 2021, doi: 10.1520/C1611_C1611M-21.

[146] ASTM C192-19, "Standard Practice for Making and Curing Concrete Test Specimens in the Laboratory," *ASTM*, pp. 1–8, 2019, doi: 10.1520/C0192_C0192M-19.

[147] AASHTO T 358-15, "Standard Method of Test for Surface Resistivity Indication of Concrete's Ability to Resist Chloride Ion Penetration," *AASHTO*, pp. 1–10, 2015, [Online]. Available: www.salmanco.comwww.salmanco.com

[148] AASHTO TP 119-19, "Standard Method of Test for Electrical Resistivity of a Concrete Cylinder Tested in a Uniaxial Resistance Test," *AASHTO*, pp. 1–2, 2019.

[149] ASTM C1012-18, "Standard Test Method for Length Change of Hydraulic-Cement Mortars Exposed to a Sulfate Solution," *ASTM*, pp. 1–8, 2018, doi: 10.1520/C1012_C1012M-18.

[150] ASTM C39-09, "Standard Test Method for Compressive Strength of Cylindrical Concrete Specimens," *ASTM*, pp. 1–7, 2010, doi: 10.1520/C0039_C0039M-09a.

[151] W. Zhan *et al.*, "Evaluating the effect of mgo/al2o3 ratio on thermal behaviors and structures of blast furnace slag with low carbon consumption," *Crystals (Basel)*, vol. 11, no. 11, Nov. 2021, doi: 10.3390/cryst11111386.

[152] D. A. Koleva, O. Copuroglu, K. van Breugel, G. Ye, and J. H. W. de Wit, "Electrical resistivity and microstructural properties of concrete materials in conditions of current flow," *Cem Concr Compos*, vol. 30, no. 8, pp. 731–744, Sep. 2008, doi: 10.1016/j.cemconcomp.2008.04.001.

[153] M. A. Megat Johari, J. J. Brooks, S. Kabir, and P. Rivard, "Influence of supplementary cementitious materials on engineering properties of high strength concrete," *Constr Build Mater*, vol. 25, no. 5, pp. 2639–2648, May 2011, doi: 10.1016/j.conbuildmat.2010.12.013.

[154] ACI 201.2-23, "Durable Concrete- Guide," *American Concrete Institute*, pp. 1–100, 2023, [Online]. Available: www.concrete.org